

**AN INVESTIGATION OF INTERACTIONS
BETWEEN PLANTS AND WATER, ENERGY AND CARBON BUDGETS
IN THE SOIL-PLANT-ATMOSPHERE CONTINUUM**

by

Xiangyu Luo

B.S., Tsinghua University, Beijing, China, 1998

M.S., China Institute of Water Resources and Hydropower Research, Beijing, China, 2003

Submitted to the Graduate Faculty of
Swanson School of Engineering in partial fulfillment
of the requirements for the degree of
Doctor of Philosophy

University of Pittsburgh

2013

UNIVERSITY OF PITTSBURGH
SWANSON SCHOOL OF ENGINEERING

This dissertation was presented

by

Xiangyu Luo

It was defended on

October 11, 2013

and approved by

Jeen-Shang Lin, Ph.D., Associate Professor, Department of Civil and Environmental Engineering

Jorge D. Abad, Ph.D., Assistant Professor, Department of Civil and Environmental Engineering

Tin-Kan Hung, Ph.D., Professor, Department of Bioengineering

Zhi-Hong Mao, Ph.D., Associate Professor, Department of Electrical and Computer Engineering

Dissertation Director: Xu Liang, Ph.D., Professor, Department of Civil and Environmental
Engineering

Copyright © by Xiangyu Luo

2013

**AN INVESTIGATION OF INTERACTIONS
BETWEEN PLANTS AND WATER, ENERGY AND CARBON BUDGETS
IN THE SOIL-PLANT-ATMOSPHERE CONTINUUM**

Xiangyu Luo, PhD

University of Pittsburgh, 2013

Exchange of energy and substance (water, carbon dioxide, etc.) between land surface and atmosphere has a significant impact on climate. Considerable part of this exchange occurs through the soil-plant-atmosphere continuum (SPAC) where plants play an important role. Therefore functions of plants in water, energy and carbon cycles of the SPAC need to be extensively studied.

When dry climatic conditions appear, plants can cope with the adverse circumstances by taking advantage of some biological or hydrological processes. In this study, the Three-Layer Variable Infiltration Capacity (VIC-3L) land surface model is extended to include some important biological or hydrological processes under water-limited climatic conditions: (1) movement of soil water from wet to dry regions through hydraulic redistribution (HR); (2) groundwater dynamics; (3) plant water storage; and (4) photosynthetic process. The extended VIC-3L model (referred to as VIC+ model) is evaluated with an analytical solution under simple conditions and with observed data at two AmeriFlux sites. Scenario simulations demonstrate that: (1) HR has significant impacts on water, energy and carbon budgets during the dry season; (2) Rise of groundwater table, increase of root depth, HR, and plant water storage can increase dry-season latent heat flux; (3) Plant water storage can weaken the intensity of upward HR; (4) Frozen soil can restrict downward HR in the wet winter and reduce the soil water reserves for the dry season.

Groundwater can have significant impacts on the interactions between land surface and atmosphere by way of mechanisms such as influencing plant transpiration. The VIC+ model is used to conduct numerical experiments to study impacts of groundwater on transpiration. The relationship between transpiration and groundwater dynamics, and the related subsurface processes under various conditions are revealed and analyzed through results of numerical experiments.

In order to predict interactions between land surface and atmosphere in the future, vegetation needs to be represented dynamically in modeling studies. To this end, the CASACNP biogeochemical model has been coupled with the VIC+ model. This coupled model is used to conduct scenario simulations to demonstrate impacts of vegetation on water and energy cycles when dynamic growth of vegetation is represented.

TABLE OF CONTENTS

ACKNOWLEDGEMENTS	XXI
1.0 INTRODUCTION.....	1
1.1 BACKGROUND AND MOTIVATION	1
1.2 RESEARCH OBJECTIVES.....	6
1.3 DISSERTATION ORGANIZATION.....	7
2.0 MODELING METHODS.....	8
2.1 MODELING OF HYDRAULIC REDISTRIBUTION AND GROUNDWATER	8
2.1.1 Soil Water Dynamics	8
2.1.2 Water Transport in the Root System.....	10
2.1.3 Water Exchange between Roots and the Soil.....	11
2.1.4 Representation of the Saturated Zone	12
2.1.5 Frozen Soil.....	13
2.1.6 Solving the Coupled Equations	14
2.1.7 Root Parameters	15
2.1.7.1 Vertical Distribution of Roots	16
2.1.7.2 Root Hydraulic Conductivities	17
2.2 MODELING OF PLANT TRANSPIRATION.....	18

2.2.1	Ohm’s Law Analogy	19
2.2.2	Penman-Monteith Method Coupled with Photosynthesis	21
2.2.2.1	Stomatal Conductance.....	21
2.2.2.2	Carbon Assimilation	23
	Diffusion Method.....	23
	Modified Farquhar Model.....	24
2.2.3	Calculation Procedure for Plant Transpiration	25
2.3	COUPLING WITH THREE-LAYER VARIABLE INFILTRATION CAPACITY (VIC-3L) MODEL	25
2.3.1	Incorporation of the Soil-Root Module	26
2.3.2	Incorporation of the New Transpiration Module.....	29
3.0	MODEL VALIDATION.....	30
3.1	VALIDATION OF SOIL-ROOT MODULE UNDER A SIMPLIFIED CONDITION.....	30
3.2	VALIDATION AT DUKE SITE	32
3.2.1	Site Description and Model Setup.....	32
3.2.2	Comparison to Observations	37
3.3	VALIDATION AT BLODGETT SITE	44
3.3.1	Site Description and Model Setup.....	44
3.3.2	Comparison to Observations	46
4.0	IMPACTS OF BIOLOGICAL/HYDROLOGICAL PROCESSES ON WATER, ENERGY AND CARBON BUDGETS	49
4.1	SCENARIO SIMULATIONS AT DUKE SITE.....	49

4.1.1	Impact of Hydraulic Redistribution on Root Uptake.....	50
4.1.2	Impact of Hydraulic Redistribution on Soil Moisture	52
4.1.3	Impact of Hydraulic Redistribution on Transpiration, Latent Heat, Sensible Heat and GPP	56
4.1.4	Summary	58
4.2	SCENARIO SIMULATIONS AT BLODGETT SITE.....	58
4.2.1	Impacts of Hydraulic Redistribution, Groundwater and Plant Storage on Latent Heat Flux	59
4.2.2	Interactions among the Impacts of Root Depth, Hydraulic Redistribution and Groundwater	64
4.2.2.1	Impact of Root Depth	65
4.2.2.2	Impact of Hydraulic Redistribution.....	66
4.2.2.3	Impact of Groundwater.....	67
4.2.3	Impact of Plant Storage on Hydraulic Redistribution.....	68
4.2.4	Impact of Frozen Soil on Hydraulic Redistribution.....	70
4.2.5	Summary	74
5.0	RELATIONSHIPS BETWEEN PLANT TRANSPIRATION AND GROUNDWATER DYNAMICS.....	76
5.1	INTRODUCTION	76
5.2	MODEL DESCRIPTION	79
5.3	DESIGN OF NUMERICAL EXPERIMENTS.....	80
5.3.1	Description of One Numerical Experiment.....	81
5.3.2	Differences among Numerical Experiments.....	83

5.4	SIMULATION RESULTS AND DISCUSSION.....	86
5.4.1	Transpiration–GWTD Relationships	86
5.4.1.1	Impact of Precipitation on Transpiration–GWTD Relationships..	86
5.4.1.2	Comparisons among Different Vegetation Types	88
5.4.1.3	Impact of Soil Type on Transpiration–GWTD Relationships	90
5.4.1.4	Impact of HR on Transpiration–GWTD Relationships	91
5.4.2	Upward Diffusion of Soil Water	94
5.4.2.1	Impact of Precipitation on Upward Diffusion of Soil Water	95
5.4.2.2	Impact of Soil Type on Upward Diffusion of Soil Water	97
5.4.2.3	Impact of HR on Upward Diffusion of Soil Water	98
5.4.3	Hydraulically Redistributed Water	99
5.4.3.1	Impact of Precipitation on Hydraulically Redistributed Water...	100
5.4.3.2	Impact of Soil Type on Hydraulically Redistributed Water	102
5.4.4	Daytime Uptake by Roots	103
5.4.4.1	Impact of Precipitation on Daytime Uptake by Roots.....	104
5.4.4.2	Impact of HR on Daytime Uptake by Roots	105
5.4.5	Effects of Forcing Type on Transpiration – GWTD Relationship.....	107
5.4.5.1	Transpiration – GWTD Relationships.....	107
5.4.5.2	Hydraulically Redistributed Water.....	109
5.4.5.3	Upward Diffusion of Soil Water	112
5.4.5.4	Daytime Uptake by Roots.....	114
5.5	SUMMARY	116
6.0	DYNAMIC REPRESENTATION OF VEGETATION	121

6.1	INTRODUCTION	121
6.2	CASACNP BIOGEOCHEMICAL MODEL	122
6.3	COUPLING CASACNP MODEL WITH VIC+ MODEL	124
6.4	SCENARIO SIMULATIONS.....	125
7.0	SUMMARY AND CONCLUSIONS	129
7.1	VIC+ MODEL.....	129
7.2	MODEL VALITATION	129
7.3	IMPACTS OF BIOLOGICAL/HYDROLOGICAL PROCESSES.....	131
7.4	TRANSPIRATION – GROUNDWATER INTERACTIONS.....	132
7.5	DYNAMIC REPRESENTATION OF VEGETATION.....	134
7.6	FUTURE WORK.....	134
	APPENDIX.....	135
	BIBLIOGRAPHY.....	150

LIST OF TABLES

Table 3.1	Values of model parameters for this study	35
Table 3.2	Water balance of the surface layer in ten nights.....	40
Table 4.1	Comparison of the modeled results of the two scenarios.	57
Table 4.2	Setup of scenarios for studying impacts of HR, groundwater depth and plant water storage on water and energy cycles ^a	59
Table 4.3	Comparison of dry-season latent heat flux among different scenarios.....	61
Table 4.4	Setup of groups for studying interactions among HR, groundwater and root depth ^a . ..	64
Table 4.5	Comparison of hydraulically redistributed water (HRW) amounts ^a	69
Table 6.1	Setup of scenarios for studying impacts of dynamic vegetation	125

LIST OF FIGURES

- Figure 2.1 Diagram of water movement in plants. E_r : plant transpiration; F_{ru} : sap flux at the root collar; q : plant-storage flux; R : hydraulic resistance from the soil to leaves; r : plant-storage hydraulic resistance; C : plant capacitance; ψ_l : leaf water potential; ψ_p : plant-storage water potential; ψ_{soil} : soil water potential. 19
- Figure 2.2 A flow chart illustrating the main procedures for calculating the plant transpiration. Rectangles indicate calculation processes. Parallelograms represent variables. 26
- Figure 2.3 Schematic diagram for coupling of the new transpiration module, the soil-root module and the VIC-3L model. 27
- Figure 3.1 Comparison of the initial (i.e., derived theoretical) and final soil moisture profiles in the simple numerical experiment. 31
- Figure 3.2 Comparison between the modeled soil water content (SWC) and the observed data at the Duke site for years 2004 and 2005. The SWC values are average values of the surface soil layer (0 – 30 cm depth). “Observed mean” shows the mean values of one group of data from four measurement points. “Observed range” shows the variation range of the group of data. a) Daily values of year 2004; b) Hourly values from 18:00, 20 May to 18:00, 3 June in year 2004; c) Daily values of year 2005; d) Hourly values from 18:00, 23 August to 18:00, 6 September in year 2005. 38

Figure 3.3	Comparison of modeled energy results with the observed data at daily time scale for the year 2005. (a) Net radiation; (b) Latent heat flux; (c) Sensible heat flux; (d) Ground heat flux; (e) Ground temperature. The observed ground heat flux is not available and not included here.....	43
Figure 3.4	Comparison of modeled results with the observations at Duke site for the year 2004. a) Latent heat flux; b) Gross primary productivity (GPP).	44
Figure 3.5	Comparison of modeled soil moisture results with the observed data at the Blodgett site for the year 2004. a) At the depth of 10 cm; b) At the depth of 30 cm. Hydraulic redistribution (HR) is considered in the “HR” scenario simulation and not considered in the “no-HR” scenario simulation.....	46
Figure 3.6	Comparison of modeled results with the observations at the Blodgett site for the year 2004. a) Latent heat flux; b) Gross primary productivity (GPP). The modeled results of both the “HR” scenario and the “no-HR” scenario are shown.	48
Figure 4.1	Profiles of total daytime uptake in one year for Case A (without HR) and Case R (with HR): a) From ground surface to 0.5 m depth; b) From 0.5 m to 5 m depth. ..	51
Figure 4.2	Relative differences between daytime uptake profiles of Case A and Case R. Positive values mean that uptake of Case R is larger than that of Case A and the vice versa.	51
Figure 4.3	Profile of total nighttime uptake in one year for Case R (with HR): a) From ground surface to 0.5 m depth; b) From 0.5 m to 5 m depth. (Negative values mean that roots release water into the soil.)	52
Figure 4.4	Average volumetric soil water content (SWC) of the top layer (0-30 cm) for Case A (without HR) and Case R (with HR).....	53

Figure 4.5 Comparison of SWC profiles between Case A (without HR) and Case R (with HR):
a) Mean SWC profiles of one year for Case A and Case R; b) Relative differences between the mean SWC profile of Case R and that of Case A (Positive values mean that SWC of Case R is higher than that of Case A and the vice versa). The abrupt changes on the SWC profiles are due to heterogeneous soil properties. 53

Figure 4.6 Comparison of SWC profiles between Case A (without HR) and Case R (with HR) for a) a wet period (from 3/9 to 3/11, the three days after a rain event on 3/8) and b) a dry period (from 8/23 to 9/2, when potential evapotranspiration overwhelms precipitation). 54

Figure 4.7 Comparison of SWC profiles between Case A (without HR) and Case R (with HR) for three days: a) March 31, approximate the end of the wet period; b) September 30, approximate the end of the dry period; c) December 31, the end of three wet months. 55

Figure 4.8 Comparison of precipitation to potential transpiration at the monthly time scale. 56

Figure 4.9 Comparison of latent heat flux between the benchmark scenario and other scenarios when the maximum root depth is 2 m (a, b, c and d) or 8 m (e, f, g and h). a) and e): Scenario 2 vs. Benchmark Scenario (HR vs. no-HR); b) and f): Scenario 3 vs. Benchmark Scenario (Shallower groundwater table vs. Deeper groundwater table); c) and g): Scenario 4 vs. Benchmark Scenario (With plant storage vs. Without plant storage); d) and h): Scenario HRGWC vs. Benchmark Scenario. 60

Figure 4.10 Comparison of root uptake profiles between the Benchmark Scenario (no-HR) and the Scenario 1 (HR). The profiles show annual total root uptake at daytime and nighttime, respectively. Negative values mean that roots release water into the soil.

When the maximum root depth is 2 m, results are shown in a) (from ground surface to 1 m depth) and b) (from 1 m to 2 m depth). When the maximum root depth is 8 m, results are shown in c) (from ground surface to 1 m depth) and d) (from 1 m to 8 m depth). 62

Figure 4.11 (a) Relationships between dry-season latent heat fluxes and root depths for the four groups of scenarios in Table 3; (b) Relationships between average groundwater table depths and root depths for the four groups of scenarios. “GWT” is the abbreviation of “groundwater table”..... 65

Figure 4.12 Comparison of amounts of hydraulically redistributed water in the shallow soil layer between the scenario with plant storage and the scenario without plant storage. a) The maximum root depth is 2 m; b) The maximum root depth is 8 m. 68

Figure 4.13 Comparison of daily downward HRW (Hydraulically Redistributed Water) for the “Frozen soil” scenario and the “No frozen soil” scenario in the year 2004 at the Blodgett site. 71

Figure 4.14 Comparison of profiles of total root uptake in the winter for the “Frozen soil” scenario and the “No frozen soil” scenario: (a) 0 – 1 m root zone; (b) 1 – 8 m root zone. Negative values mean that roots release water into the soil. Root uptake values of each 2 cm sublayer are shown. 71

Figure 4.15 Comparison of daily downward HRW (Hydraulically Redistributed Water) for the “Frozen soil” scenario and the “No frozen soil” scenario (the lower panel) when the air temperature is lowered by 3 degrees Celsius for each hour of year 2004. The adjusted daily air temperature and daily precipitation are shown in the upper panel. 72

Figure 4.16	Comparison of profiles of total root uptake in the winter for the “Frozen soil” scenario and the “No frozen soil” scenario when the air temperature is lowered by 3 degrees Celsius. (a) 0 – 1 m root zone; (b) 1 – 8 m root zone. Negative values mean that roots release water into the soil. Root uptake values of each 2 cm sublayer are shown.	73
Figure 5.1	Comparisons of Transpiration – GWTD relationships under three precipitation conditions: (a) When HR is considered; (b) When HR is not considered. The vegetation type is tree and the soil type is loam.	87
Figure 5.2	Comparisons of Transpiration – GWTD relationships of three vegetation types: (a) When HR is considered; (b) When HR is not considered. The soil type is loam and the precipitation condition is P50.	89
Figure 5.3	Comparisons of Transpiration – GWTD relationships of three soil types: (a) When HR is considered; (b) When HR is not considered. The vegetation type is tree and the precipitation condition is P50.	90
Figure 5.4	Comparisons of Transpiration – GWTD relationships between HR and no-HR scenarios under three precipitation conditions: (a) P50; (b) P70; (c) P100. The vegetation type is tree and the soil type is loam.	92
Figure 5.5	Comparisons of Transpiration – GWTD relationships between HR and no-HR scenarios for three soil types: (a) Loam; (b) Sand; (c) Clay. The vegetation type is tree and the precipitation condition is P50.....	93
Figure 5.6	Comparisons of Transpiration – GWTD relationships between HR and no-HR scenarios for three vegetation types: (a) Tree; (b) Shrub; (c) Grass. The soil type is loam and the precipitation condition is P50.....	94

Figure 5.7 Comparisons of upward diffusion of soil water under three precipitation conditions (P50, P70 and P100) for (a) HR scenarios and (b) no-HR scenarios. The soil type is loam and the vegetation type is tree. The upward diffusion occurs at the depth of 5.5m (i.e., 0.5 m below the root zone bottom)..... 96

Figure 5.8 Comparisons of upward diffusion of soil water for three soil types (loam, sand and clay): (a) When HR is considered; (b) When HR is not considered. The precipitation condition is P50 and the vegetation type is tree. The upward diffusion occurs at the depth of 5.5m (i.e., 0.5m below the root zone bottom). 97

Figure 5.9 Comparisons of upward diffusion of soil water between HR scenarios and no-HR scenarios for three soil types: (a) Loam; (b) Sand; (c) Clay. The precipitation condition is P50 and the vegetation type is tree. The upward diffusion occurs at the depth of 5.5m (i.e. 0.5m below the root zone bottom)..... 98

Figure 5.10 Comparisons of hydraulically redistributed water (HRW) – GWTD relationships under three precipitation conditions (P50, P70 and P100) for both (a) the shallow root zone (0-1m depth) and (b) the deep root zone (1-5m depth). The vegetation type is tree and the soil type is loam. 100

Figure 5.11 Comparisons of HRW – GWTD relationships among three soil types (loam, sand and clay) for both (a) the shallow root zone (0-1m depth) and (b) the deep root zone (1-5m depth). The vegetation type is tree and the precipitation condition is P50. 102

Figure 5.12 Comparisons of Daytime Root Uptake – GWTD relationships under three precipitation conditions (P50, P70 and P100) for both (a) the shallow root zone (0-1m depth) and (b) the deep root zone (1-5m depth). The vegetation type is tree, the soil type is loam and the HR process is considered. 104

Figure 5.13 Comparisons of daytime root uptake between HR and no-HR scenarios for both (a) the shallow root zone (0-1m depth) and (b) the deep root zone (1-5m depth). The vegetation type is tree, the soil type is loam and the precipitation condition is P50. 106

Figure 5.14 Comparisons of Transpiration – GWTD relationships between HR and no-HR scenarios for different forcing data: (a) Blodgett forcing data; (b) Duke forcing data. The vegetation type is tree, the soil type is loam and the precipitation condition is P50. 108

Figure 5.15 Comparisons of daily transpiration between HR and no-HR scenarios for different forcing data: (a) Blodgett forcing data; (b) Duke forcing data. The vegetation type is tree and the soil type is loam. The precipitation condition is P50 and the groundwater table depth is 6 meters. 109

Figure 5.16 HRW – GWTD relationships for the shallow root zone (0-1m depth) and the deep root zone (1-5m depth) under different forcing conditions: (a) Blodgett forcing data; (b) Duke forcing data. The vegetation type is tree, the soil type is loam and the precipitation condition is P50. 110

Figure 5.17 Daily HRW of the shallow root zone (0-1m depth) and the deep root zone (1-5m depth) under different forcing conditions: (a) Blodgett forcing data; (b) Duke forcing data. The vegetation type is tree and the soil type is loam. The precipitation condition is P50 and the groundwater table depth is 6 meters. 111

Figure 5.18 Comparisons of Upward Diffusion – GWTD relationships between HR scenarios and no-HR scenarios for different forcing conditions: (a) Blodgett forcing data; (b) Duke forcing data. The vegetation type is tree, the soil type is loam and the

	precipitation condition is P50. The upward diffusion occurs at the depth of 5.5m (i.e. 0.5m below the root zone bottom).....	112
Figure 5.19	Comparisons of daily upward diffusion of soil water between HR scenarios and no-HR scenarios for different forcing conditions: (a) Blodgett forcing data; (b) Duke forcing data. The vegetation type is tree and the soil type is loam. The precipitation condition is P50 and the groundwater table depth is 6 meters. The upward diffusion occurs at the depth of 5.5m (i.e. 0.5m below the root zone bottom).	113
Figure 5.20	Daytime Root Uptake – GWTD relationships for the shallow root zone (0-1m depth) and the deep root zone (1-5m depth) under different forcing conditions: (a) Blodgett forcing data; (b) Duke forcing data. The vegetation type is tree and the soil type is loam. The precipitation condition is P50 and the HR process is considered.	114
Figure 5.21	Daily daytime uptake by roots for the shallow root zone (0-1m depth) and the deep root zone (1-5m depth) under different forcing conditions: (a) Blodgett forcing data; (b) Duke forcing data. The vegetation type is tree and the soil type is loam. The precipitation condition is P50 and the groundwater table depth is 6 meters. The HR process is considered.....	115
Figure 6.1	Comparison of observed leaf area index (LAI) to simulated results from the CASACNP model when using the observed precipitation data.....	127
Figure 6.2	Comparison of transpiration modeled by VIC+ to that of the coupled model (CASACNP + VIC+) when using the observed precipitation data	127
Figure 6.3	Comparison of observed leaf area index (LAI) to simulated results from the CASACNP model when using the decreased precipitation.....	128

Figure 6.4 Comparison of transpiration modeled by VIC+ to that of the coupled model (CASACNP + VIC+) when using the decreased precipitation..... 128

ACKNOWLEDGEMENTS

I would like to express my sincere thanks to my advisor Dr. Xu Liang. She provided me the opportunity to study and carry out research in the United States, and guidance and support over the course of this work.

Appreciation is extended to the other members of my doctoral committee: Dr. Jeen-Shang Lin, Dr. Jorge D. Abad, Dr. Tin-Kan Hung and Dr. Zhi-Hong Mao, for their precious advice and time.

Special thanks to the other members of the preliminary examination committee: Dr. Rafael G. Quimpo and Dr. Ravi Sharma, for their guidance and suggestions.

Thanks to former and current members of our research group for all their big or small help. Thanks to fellow students of the CEE department for their help.

Thanks to the staff and faculty of the Department of Civil and Environmental Engineering for their assistance and support.

Thanks to colleagues in my former employer, the IWHR (China Institute of Water Resources and Hydropower Research). I studied and worked there for eight years before I came to pursue the doctoral degree. From those colleagues I obtained part of the motivation to study abroad.

Finally, deep gratitude to my family.

1.0 INTRODUCTION

1.1 BACKGROUND AND MOTIVATION

Exchange of energy and substance (water, carbon dioxide, etc.) between land surface and atmosphere has a significant impact on climate. Considerable part of this exchange occurs through the soil-plant-atmosphere continuum (SPAC) since the total forested area on the earth surface is about 3.6 billion hectares (9 billion acres) – covering one third of the landmass [Gore, 2009]¹. Transpiration from vegetation accounts for the major part of water vapor from land surface to atmosphere. At the same time, water cycle in the SPAC determines the partition of precipitation and hence affects runoff and amount of freshwater available to human beings. Therefore functions of plants in water, energy and nutrient cycles of the SPAC have been extensively studied in both the climatic area and the hydrological area. However, our understanding of hydrological and biogeochemical processes in the SPAC is still limited.

Many important hydrological and biogeochemical processes related to plants have been included in land surface models, which are often employed in climate models, in hopes of properly reproducing and predicting water, energy and carbon cycles in the soil-plant-

¹ Although at present the forest cover on the earth is only half of that 300 years ago, and is constantly declining due to deforestation. The net loss of forests each year is about 7.3 million hectares (18 million acres). [Gore, 2009]

atmosphere continuum [e.g., *Sellers et al.*, 1986, 1996; *Bonan*, 1995; *Foley et al.*, 1996]. However, significance of a process may vary under different climatic and environmental conditions. Processes that are not important in the humid environment, for example, may have evident impacts on water, energy and carbon cycles under water-limited conditions and thus, should not be ignored in the corresponding model simulations[e.g., *Lee et al.*, 2005; *Wang*, 2011].

Plant growth relies on climatic and environmental conditions. Plants have the ability to adjust their strategies to adapt to the environment. When dry climatic conditions appear, plants may try to cope with the adverse circumstances by taking advantage of some biological and hydrological processes (e.g., hydraulic redistribution, ground water dynamics, plant water storage, etc.) [e.g., *Caldwell et al.*, 1998; *Wang et al.*, 2002; *Soylu et al.*, 2011]. Therefore these processes can play important roles in the soil-plant-atmosphere continuum and should be included in models.

Hydraulic redistribution (HR) is the movement of water from soil of higher water potential to soil of lower water potential, usually from moist regions to dry regions, through plant roots. HR has been verified to exist for many plant species at different geographical locations around the world [*Caldwell et al.*, 1998]. Experimental and modeling studies show that HR is an important process not only in the arid and semi-arid regions [*Caldwell and Richards*, 1989; *Dawson*, 1993; *Ryel et al.*, 2002] but also in wet regions which experience dry seasons (e.g., partial region of the Amazonia) [*Lee et al.*, 2005; *Wang*, 2011]. For example, it has been found that HR can contribute to dry-season transpiration and carbon assimilation [*Ryel et al.*, 2002; *Lee et al.*, 2005; *Amenu and Kumar*, 2008; *Wang*, 2011].

HR has been investigated in a number of modeling studies. Most of these used conceptual formulae to represent the HR process [e.g., *Ryel et al.*, 2002]. In some of these studies, conceptual representations of HR were incorporated into land surface models or General Circulation Models (GCMs) to investigate its impacts at large spatial scales [e.g., *Ren et al.*, 2004; *Lee et al.*, 2005; *Baker et al.*, 2008; *Wang*, 2011; *Li et al.*, 2012]. However, in those conceptual formulae for the HR process, it is challenging to estimate parameter values [*Ryel et al.*, 2002; *Wang*, 2011; *Neumann and Cardon*, 2012]. In addition to conceptual formulae, some process-based schemes have also been put forward to model the HR process [e.g., *Mendel et al.*, 2002; *Amenu and Kumar*, 2008; *Quijano et al.*, 2012]. For parameters in these process-based schemes, physical meanings are straightforward and the parameter values can be estimated from the measured data. In the previous studies, process-based HR schemes have been coupled with other biological and hydrological processes. *Mendel et al.* [2002] considered interactions between HR, transpiration and groundwater in their model, and applied the model in a two-dimensional domain under a simplified condition. *Amenu and Kumar* [2008] coupled their process-based HR scheme with a big-leaf canopy model of plant transpiration, and applied the coupled model at the Sierra Nevada eco-region. This HR scheme was also used to model the HR processes of overstory and understory simultaneously and the interactions between vegetation species were investigated [*Quijano et al.*, 2012]. In this study, a process-based HR scheme has been coupled with a few biological or hydrological processes (e.g., groundwater dynamics, plant water storage, etc.), which can play important roles under water-limited conditions. The HR scheme and representations of these processes have been integrated into the Three-layer Variable Infiltration Capacity (i.e., VIC-3L) land surface model and the dynamic interactions between HR

and other biological and hydrological processes of land surface are represented. The extended VIC-3L model is also referred to as VIC+ model in this dissertation.

Groundwater can have significant impacts on the land surface and atmospheric processes under dry climatic conditions by way of mechanisms such as exerting influence on soil moisture of the root zone. Groundwater dynamics have been represented in some land surface models [e.g., *Liang et al.*, 2003; *Kollet and Maxwell*, 2008]. HR influences the distribution of soil moisture in the root zone and can enhance the utilization of groundwater by plants. Previous experimental studies indicated that the existence of groundwater, together with the effect of HR, could provide more potential transpirational water to plants [e.g., *Dawson*, 1996]. Therefore, it is meaningful to consider the interaction between HR and groundwater in modeling studies. Groundwater was represented in a few previous modeling studies on HR. For example, in the HR modeling study by *Ryel et al.*[2002], the groundwater table is represented but is “fixed” at a certain position below the root zone (i.e., the depth from the ground surface to the groundwater table is assumed to be constant). *Mendel et al.*[2002] considered the HR-groundwater coupling in the context of a simplified scenario. In this study, groundwater dynamics is explicitly modeled and the coupling between HR and groundwater dynamics is represented in the context of the land surface model. The HR-groundwater coupling is integrated with other land surface processes in the VIC+ model.

Besides groundwater dynamics, frozen soil can also affect the amount of water stored in the soil. During the wet season, soil water in shallow layers may be transferred to the deep soil through downward HR, if the water potential of the shallow layer is higher than that of the deep soil [e.g., *Caldwell et al.*, 1998; *Amenu and Kumar*, 2008; *Neumann and Cardon*, 2012]. However, if the wet season is in winter (e.g., the Mediterranean climate), soil water in the shallow layer may be frozen, thus reducing the magnitude of downward HR and decreasing the

amount of water stored in the deep soil which can be used by plants during the dry periods. In this study, the impact of frozen soil on HR is represented in the model.

Besides soil moisture, water stored in plant can also affect water, energy and nutrient cycles in the soil-plant-atmosphere continuum. Water absorbed by roots can be stored in plant tissues (e.g., stems and leaves) and used to partially supply transpiration at a later time when root uptake cannot satisfy the transpiration demand [e.g., *Katerji et al.*, 1986; *Lhomme et al.*, 2001]. Therefore this plant water storage (also referred to as “plant storage”) can promote plant transpiration and hence latent heat flux, especially under dry soil conditions [e.g., *Wang et al.*, 2002]. This process affects the water cycle in plants and causes time-lag between root uptake and transpiration, as well as decreases maximum instantaneous rate of water uptake by roots [*Hunt et al.*, 1991]. In this study, the representation of plant water storage is included in the VIC+ model.

In addition to the above biological or hydrological processes, the photosynthetic process is also coupled into the VIC+ model. Stomata of leaves regulate both vapor flux and uptake of CO₂ simultaneously and transpiration is closely related to photosynthesis [e.g., *Collatz et al.*, 1991; *Daly et al.*, 2004]. In this study, the transpiration process is coupled with the photosynthetic process through linking the stomatal conductance with carbon assimilation, using a variant of the Ball-Berry-Leuning model [*Tuzet et al.*, 2003]. This *Tuzet et al.* model has a solid mechanistic basis and accounts for the effect of water stress on stomatal conductance. In addition, in this coupling method the photosynthetic capacity is effectively reduced under dry conditions, which can result in decreases of both photosynthesis and transpiration.

The VIC-3L land surface model is extended in the above ways in this study [*Luo et al.*, 2013]. Many hydrological or biological processes have been coupled with each other in this model, which makes it possible to employ this model to study the interactions between these

processes. Groundwater can have significant impacts on the subsurface, land surface and atmospheric processes, especially under water limited conditions. Understanding of land surface – groundwater interactions is helpful for development and application of land surface models. Plant transpiration is one of the primary land surface processes. In this study, the relationship between transpiration and groundwater table depth under different conditions are investigated through conducting numerical experiments using the VIC+ model.

In the above studies, static representation of vegetation is used. However, dynamic representation of vegetation is necessary in some modeling studies, for example, to conduct scenario simulations under future conditions. The reason is that the environment exerts influence on plants and affects their growth and, at the same time, dynamic variation of vegetation sends feedback to the environment. In this study, the VIC+ model has been coupled with the CASACNP biogeochemical model where plant growth is represented. The coupling of the two models is favorable to modeling the dynamic role of vegetation in the soil-plant-atmosphere continuum.

1.2 RESEARCH OBJECTIVES

The primary research objectives of this study are listed as follow:

- (a) To improve capabilities of the land surface model under water-limited conditions by incorporating biological and hydrological processes;
- (b) To investigate the impacts of biological and hydrological processes on water, energy and carbon budgets in the soil-plant-atmosphere continuum;

(c) To investigate the interactions between biological and hydrological processes in the soil-plant-atmosphere continuum.

1.3 DISSERTATION ORGANIZATION

In this dissertation, Chapter 2 describes the parameterizations of the biological and hydrological processes, as well as the method for coupling these parameterizations with the VIC-3L model; Chapter 3 demonstrates the validation of the VIC+ model; Chapter 4 presents impacts of biological/hydrological processes on water, energy and carbon budgets in the soil-plant-atmosphere continuum, and interactions between biological and hydrological processes; Chapter 5 discusses the transpiration – groundwater interactions; Chapter 6 describes dynamic representation of vegetation in the land surface model; Chapter 7 provides summary and conclusions.

2.0 MODELING METHODS

2.1 MODELING OF HYDRAULIC REDISTRIBUTION AND GROUNDWATER

In this study, water movement in the soil and root system is modeled simultaneously. The Richards equation is used to represent the soil water dynamics and the Poiseuille law is used to approximate the water transport along roots. The movement of water in the soil and in roots is connected through the water exchange at the interface between roots and the soil.

2.1.1 Soil Water Dynamics

Water movement in the soil is represented by a mixed-form of the Richards equation [Richards, 1931]:

$$\frac{\partial \theta}{\partial t} - \frac{\partial}{\partial z} \left[K_s \cdot \frac{\partial (\psi_s - \rho_w g z)}{\partial z} \right] + F_{sr} = 0 \quad (2-1)$$

where θ [m^3m^{-3}] is the volumetric soil water content (SWC); t is time; z [m] is the vertical coordinate originating from the ground surface with downward being positive; K_s [$\text{m}^2 \text{s}^{-1} \text{Pa}^{-1}$] is the soil hydraulic conductivity; ψ_s [Pa] is the soil water potential; $(-\rho_w g z)$ [Pa] is the gravitational potential; ρ_w [kg m^{-3}] is the water density; g [m s^{-2}] is the gravitational acceleration; F_{sr} [s^{-1}] is the water exchange between roots and the soil and can be

a sink term (roots absorb water) or source term (roots release water). Here “water potential” specifically refers to the pressure component of the total water potential. The pressure component can be either negative or positive.

For unsaturated soil, the soil water content (θ) is linked to the soil water potential (ψ_s) through the equation of van Genuchten [1980]:

$$\theta(\psi_s) = \theta_r + (\theta_s - \theta_r) \cdot \left[1 + (\alpha |\psi_s|)^n \right]^{\frac{1-n}{n}} \quad (2-2)$$

where θ_r [m^3m^{-3}] is the residual soil water content; θ_s [m^3m^{-3}] is the saturated soil water content; parameters α [m^{-1}] and n are experimentally determined for different soil types.

The soil hydraulic conductivity (K_s) is predicted from the soil water potential (ψ_s) by using the Mualem–van Genuchten formula [van Genuchten, 1980]:

$$K_s(\psi_s) = K_{sat} \cdot \left[1 + (\alpha |\psi_s|)^n \right]^{\frac{1-n}{2n}} \cdot \left\{ 1 - (\alpha |\psi_s|)^{n-1} \cdot \left[1 + (\alpha |\psi_s|)^n \right]^{\frac{1-n}{n}} \right\}^2 \quad (2-3)$$

where K_{sat} [$\text{m}^2 \text{s}^{-1} \text{Pa}^{-1}$] is the hydraulic conductivity of saturated soil; parameters α and n are the same as that of Equation (2-2). The reason of using Equations (2-2) and (2-3) instead of the Clapp–Hornberger type of equations for the θ , ψ_s , and K_s relationship is that the former leads to a smoother transition for the soil moisture profile from the unsaturated zone to the saturated zone.

Flux boundary conditions are used for the Richards equation. At the upper boundary, the fluxes are infiltration and evaporation. At the lower boundary zero flux is prescribed since it is assumed that the soil domain is underlain by impervious bedrock.

2.1.2 Water Transport in the Root System

Water flows in xylem vessels of primary roots which stretch to soil layers of different depths. It has been shown that water flow in xylem vessels can be well represented by the Poiseuille law for laminar viscous and incompressible flow in a long cylindrical pipe [Frensch and Steudle, 1989]. Therefore the total flow rate Q_{vessel} [$\text{m}^3 \text{s}^{-1}$] in all vessels which go through the area S [m^2] can be approximated by

$$Q_{vessel} = \sum_{i=1}^n \left[k_{a,i} \cdot \frac{\partial(\psi_{r,i} - \rho_w g z)}{\partial z} \right] \quad (2-4)$$

where n is the number of vessels; $k_{a,i}$ [$\text{m}^4 \text{s}^{-1} \text{Pa}^{-1}$] is the axial hydraulic conductance of vessel i ; $\psi_{r,i}$ [Pa] is the root water potential in vessel i ; the meanings of other symbols are the same as that of Equation (2-1). For flow rate Q_{vessel} upward is positive.

Assuming the same distribution of water potential in all vessels and dividing both sides of Equation (2-4) by the area S , one obtains the expression of vessel flux per unit area (q_{vessel} [m s^{-1}]) as:

$$q_{vessel} = K_{ra} \cdot \frac{\partial(\psi_r - \rho_w g z)}{\partial z} \quad (2-5)$$

where K_{ra} [$\text{m}^2 \text{s}^{-1} \text{Pa}^{-1}$] is the axial hydraulic conductivity of roots per unit area and is equal to $\sum_{i=1}^n k_{a,i} / S$; ψ_r [Pa] is the root water potential.

K_{ra} is estimated based on the distribution of primary roots in the vertical direction and the specific hydraulic conductivity per unit lumen area. The former can be described by an asymptotic equation [Gale and Grigal, 1987; Jackson *et al.*, 1996]. The latter can be measured [e.g., Pate *et al.*, 1995] or be approximately estimated using the Poiseuille law. The method for estimating K_{ra} is described in the Section 2.1.7.

From the mass conservation, one has the change rate of vessel flux along the vertical direction and the local water exchange between roots and the soil satisfy the following relationship:

$$\frac{\partial q_{vessel}}{\partial z} = -F_{sr} \quad (2-6)$$

Substituting Equation (2-5) into Equation (2-6), one has

$$\frac{\partial}{\partial z} \left[K_{ra} \cdot \frac{\partial(\psi_r - \rho_w g z)}{\partial z} \right] + F_{sr} = 0 \quad (2-7)$$

For this equation, the upper boundary condition is the sap flux at the root collar (i.e., the interface between the plant stem and roots). This sap flux can be derived from the plant transpiration which will be discussed below. At the lower boundary zero flux is assumed.

2.1.3 Water Exchange between Roots and the Soil

Water uptake by plant roots is primarily a passive process, i.e., water passively moves from the soil into xylem vessels under water potential gradient [Stedle and Peterson, 1998]. The uptake flux can be considered to be proportional to the difference between the soil water potential and the root water potential [Fiscus, 1975; Herkelrath *et al.*, 1977; Landsberg and Fowkes, 1978]. In

this study the water exchange between roots and the soil is represented by the following equation similar to that of Landsberg and Fowkes :

$$F_{sr} = K_{rr} S_r (\psi_s - \psi_r) \quad (2-8)$$

where K_{rr} [$\text{m s}^{-1} \text{Pa}^{-1}$] is the root radial hydraulic conductivity per unit of root surface area; S_r [$\text{m}^2 \text{m}^{-3}$] is the surface area of roots which absorb or release water per unit volume of soil; ψ_s [Pa] is the soil water potential; ψ_r [Pa] is the root water potential.

It is worth mentioning that the root axial hydraulic conductivity (K_{ra}) is the flux density per unit of potential gradient and the root radial hydraulic conductivity (K_{rr}) is the flux density per unit of potential difference. The units of these two parameters are different.

The water exchange (F_{sr}) could be positive (roots absorb water) or negative (roots release water) depending on the potential difference between the soil water potential and the root water potential. Representations similar to Equation (2-8) for the water exchange were also employed by previous studies [e.g., Mendel *et al.*, 2002; Amenu and Kumar, 2008]. Effect of osmotic potential on the water exchange is not taken into account since HR is primarily a hydraulic process, which is also supported by Mendel *et al.* [2002] through numerical simulations.

2.1.4 Representation of the Saturated Zone

The Richards equation (i.e., Equation (2-1)) is also employed to describe the water dynamics of the saturated zone [van Dam and Feddes, 2000]. The Richards equation is simultaneously solved for the unsaturated zone and the saturated zone. Solutions of soil water potential for the equation

would indicate whether the soil is saturated or not. When the soil water potential value becomes zero or positive, it means that the soil is saturated. In fact the positive soil water potential is the hydrostatic pressure. The interface between the unsaturated zone and the saturated zone (i.e. the groundwater table) is dynamic, since the unsaturated soil can become saturated and vice versa.

The sink or source term (F_{sr}) of Equation (2-1) appears no matter whether the soil is saturated or not, as long as there are roots in the soil. If the soil becomes saturated, the water exchange between roots and the saturated soil can also be simulated.

2.1.5 Frozen Soil

The primary part of the frozen soil algorithm for the VIC-3L land surface model [*Cherkauer and Lettenmaier, 1999; Jeong, 2009*] is kept in this VIC+ model. A multilayer snow submodel is used in the VIC-3L model [*Jeong, 2009*]. The thermal fluxes in the snowpack and the soil are simultaneously solved and the solution gives the temperature profiles in the snowpack and the soil column along the vertical direction. At different depths of the soil column, if the local soil temperature drops below the freezing point, then partial soil water turns into ice. The fraction of unfrozen water is calculated using the method by Flerchinger and Saxton [1987].

Water movement in the soil and roots is computed after the ice content is updated. When the ice content increases, flow paths in the soil become narrower and unfrozen soil water decreases, which reduce moisture fluxes in the soil and water uptake by roots. When partial liquid soil water changes into ice, soil matric potential and soil hydraulic conductivity are described with a modified version of the van Genuchten equation [*Wang et al., 2010a*]. The soil matric potential of node j is expressed as

$$\psi_j = \frac{1}{\alpha} \left[\left(\frac{\theta_{liq,j} - \theta_r}{\theta_s - \theta_{ice,j} - \theta_r} \right)^{-1/m} - 1 \right]^{1/n} \quad (2 - 9)$$

Where $\theta_{ice,j}$ is soil ice content and $\theta_{liq,j}$ is soil liquid water content; The other parameters and variables are typical ones in the van Genuchten equation.

The soil hydraulic conductivity of node j is expressed as

$$K_j = f_{ice,j} K_{sat,j} \left(\frac{\theta_{liq,j} - \theta_r}{\theta_s - \theta_r} \right)^{1/2} \left[1 - \left(1 - \left(\frac{\theta_{liq,j} - \theta_r}{\theta_s - \theta_r} \right)^{-1/m} \right)^m \right]^2 \quad (2 - 10)$$

Where $f_{ice,j}$ is a reduction factor and is defined as:

$$f_{ice,j} = \exp(-10 \cdot (T_f - T_{soil,j})) \quad (2 - 11)$$

Where T_f is freezing point of water and $T_{soil,j}$ is soil temperature. $f_{ice,j}$ should fall within the range [0.05, 1].

After the calculation of water movement in the soil and roots, the updated soil water and ice contents are used to estimate the thermal properties of soil. The thermal conductivity is estimated with the method of Johansen [1977]. The volumetric heat capacity is calculated using the method of Flerchinger and Saxton [1987]. The updated thermal properties will be used in the thermal flux calculation of the next time step.

2.1.6 Solving the Coupled Equations

The soil water dynamics (Equation (2-1)) and the water transport in roots (Equation (2-7)) are linked via the sink or source term (F_{sr}) given by Equation (2-8). Equations (2-1), (2-7) and (2-8)

are simultaneously solved with a finite difference method in which central difference is used for the space derivative and implicit backward difference is used for the time derivative. The soil domain is divided into n layers by $n+1$ nodes. For each node there are two difference equations: one for the soil water flow and the other for the root water flow.

At the upper boundary, the water balance equation for the top half layer is discretized to get the difference equation of the soil water flow for the top node. This approach is employed for the stability and mass conservation of the computation, especially when the boundary fluxes vary rapidly [Šimůnek *et al.*, 2005]. At the lower boundary the same treatment is applied. The resulted algebraic equations are solved with the Gaussian elimination algorithm. For each time step an iterative process is used to obtain the solution when prescribed convergence criteria are satisfied. For all nodes of the unsaturated zone, the relative change in soil water content between two successive iterations needs to be less than a specified tolerance. For the saturated zone, the soil water potential (hydrostatic pressure) results of two successive iterations need to meet a prescribed convergence criterion.

After a solution is obtained for soil water potential and root water potential, mass balance is checked for both the soil and the root systems. For the soil porous media, the amount of water entering (e.g. infiltration) and exiting (e.g. water uptake by roots) should be balanced by the change of the water storage. For the root system, the summation of water exchange between roots and the soil should be equal to the sap flux at the root collar.

2.1.7 Root Parameters

Root distribution and root hydraulic properties have impact on water exchange between roots and the soil, as well as water transport in roots. Therefore the parameters for describing

distribution and hydraulic properties of roots are important to the simulations of the water dynamics in roots and the soil. The estimation of the vertical distribution and the hydraulic conductivities of roots is described in the following sections.

2.1.7.1 Vertical Distribution of Roots

Root distribution has been investigated by many studies. Gale and Grigal [1987] assembled 19 studies and 123 vertical root distributions, then proposed an asymptotic equation as follows to describe the vertical root distribution (also abbreviated as “root distribution” hereinafter).

$$Y = 1 - \beta^d \quad (2-12)$$

where Y is the root fraction from the ground surface to depth d (in centimeters) and β is the fitted coefficient. This equation was adopted by Jackson et al. [1996, 1997]. Based on previous 250 root studies, they analyzed the root distributions of different terrestrial biomes and obtained the fitted coefficient for each biome [Jackson et al., 1996]. They also applied Equation (2-12) to the vertical distribution of live fine roots and obtained corresponding fitted coefficients [Jackson et al., 1997]. This asymptotic equation and the fitted coefficients from Jackson et al. [1996, 1997] are employed in this study.

In Equation (2-8) we need to know the surface area density (S_r) of roots which absorb or release water. Assuming the water exchange occurs at live fine roots, we need to estimate the surface area density of live fine roots. This density distribution can be derived from the distribution function for surface area of live fine roots and the LFRAI (Live Fine Root Area Index, i.e. the total surface area of live fine roots per unit ground area). Equation (2-12) can be used as the distribution function for the surface area of live fine roots assuming the tissue density and the radius of live fine roots are uniform.

2.1.7.2 Root Hydraulic Conductivities

The root radial hydraulic conductivity (K_{rr}) in Equation (2-8) ranges from 1.0×10^{-14} to $4.6 \times 10^{-13} \text{ m s}^{-1} \text{ Pa}^{-1}$ for different species [Huang and Nobel, 1994]. It is assumed that the root permeability is symmetric and the same K_{rr} value is used to calculate the water release by roots.

From the above Section 2.1.2 we know that the axial hydraulic conductivity of roots per unit area is given by

$$K_{ra} = \sum_{i=1}^n k_{a,i} / S \quad (2-13)$$

This expression can be rewritten in the form

$$K_{ra} = \left(\sum_{i=1}^n k_{a,i} / S_{lumen} \right) \cdot \frac{S_{lumen}}{S_{root}} \cdot \frac{S_{root}}{S} \quad (2-14)$$

where S_{lumen} [m^2] is the transectional area of vessel lumens; S_{root} [m^2] is the transectional area of primary roots which go through the area S . $\left(\sum_{i=1}^n k_{a,i} / S_{lumen} \right)$ is the specific hydraulic conductivity per unit lumen area and denoted as K_{rs} [$\text{m}^2 \text{ s}^{-1} \text{ Pa}^{-1}$].

Specific hydraulic conductivity can be measured or approximately estimated using Poiseuille law. Pate et al. [1995] examined specific hydraulic conductivities of primary roots in variously-aged tree or shrub species of Proteaceae and found that K_{rs} values range from 3.0×10^{-8} to $7.8 \times 10^{-7} \text{ m}^2 \text{ s}^{-1} \text{ Pa}^{-1}$. The ratio S_{lumen} / S_{root} is assumed to be 0.1, which is based on Figure 2 of McElrone et al. [2004]. The procedure for approximately estimating the ratio S_{root} / S is described as follows.

- (1) At first, the vertical distribution of the volume density of coarse roots (i.e. the volume of coarse roots per unit volume of soil) is derived from the distribution function for volume of coarse roots and the total volume of coarse roots per unit ground area. Equation (2-12) is used as the distribution function for volume of coarse roots assuming the tissue density of the coarse roots is uniform.
- (2) The volume density of primary roots is assumed to be half of the volume density of the coarse roots.
- (3) The ratio S_{root}/S is equal to the volume density of primary roots assuming that all primary roots are perpendicular to the horizontal plane.

2.2 MODELING OF PLANT TRANSPIRATION

Plant transpiration plays an important role in the soil-plant-atmosphere continuum. In this study, plant transpiration is estimated by combining the method of Ohm's law analogy, where the plant storage is considered, with the Penman-Monteith method, where the stomatal conductance is linked with the photosynthesis process.

2.2.1 Ohm's Law Analogy

The water movement in plants is described by using Ohm's law analogy and is represented by the capacitance-resistance circuit shown in Figure 2.1, which is similar to that of some previous studies [Landsberg *et al.*, 1976; Katerji *et al.*, 1986; Lhomme *et al.*, 2001].

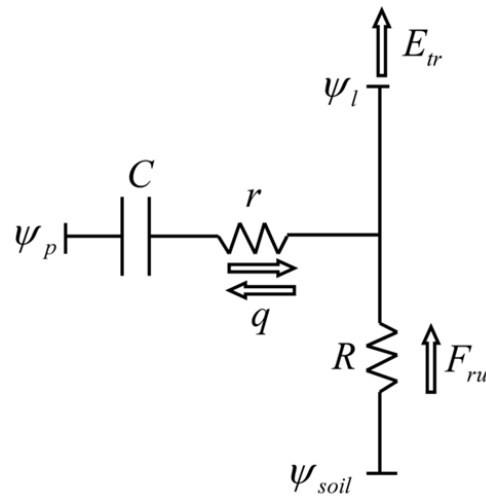


Figure 2.1 Diagram of water movement in plants. E_{tr} : plant transpiration; F_{ru} : sap flux at the root collar; q : plant-storage flux; R : hydraulic resistance from the soil to leaves; r : plant-storage hydraulic resistance; C : plant capacitance; ψ_l : leaf water potential; ψ_p : plant-storage water potential; ψ_{soil} : soil water potential.

The plant transpiration (E_{tr} [m s^{-1}]) is thus assumed to be the sum of the sap flux (F_{ru} [m s^{-1}]) at the root collar and the plant-storage flux (q [m s^{-1}]):

$$E_{tr} = F_{ru} + q \quad (2-15)$$

The sap flux is derived by [van den Honert, 1948]

$$F_{ru} = \frac{\psi_{soil} - \psi_l}{R} \quad (2-16)$$

where ψ_{soil} [Pa] is the lumped soil water potential in the root zone; ψ_l [Pa] is the leaf water potential; R [Pa s m⁻¹] is the hydraulic resistance from the soil to leaves.

The plant-storage flux is calculated from

$$q = \frac{\psi_p - \psi_l}{r} \quad (2-17)$$

where ψ_p [Pa] is the water potential of plant storage; r [Pa s m⁻¹] is the hydraulic resistance between plant storage and leaves.

The plant-storage flux can be also expressed as

$$q = -C \left(\frac{d\psi_p}{dt} \right) \quad (2-18)$$

where C [m Pa⁻¹] is the parameter “plant capacitance”; t is time.

Based on the above equations, the plant transpiration can be estimated if the leaf water potential (ψ_l) of the current time step is known. To this end, Equation (2-15) is combined with the Penman-Monteith method to determine the proper leaf water potential and the plant transpiration.

2.2.2 Penman-Monteith Method Coupled with Photosynthesis

From the Penman-Monteith method the plant transpiration can be calculated by

$$E_{tr} = \frac{\Delta(R_n - G) + \rho_a C_p \delta e \bar{g}_a}{\rho_w \lambda_w \left(\Delta + \gamma_w + \frac{\gamma_w \bar{g}_a}{LAI g_s} \right)} \quad (2-19)$$

where Δ [Pa K⁻¹] is the rate of change of saturation vapor pressure with air temperature; R_n [W m⁻²] is the net radiation; G [W m⁻²] is the ground heat flux; ρ_a [kg m⁻³] is the air density; C_p [J kg⁻¹ K⁻¹] is the specific heat capacity of air; δe [Pa] is the vapor pressure deficit; \bar{g}_a [m s⁻¹] is the conductance of the atmospheric boundary layer (per unit ground area); ρ_w [kg m⁻³] is the water density; λ_w [J kg⁻¹] is the latent heat of water vaporization; γ_w [Pa K⁻¹] is the psychrometric constant; LAI is the leaf area index; and g_s [m s⁻¹] is the stomatal conductance per unit leaf area which is discussed below.

2.2.2.1 Stomatal Conductance

The stomatal conductance is usually estimated with empirical approaches such as the Jarvis-type formulation which relates stomatal conductance with soil wetness, air temperature, incoming solar radiation and air vapor pressure deficit [Jarvis, 1976; Lhomme *et al.*, 1998]. In this study the stomatal conductance is estimated through establishing the link with the parameterization of photosynthesis like others [Ball *et al.*, 1987; Leuning, 1995; Tuzet *et al.*, 2003; Daly *et al.*, 2004; Runkle, 2009]. The stomata regulate vapor flux and CO₂ flux at the same time. Therefore the stomatal conductance for water vapor is related to the stomatal conductance for CO₂. The former

(g_{s,H_2O} [$\text{mol}_{H_2O} \text{ m}^{-2} \text{ s}^{-1}$]) can be assumed to be equal to the latter (g_{s,CO_2} [$\text{mol}_{CO_2} \text{ m}^{-2} \text{ s}^{-1}$]) multiplied by 1.6 [Jones, 1992]. The stomatal conductance (g_{s,H_2O}) is in the unit of [molar] while in the previous Penman-Monteith equation the stomatal conductance (g_s) is in the unit of [m s^{-1}]. The unit conversion can be done using the method of Pearcy et al. [1989].

The CO_2 stomatal conductance (g_{s,CO_2}) is expressed as a function of the net carbon assimilation in the Ball-Berry-Leuning model [Ball et al., 1987; Leuning, 1995]. Tuzet, Perrier and Leuning [2003] proposed a variant of the Ball-Berry-Leuning model. This variant accounts for the effect of leaf water potential on CO_2 stomatal conductance and is more appropriate for plants that could be under water stress conditions. The variant is written as

$$g_{s,CO_2} = g_0 + \frac{aA_n}{c_i - \Gamma} \cdot f(\psi_l) \quad (2-20)$$

where g_0 [$\text{mol m}^{-2} \text{ s}^{-1}$] is the residual conductance; a is an empirical coefficient; A_n [$\text{mol m}^{-2} \text{ s}^{-1}$] is the net carbon assimilation per unit leaf area (also referred to as “carbon assimilation rate” or “assimilation rate” hereinafter); c_i [mol mol^{-1}] is the CO_2 concentration in leaf pores; Γ [mol mol^{-1}] is the CO_2 compensation point; $f(\psi_l)$ is an empirical function which is given by

$$f(\psi_l) = \frac{1 + \exp(s_f \psi_f)}{1 + \exp(s_f \psi_f - s_f \psi_l)} \quad (2-21)$$

where ψ_l [Pa] is the leaf water potential; S_f [Pa^{-1}] is a sensitivity parameter; ψ_f [Pa] is a reference potential.

With Equation (2-20) the CO₂ stomatal conductance is derived from the assimilation rate which is estimated using the following algorithms.

2.2.2.2 Carbon Assimilation

Both the diffusion method and the Modified Farquhar model are used to derive the carbon assimilation. The carbon assimilation results from the two methods should be the same in the final adopted solution.

Diffusion Method

Carbon dioxide diffuses from air into leaf pores, the net carbon assimilation per unit leaf area can be written as [Daly et al., 2004]

$$A_n = g_{sba,CO_2} (c_a - c_i) \quad (2-22)$$

where c_a [mol mol⁻¹] is the CO₂ concentration in the ambient air; c_i [mol mol⁻¹] is the CO₂ concentration in leaf pores; the conductance g_{sba,CO_2} [mol m⁻² s⁻¹] is calculated by

$$g_{sba,CO_2} = (g_{s,CO_2}^{-1} + g_{b,CO_2}^{-1} + g_{a,CO_2}^{-1})^{-1} \quad (2-23)$$

where g_{s,CO_2} [mol m⁻² s⁻¹] is the CO₂ stomatal conductance and assumed to be equal to $g_s/1.6$; g_{b,CO_2} [mol m⁻² s⁻¹] is the CO₂ leaf boundary layer conductance and is equal to $g_b/1.37$; g_{a,CO_2} [mol m⁻² s⁻¹] is the atmospheric conductance and is equal to g_a in value.

The assimilation rate can be derived by combining Equations (2-20) and (2-22) once the CO₂ concentration in leaf pores (c_i) is given.

Modified Farquhar Model

Carbon assimilation rate is also estimated by using the modified Farquhar model [Farquhar *et al.*, 1980; Daly *et al.*, 2004] :

$$A_n = A_{\psi_l}(\psi_l) \times A_{\phi, c_i, T_l}(\phi, c_i, T_l) \quad (2-24)$$

where the function $A_{\psi_l}(\psi_l)$, which reflects the reduction of carbon assimilation under water-stress conditions, is defined as

$$A_{\psi_l}(\psi_l) = \begin{cases} 0 & (\psi_l < \psi_{l_{A0}}) \\ \frac{\psi_l - \psi_{l_{A0}}}{\psi_{l_{A1}} - \psi_{l_{A0}}} & (\psi_{l_{A0}} \leq \psi_l \leq \psi_{l_{A1}}) \\ 1 & (\psi_l > \psi_{l_{A1}}) \end{cases} \quad (2-25)$$

where ψ_l [Pa] is the leaf water potential; $\psi_{l_{A1}}$ [Pa] is the leaf water potential value indicating well-watered condition; $\psi_{l_{A0}}$ [Pa] is the leaf water potential value when stomata are completely closed.

$A_{\phi, c_i, T_l}(\phi, c_i, T_l)$ in Equation (2-24) is the assimilation rate under well-watered condition and is given by the minimum of A_q , A_c and A_s . A_q is the assimilation rate limited by RuBP (Ribulose-1,5-bisphosphate) regeneration when photosynthetically active radiation is low; A_c is the assimilation rate restricted by rubisco activity (i.e. restricted by CO₂ concentration in leaf pores (c_i)); and A_s is the assimilation rate constrained only by leaf temperature.

The assimilation rate can be estimated by the modified Farquhar model when the CO₂ concentration in leaf pores (C_i) and the leaf water potential are given.

2.2.3 Calculation Procedure for Plant Transpiration

The calculation procedure for plant transpiration is illustrated in Figure 2.2. At first the leaf water potential of the current time step is assumed and a preliminary value of plant transpiration (E_{tr1}) can be estimated with the method of Ohm's law analogy described in Section 2.2.1. A trial-and-error method is used to search the proper CO₂ concentration in leaf pores (C_i) with which the assimilation rate from the diffusion method is the same as that from using the modified Farquhar model. Then the assimilation rate is substituted into the variant of the Ball-Berry-Leuning model (i.e., Equation (2-20)) to obtain the CO₂ stomatal conductance which is then converted to the stomatal conductance. The stomatal conductance is employed to obtain a second value of plant transpiration (E_{tr2}) using the Penman-Monteith equation. If E_{tr2} is different from E_{tr1} , the leaf water potential is adjusted and the above steps are repeated. The calculation is completed when the difference between E_{tr2} and E_{tr1} is smaller than a prescribed criterion.

2.3 COUPLING WITH THREE-LAYER VARIABLE INFILTRATION CAPACITY

(VIC-3L) MODEL

The approach for representing the water movement in the soil and roots is implemented as a soil-root module. The approach for representing the plant transpiration is implemented as a new

transpiration module. These two modules are incorporated into the Three-Layer Variable Infiltration Capacity (VIC-3L) land surface model. The coupling approach is illustrated in Figure 2.3. For details of the VIC-3L model and its previous versions the reader is referred to Liang et

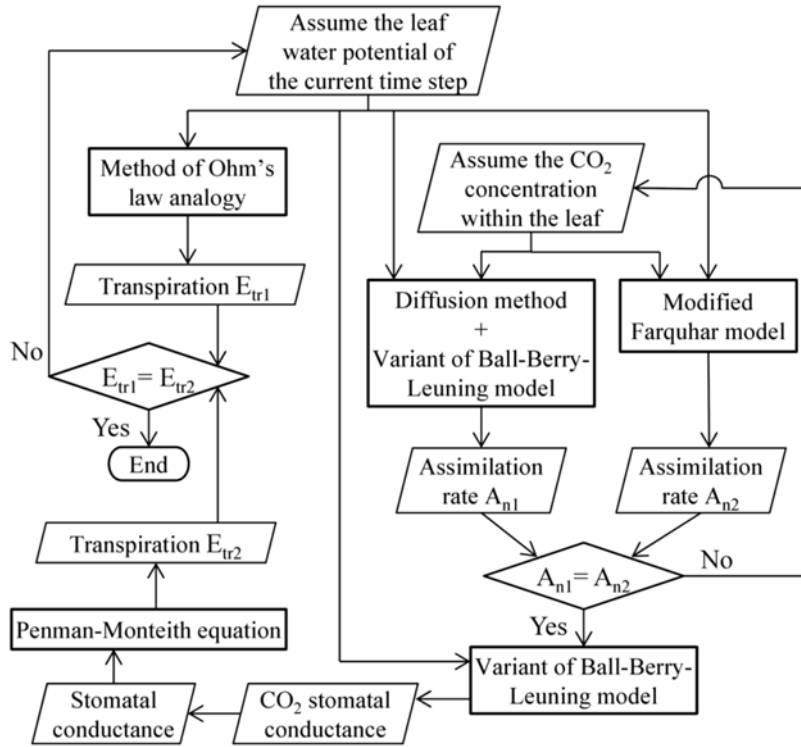


Figure 2.2 A flow chart illustrating the main procedures for calculating the plant transpiration. Rectangles indicate calculation processes. Parallelograms represent variables.

al. [1994, 1996a, 1996b, 1999, 2003], Cherkauer and Lettenmaier [1999], Liang and Xie [2001], and Huang and Liang [2006].

2.3.1 Incorporation of the Soil-Root Module

The land-surface water balance calculation in the VIC-3L model provides the water flux at the ground surface. The water flux can be infiltration or soil evaporation and is used as the upper

boundary condition for the Richards equation in the soil-root module. The new transpiration module provides the sap flux at the root collar which is the upper boundary condition for the water transport in roots. Driven by these boundary conditions, the soil-root module can update

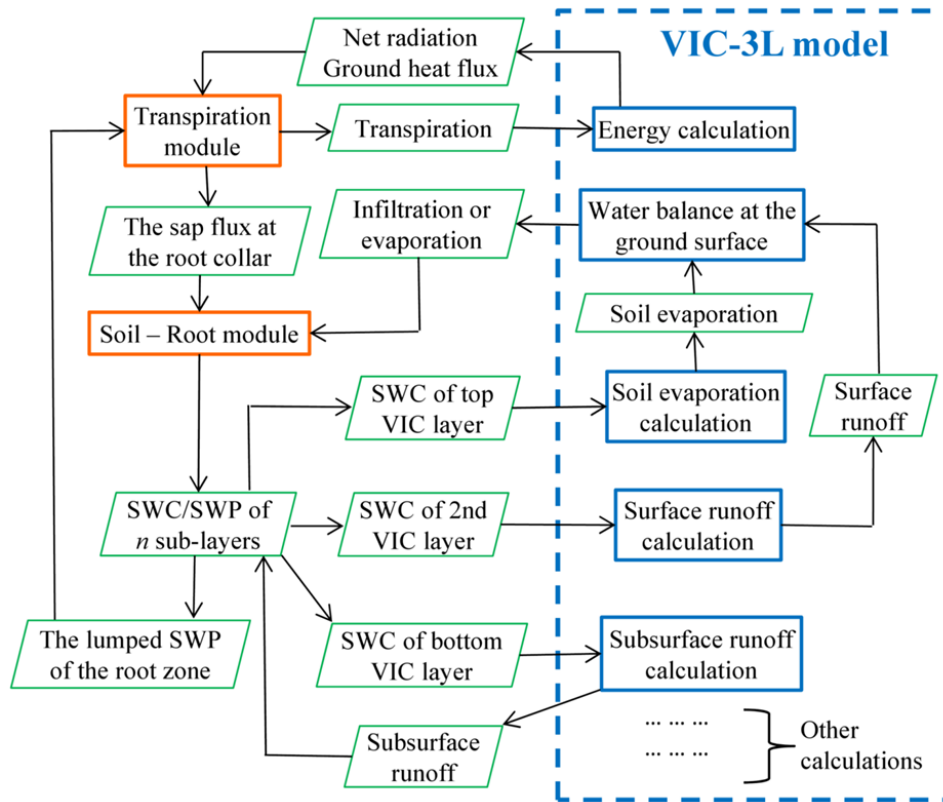


Figure 2.3 Schematic diagram for coupling of the new transpiration module, the soil-root module and the VIC-3L model.

the distribution of soil moisture content (or soil water potential) in the soil domain. As described in Section 2.1, the soil domain is divided into n layers when the finite difference method is applied to solve the coupled differential equations for the water movement in the soil and the root system. The n layers are referred to as sub-layers hereinafter in order to distinguish them

from the three layers in the VIC-3L model, which are abbreviated to “VIC layer” hereinafter. The sub-layers are finer than the VIC layers. Therefore each of the three VIC layers comprises a number of the sub-layers.

Soil moisture values of sub-layers are averaged to give soil moisture values of the three VIC layers respectively. For example, the soil moisture value of the top VIC layer is obtained by averaging all the soil moisture values of the sub-layers within this VIC layer. The soil moisture values of the top and the second VIC layers will be used to calculate soil evaporation and surface runoff respectively in the next time step. The soil moisture value of the bottom VIC layer is used by the ARNO algorithm [*Franchini and Pacciani, 1991*] to calculate the subsurface runoff, which is subsequently deducted from the sub-layers within the bottom VIC layer.

After the soil moisture adjustment, the soil water potential values of the sub-layers within the root zone are used to calculate the weighted average soil water potential of the root zone. For each sub-layer, the weighting coefficient is the ratio of the live fine roots in the current sub-layer to the total live fine roots in terms of biomass. The weighted average soil water potential is used by the new transpiration module to calculate the transpiration for the next time step.

It is worth mentioning that in this extended model, the dynamic movement of the ground water table (GWT) is calculated based on the mixed form of the Richards Equation when the soil water potential becomes zero using the finite difference method described in the previous section. In other words, the calculation of the GWT is not based on the moving boundary approach which uses the finite element method and is coupled with the VIC-3L model [*Liang et al., 2003*]. The two main reasons are: (1) to use a consistent numerical method (i.e., finite difference method) to deal with the unsaturated and saturated zones rather than using the finite difference method for the unsaturated zone and the finite element method for the saturated zone;

and (2) to have the entire extended model in C language rather than C and Fortran combined since the moving boundary approach associated with the finite element method is written in Fortran language.

2.3.2 Incorporation of the New Transpiration Module

The net radiation and the ground heat flux from the VIC-3L model and the above weighted average soil water potential of the root zone are provided to the new transpiration module which subsequently gives the water flux results, including the sap flux at the root collar and the plant transpiration. The sap flux is supplied to the soil-root module. The plant transpiration is used in the calculation of energy balance of the VIC-3L model.

3.0 MODEL VALIDATION

3.1 VALIDATION OF SOIL-ROOT MODULE UNDER A SIMPLIFIED CONDITION

A simple numerical experiment is used to evaluate the VIC+ model simulation results related to water movement in roots and the soil, where interactions between the unsaturated and saturated zones are considered. First we analytically derived a hydrostatic equilibrium soil moisture distribution along the vertical direction in the soil domain. Using this distribution as the initial condition of the soil domain and assuming that there is no water flux at all boundaries of the soil domain and the root system, we run the new coupled model for a period of time and check whether the initial soil moisture profile is maintained.

If there is no water flux at all boundaries of the study soil domain and the corresponding root system, namely there is no infiltration, soil evaporation, subsurface flow and plant transpiration, then soil water should be at the hydrostatic equilibrium state and the total water potential (i.e., matric potential plus gravitational potential) should be a constant within the soil domain. Based on this principle, the new coupled model can be evaluated under a given ideal condition. In this test, we use the van Genuchten formulation to represent the relationship between soil moisture and soil matric potential, and derive the ideal steady-state soil moisture distribution within the soil domain to compare with the numerical results from the VIC+ model.

In this simple numerical experiment, the soil domain is composed of loam and has a depth of 3.44 m. The groundwater table depth is set to be 2 m. The vertical coordinate originates from the ground surface with upward being positive. Therefore the constant total water potential of the hydrostatic equilibrium state is -2 m. The derived steady-state soil moisture distribution is shown in Figure 3.1.

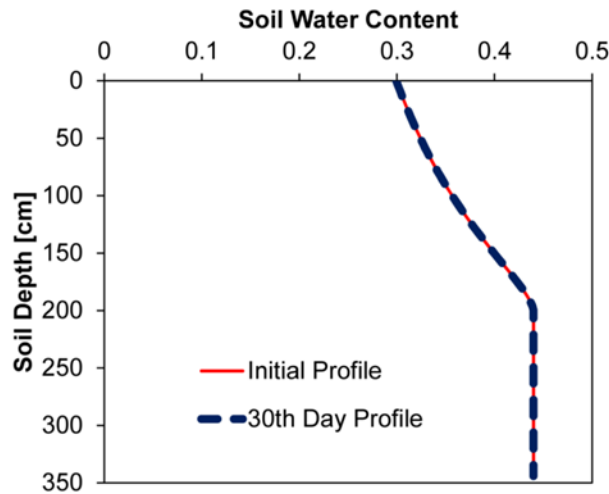


Figure 3.1 Comparison of the initial (i.e., derived theoretical) and final soil moisture profiles in the simple numerical experiment.

In the numerical simulation, the soil domain is evenly discretized into 100 layers of which each is 3.44 cm thick. The time step is hourly. The theoretical steady-state soil moisture distribution derived is used as the initial condition of the soil domain and all the boundary conditions are set to be zero-flux for the soil domain and the root system. The model was run for 30 days and the initial soil moisture profile was found to be always maintained. This result verifies that the VIC+ model is reliable in terms of its numerical modeling of the soil water dynamics. This model does not have the numerical deficiencies of the Community Land Model, version 3 (i.e., CLM3) when it includes the groundwater module of Niu *et al.* [2007] as

indicated by Zeng and Decker [2009]. This result also demonstrates that the simulation for the coupling of soil water dynamics and root water transport is reliable under the simplified condition of this numerical experiment.

3.2 VALIDATION AT DUKE SITE

3.2.1 Site Description and Model Setup

The VIC+ model is tested using the observed data from an AmeriFlux site (Duke Forest Loblolly Pine (US-Dk3)) located within the Blackwood Division of Duke Forest near Durham, North Carolina, USA (35.98° N, 79.09° W). The average elevation is about 163m above sea level. The vegetation is dominated by *Pinus taeda* L. (loblolly pine) trees, which were uniformly planted in 1983, with a mean canopy height of about 19 m in 2006. The understory is composed of different hardwood species. The soil types are loam and clay. The climate is characterized by mean annual precipitation of 1145 mm and mean air temperature of 15.5 °C. This site is chosen because there are usually dry periods during a year. The biological and hydrological processes included in the VIC+ model are expected to play important roles in the water, energy and carbon cycles under dry conditions. Also, the observed soil moisture data there shows a nighttime increase in soil moisture which seems to indicate the existence of hydraulic redistribution. In addition, previous studies have observed the HR phenomenon for the same vegetation (i.e., loblolly pine) in that area [e.g., Domec *et al.*, 2010].

The soil information is from the Web Soil Survey (WSS) database, which is operated by Natural Resources Conservation Service (NRCS) of United States Department of Agriculture

(USDA). At this site the typical soil profile is composed of sandy clay loam (from the ground surface to 30 cm depth), clay (from 30 cm to 80 cm depth) and loam (below 80 cm depth). The WSS data indicate that the soil depth is greater than 80 inches (203 cm), but the maximum soil depth is unknown. For each soil class, class-average values of soil parameters, including saturated hydraulic conductivity, porosity, residual soil water content and van Genuchten parameters, are obtained from the database of the ROSETTA model developed by the Agricultural Research Service of USDA. The leaf area index (LAI) data is from a study performed at the Duke Free Air CO₂ Enrichment (FACE) experiment [McCarthy *et al.*, 2007]. The Duke FACE facilities are located in the same forest as the AmeriFlux tower.

The plant capacitance is estimated based on data from the literature. Wronski *et al.* [1985] found that the capacitance of 20 ~ 25 m tall *Pinus radiata* trees ranges from 1.5 to 2.1 kg MPa⁻¹. The vegetation type and height are close to that of the US-Dk3 site. Therefore this capacitance value for a single tree is converted to the capacitance in Equation (2 - 18) by using the equation

$$C = \frac{C_{tree} \cdot n_{tree}}{\rho_w} \quad (3-1)$$

where C [m Pa⁻¹] is the capacitance per unit area; C_{tree} [kg Pa⁻¹] is the capacitance per tree; n_{tree} [m⁻²] is the number of trees per unit area; ρ_w [kg m⁻³] is the water density. The value of n_{tree} is about 0.17 m⁻² since loblolly pines were uniformly planted at 2.4 m by 2.4 m spacing. With Equation (3-1) the capacitance is estimated to be in the range $(2.6 \sim 3.6) \times 10^{-10}$ m Pa⁻¹. The smallest value (2.6×10^{-10} m Pa⁻¹) is used in the model simulations since in 2004 the average canopy height was 18 m, which is slightly smaller than the lowest value of tree height in the study by Wronski *et al.* [1985]. This estimation method does not take into account the understory (hardwood species) because the relevant information is not available. The resulting

error is assumed to be small considering that the understory only accounts for a minor part of the forest (the understory accounts for 10% of the basal area).

The climatic input data for the VIC+ model includes precipitation, air temperature, wind speed, atmospheric pressure, vapor pressure, short wave radiation, downward long wave radiation and CO₂ concentration in the atmosphere. The data of years 2004 and 2005 from the website of the AmeriFlux network is used. For years 2004 and 2005, the annual precipitation values are 983 mm and 935 mm, and the mean air temperature values are 14.8 °C and 14.7 °C, respectively.

The dominant vegetation, loblolly pine, is known to have a deep taproot. In the model simulations the maximum root depth is set as 5 m. The soil depth is set to be larger than 5 m so that the groundwater table in the soil can either rise into the root zone or drop below the root zone. In the trial model simulations using the forcing data of years 2004 and 2005, the modeled groundwater table depths are always smaller than 6.5 m. Therefore the soil depth of 7 m is adopted. The seven-meter thick soil domain is evenly discretized into 350 sublayers, i.e., each sublayer's thickness is 2 cm, in the finite difference method of the model simulation. One advantage of having this uniform discretization configuration is that the ground water table can move upward or downward smoothly. The time step is hourly.

The 30 cm top soil layer is underlain by a less pervious clay layer. In addition, the slope of this area is from 2% to 6%. These features make lateral flow in the top soil layer possible [Schäfer *et al.*, 2002]. In order to represent such specific characteristic of this site, an additional subsurface runoff calculation with the ARNO algorithm is implemented in the top layer.

Values of some model parameters for this study are listed in Table 3.1.

Table 3.1 Values of model parameters for this study

Parameter	Symbol	Units	Duke site	Blodgett site
Empirical coefficient in Eq. 2-20	a	–	2 ^a	2
Soil moisture capacity shape parameter	b	–	0.5	0.4
Capacity of plant water storage (Eq.2-18)	C	m MPa ⁻¹	2.6×10^{-4b}	1.8×10^{-4c}
Maximum subsurface runoff of one day in ARNO algorithm	D_m	mm day ⁻¹	0.5	0.3
Maximum root depth	D_{root}	m	5	8
Maximum soil depth	D_{soil}	m	7	12
Axial hydraulic conductivity of roots per unit area (Eqs. 2-5 and 2-7)	K_{ra}	m ² s ⁻¹ MPa ⁻¹	$8.9 \times 10^{-6} \sim 3.8 \times 10^{-4d}$	$8.9 \times 10^{-6} \sim 3.8 \times 10^{-4}$
Radial hydraulic conductivity of roots per unit of root surface area (Eq. 2-8)	K_{rr}	m s ⁻¹ MPa ⁻¹	$1.4 \times 10^{-7e, f}$	1.4×10^{-7}
Sensitivity parameter (Eq. 2-21)	S_f	MPa ⁻¹	3.2 ^a	3.2
Reference leaf water potential (Eq. 2-21)	Ψ_f	MPa	-1.9 ^a	-1.9
Leaf water potential below which assimilation is reduced to zero (Eq. 2-25)	$\Psi_{l_{A0}}$	MPa	-4.5 ^g	-4.5
Leaf water potential indicating well-watered condition (Eq. 2-25)	$\Psi_{l_{A1}}$	MPa	-0.5 ^g	-0.5

^a Tuzet *et al.* [2003]^b Wronski *et al.* [1985]^c Hunt *et al.* [1991]^d K_{ra} varies along the vertical direction in the root zone.^e Sands *et al.* [1982]^f Huang and Nobel [1994]^g Daly *et al.* [2004]

In the model simulations a few parameters, which cannot be adequately estimated based on the available information, are adjusted to obtain a better match between the modeled results and the observations. The goodness of fit is judged using the root mean square error. These parameters include the soil moisture capacity shape parameter associated with the VIC-3L model, the parameter in the ARNO parameterization and the hydraulic resistance from the soil to leaves. The soil moisture capacity shape parameter (referred to as b-parameter hereinafter) is an indicator of the spatial variation of the storage capacity of soil moisture in the upper layer of the soil column [e.g., *Liang and Xie*, 2001]. Reducing the b-parameter value can decrease the surface runoff and increase the infiltration and soil moisture. The b-parameter values adopted in this study fall within the typical range of (0, 5) indicated in the literature [e.g., *Huang et al.*, 2003]. The maximum subsurface runoff (D_m) in the ARNO algorithm controls the magnitude of subsurface runoff. Increasing the D_m value can lower the groundwater table and decrease soil moisture. The D_m values used in this study are consistent with the typical range (from 0 to 40 mm/day) indicated in the literature [*Huang and Liang*, 2006]. The reference resistance (R_0) is close to the total resistance from the soil to leaves when the root zone is moist. The increase of the reference resistance can reduce plant transpiration. The reference resistance values adopted in this study are comparable to the values in the literature [*Hunt et al.*, 1991; *Lhomme et al.*, 2001].

There exist uncertainties in the K_{ra} values. However, the sensitivity analysis shows that the simulated results are not sensitive to the K_{ra} values. For example we contrast two cases. In Case 1 K_{ra} values are estimated to be over a range from 1.4×10^{-9} to $3.9 \times 10^{-11} \text{ m}^2 \text{ s}^{-1} \text{ Pa}^{-1}$ along the vertical direction of the root zone when the specific hydraulic conductivity (K_{rs}) is taken as the largest value ($7.8 \times 10^{-7} \text{ m}^2 \text{ s}^{-1} \text{ Pa}^{-1}$) obtained by Pate et al. [1995]. In Case 2 K_{ra}

values range from 5.4×10^{-11} to $1.3 \times 10^{-12} \text{ m}^2 \text{ s}^{-1} \text{ Pa}^{-1}$ as K_{rs} is taken as the smallest value ($3.0 \times 10^{-8} \text{ m}^2 \text{ s}^{-1} \text{ Pa}^{-1}$) obtained by Pate et al. [1995]. Simulated results of Case 2 are only slightly different from that of Case 1. For example the annual amount of hydraulically redistributed water in the top one-meter layer decreases by less than 6%. In the simulations K_{rs} is assigned a moderate value ($2.0 \times 10^{-7} \text{ m}^2 \text{ s}^{-1} \text{ Pa}^{-1}$) within the range obtained by Pate et al. [1995] and the K_{ra} values range from 3.8×10^{-10} to $8.9 \times 10^{-12} \text{ m}^2 \text{ s}^{-1} \text{ Pa}^{-1}$ along the vertical direction in the root zone.

The modeled results are compared to the observations as follows.

3.2.2 Comparison to Observations

The modeled soil water content (SWC) values are compared with the observed data at the Duke site for the years 2004 and 2005 (Figure 3.2). Both the modeled results and the observed data are average values of the surface soil layer from 0 to 30 cm depth (abbreviated as “surface layer” hereinafter in this section). The model captures the daily variations of soil moisture fairly well (Figure 3.2a and Figure 3.2c). The coefficients of determination (R^2) between modeled and observed soil moisture for years 2004 and 2005 are 0.86 and 0.94, respectively. The root mean square errors (RMSEs) for years 2004 and 2005 are 0.029 and 0.026, respectively. For some time periods (e.g., Day 210 – 230 of year 2004 and Day 110 – 135 of year 2005), the differences between the modeled results and the observations are evident. One possible reason may be the spatial heterogeneity of soil moisture at this site. The modeled results represent the spatially averaged soil moisture of the site. The observed data are average soil moisture values of four different locations at the site and may not represent the real average condition of the site since

the actual soil moisture varies at different locations of this site due to heterogeneity of some factors such as precipitation and soil characteristics. For example, Figure 3.2 shows the range of soil moisture values obtained at the four locations of the site. The range of SWC can be as large as 0.1.

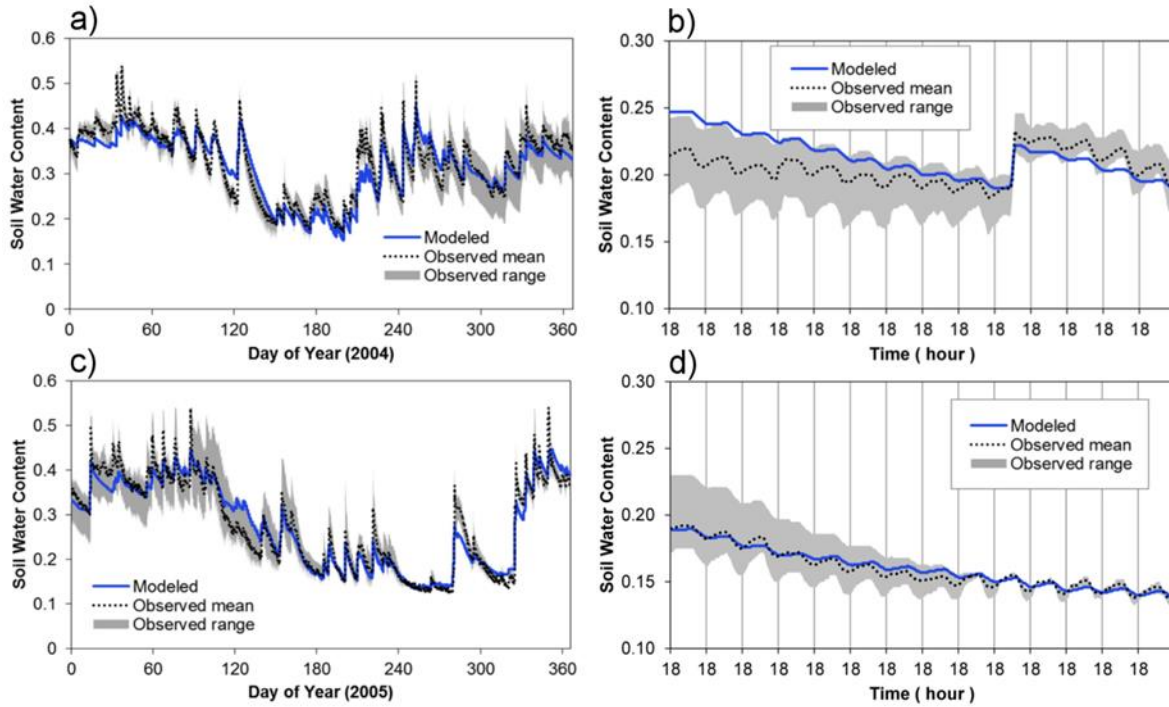


Figure 3.2 Comparison between the modeled soil water content (SWC) and the observed data at the Duke site for years 2004 and 2005. The SWC values are average values of the surface soil layer (0 – 30 cm depth). “Observed mean” shows the mean values of one group of data from four measurement points. “Observed range” shows the variation range of the group of data. a) Daily values of year 2004; b) Hourly values from 18:00, 20 May to 18:00, 3 June in year 2004; c) Daily values of year 2005; d) Hourly values from 18:00, 23 August to 18:00, 6 September in year 2005.

Figure 3.2b and Figure 3.2d show hourly SWC values of 14 days in years 2004 and 2005, respectively. On the two subfigures, we can see nighttime increases in the observed soil moisture

values of the surface layer. This phenomenon could be due to combined reasons such as HR, diffusion of soil water, and impacts of the soil temperature on the soil moisture instrument. Note that “Soil moisture” specifically refers to soil moisture of the surface layer hereinafter in this section. At this site the nighttime increases in the observed soil moisture data are relatively large. For example, in Figure 3.2b the increases are usually as large as 0.01, which means that a 3 mm depth of water is imported into the 30 cm depth of surface layer. Such a large nighttime soil moisture increase is probably mainly contributed by HR since the increase due to diffusion [e.g., Warren *et al.*, 2007] and instrument is small.

As shown in the literature, the water fluxes of the upward liquid or vapor diffusion process are usually much smaller than those caused by HR [e.g., Warren *et al.*, 2007]. This is also partially supported by the model simulations of this study. For the surface soil layer, nighttime inward water fluxes through direct upward soil water diffusion (W_{DIFF}) and through the HR process (W_{HR}) are respectively calculated each day. The ratio (W_{DIFF}/W_{HR}) ranges from close to zero to about 16% for the time periods when upward soil water diffusion exists. For example, Table 3.2 shows the inward and outward water fluxes of the surface layer in ten nights within the time period of Figure 3.2d (i.e., from August 23 to September 2 in year 2005). For all ten nights roots released water into the surface layer. At the same time, water flowed into the surface layer via direct upward soil water diffusion except one night when soil water diffusion was downward. However, the amount of upward soil water diffusion (W_{DIFF}) is much lower than that of hydraulically redistributed water (W_{HR}). In the nine nights the maximum and average values of the ratio W_{DIFF}/W_{HR} are 16.3% and 8.1% respectively.

The fluctuations in the observed soil moisture values due to the impacts of soil temperature on the instrument device are also examined in this study. At this site the soil

Table 3.2 Water balance of the surface layer in ten nights.

Start Time	End Time	Hydraulically Redistributed Water [mm]	Infiltration [mm]	Soil Water Diffusion [mm]	Subsurface Flow [mm]	Storage Change [mm]	Diff. / HRW [%]
8p.m. 8/23	7a.m. 8/24	0.2218	0	-0.0485	-0.0339	0.1394	-21.9
8p.m. 8/24	7a.m. 8/25	0.2831	0	0.0248	-0.0324	0.2755	8.7
8p.m. 8/25	7a.m. 8/26	0.3700	0	0.0601	-0.0306	0.3995	16.2
8p.m. 8/26	7a.m. 8/27	0.4946	0	0.0673	-0.0290	0.5329	13.6
8p.m. 8/27	7a.m. 8/28	0.5441	0	0.0431	-0.0284	0.5588	7.9
8p.m. 8/28	7a.m. 8/29	0.6106	0	0.0475	-0.0272	0.6310	7.8
8p.m. 8/29	7a.m. 8/30	0.6776	0	0.0410	-0.0263	0.6923	6.0
8p.m. 8/30	7a.m. 8/31	0.7351	0	0.0297	-0.0257	0.7391	4.0
8p.m. 8/31	7a.m. 9/1	0.7706	0	0.0351	-0.0246	0.7811	4.6
8p.m. 9/1	7a.m. 9/2	0.8534	0	0.0305	-0.0238	0.8601	3.6

Note: 1. Positive means flowing into the surface layer for flux results;

2. The last column is the ratio of soil water diffusion to hydraulically redistributed water.

moisture data were obtained with time domain reflectometry (TDR, CSI CS615 model). The SWC readings obtained by TDR may be affected by soil temperature as shown by some previous studies [Pepin *et al.*, 1995; Wraith *et al.*, 1995; Or and Wraith, 1999; Wraith and Or, 1999]. Experimental results indicate that either positive or negative correlation between soil temperature and TDR-measured SWC is possible, depending on soil texture and wetness. Wraith and Or [1999] put forward a hypothesis that the TDR-measured bulk apparent dielectric permittivity (ϵ_b), which is used to infer SWC, is “determined by an interplay between two competing phenomena: (1) the reduction in the dielectric permittivity of bulk water with increased temperature; and (2) the increase in TDR-measured ϵ_b with increased temperature due to release of bound water.” Different correlations between the soil temperature and TDR-measured ϵ_b for a wide range of soils and water contents can be explained by Wraith and Or’s hypothesis.

Based on the sensitivities of the TDR-measured SWC to the variation of soil temperature from previous studies and the variation range of soil temperature during nighttime at this site, it is deduced that the maximum possible increase in SWC readings caused by soil temperature is much smaller than the increase in the observed soil moisture data.

For loamy sand, the sensitivity $\Delta\theta/\Delta T$ is about $0.0004 \text{ m}^3\text{m}^{-3}\text{C}^{-1}$ when gravimetric water content is $0.135 \text{ kg}\cdot\text{kg}^{-1}$; for silt loam, the sensitivity $\Delta\theta/\Delta T$ is about $0.001 \text{ m}^3\text{m}^{-3}\text{C}^{-1}$ when gravimetric water content is $0.14 \text{ kg}\cdot\text{kg}^{-1}$ [Or and Wraith, 1999]. When SWC values measured with CS615 TDR are below 0.2, the sensitivity $\Delta\theta/\Delta T$ is smaller than $0.002 \text{ m}^3\text{m}^{-3}\text{C}^{-1}$ for both coarse-textured soils and fine-textured soils [Campbell, 2006].

At this heavily vegetated site located in a mixed forest, diurnal fluctuations of soil temperature are expected to be moderate. Soil temperature is measured with thermistor (Siemens Type M841/S1) at 10 cm depth. The nighttime soil temperature variation at 10 cm depth is smaller than $0.3 \text{ }^\circ\text{C}$ from August 24 to September 2, 2005 (the time period included in Figure 3.3). Adopting the upper bound value, it is assumed that the nighttime decrease of average soil temperature from 10 cm to 30 cm depth is $0.3 \text{ }^\circ\text{C}$. Based on the simulation results of the model, the average soil temperature from ground surface to 10 cm depth will have a mean nighttime decrease of $2.9 \text{ }^\circ\text{C}$ from August 24 to September 2.

If the sensitivity $\Delta\theta/\Delta T$ is set as $0.002 \text{ m}^3\text{m}^{-3}\text{C}^{-1}$, the maximum value obtained by Campbell [2006], the nighttime increases in SWC values caused by the variations of soil temperature could be $0.0058 \text{ m}^3\text{m}^{-3}$ and $0.0006 \text{ m}^3\text{m}^{-3}$ for the top soil layer (0-10 cm depth) and the underlying soil layer (10-30 cm depth), respectively. Then the average nighttime SWC increase weighted by the thickness of the two layers would be $0.0023 \text{ m}^3\text{m}^{-3}$. In Figure 3.2, the mean nighttime increase in SWC data (the average value of the top 30 cm layer) from August 24

to September 2 is about $0.0068 \text{ m}^3\text{m}^{-3}$. The maximum possible nighttime increase in SWC caused by variation of soil temperature could only account for 34% of the total increase in the observed SWC data during nighttime. Therefore it is concluded that the variations of soil temperature are not the major reason for the nighttime increases in the TDR-measured SWC data.

Based on the above analyses, we conclude that nighttime increases in the observed soil moisture data are primarily caused by HR. That is, at nighttime soil water is redistributed from the deep soil to the surface layer through roots, when the surface layer is much drier than the deep soil. This is a typical HR process which is evident in the observed data at this site. This phenomenon is captured by the VIC+ model simulation as there exists a nighttime increase in the modeled soil moisture as shown in Figure 3.2b and Figure 3.2d. This result validates, to some extent, the effectiveness of the HR scheme used in the VIC+ model.

The simulated energy results are compared with the observed data at the daily time scale for year 2005 (Figure 3.3). The simulated net radiation results are well consistent with the measured values (Figure 3.3a). The simulated latent heat flux results are close to the observed values for most of the time period (Figure 3.3b). The model overestimates the sensible heat flux during the growing season (Figure 3.3c). The simulated results of ground heat flux are not compared with the measured values since the latter are not available (Figure 3.3d). The modeled ground temperature values at the depth of 10 cm are close to the observed values in the warm season and tend to be lower than the observations during the cold season (Figure 3.3e).

The modeled latent heat flux results are compared to the observed data at the daily scale for year 2004 (Figure 3.4a). The model can reproduce the latent heat flux fairly well. The R^2 and RMSE between modeled and observed latent heat flux are 0.88 and 18.0 W/m^2 , respectively.

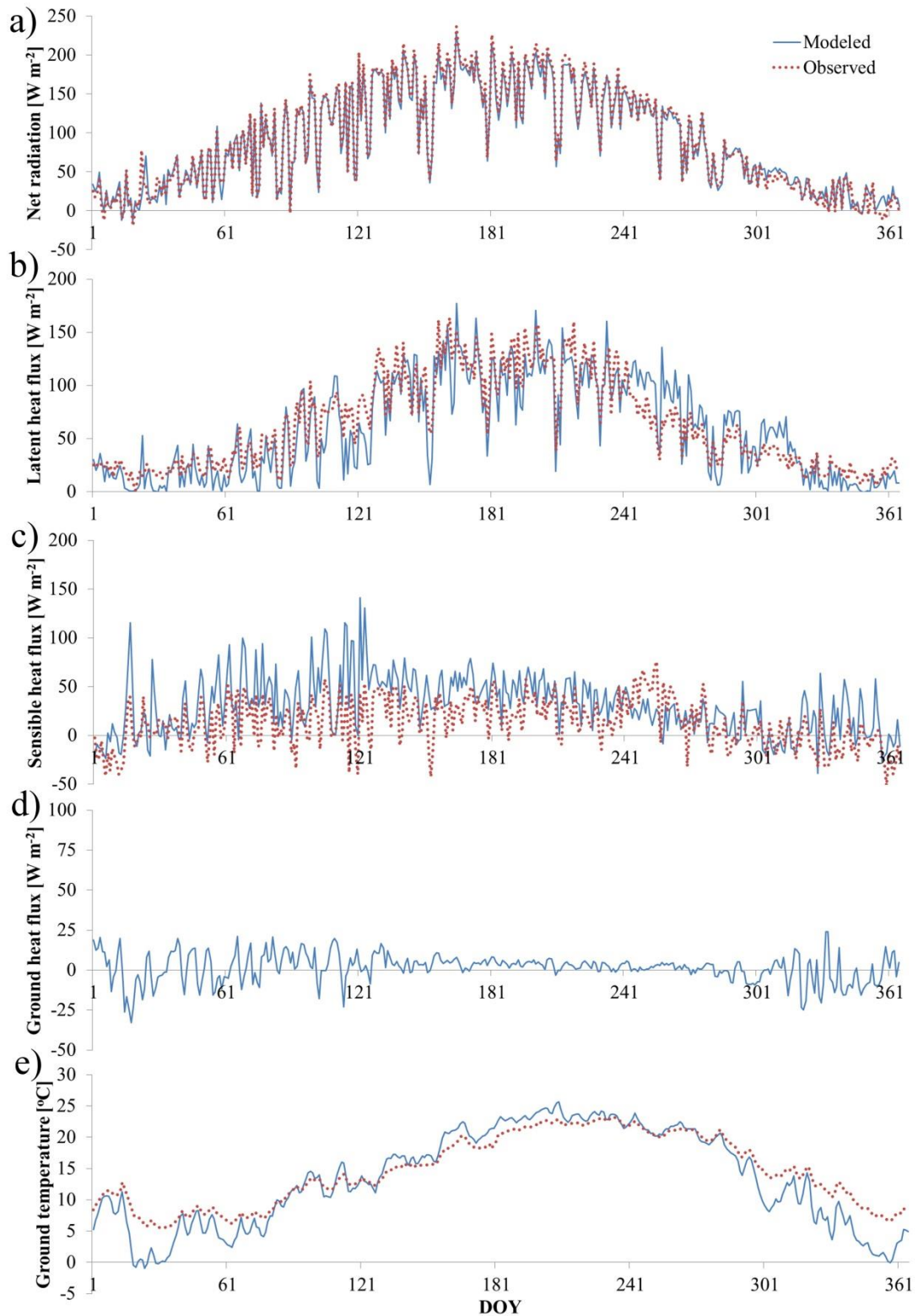


Figure 3.3 Comparison of modeled energy results with the observed data at daily time scale for the year 2005. (a) Net radiation; (b) Latent heat flux; (c) Sensible heat flux; (d) Ground heat flux; (e) Ground temperature. The observed ground heat flux is not available and not included here.

The modeled daily gross primary productivity (GPP) results are compared with the observations for year 2004 (Figure 3.4b). The daily variations of GPP are captured by the model reasonably well. The R^2 and RMSE between modeled and observed GPP are 0.73 and 2.38 $\mu\text{mol}\cdot\text{m}^{-2}\cdot\text{s}^{-1}$, respectively.

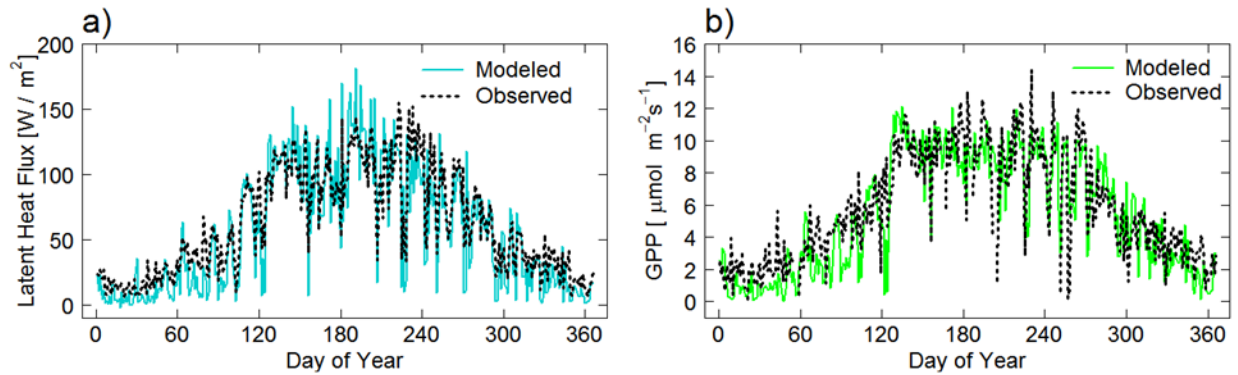


Figure 3.4 Comparison of modeled results with the observations at Duke site for the year 2004. a) Latent heat flux; b) Gross primary productivity (GPP).

3.3 VALIDATION AT BLODGETT SITE

3.3.1 Site Description and Model Setup

The VIC+ model is also applied at another AmeriFlux site (Blodgett Forest (US-Blo)) located in the Sierra Nevada range near Georgetown, California, USA (38.90° N, 120.63° W). The average elevation is about 1315m above sea level. The site is in a mixed-evergreen coniferous forest dominated by even aged ponderosa pine. Other trees and shrubs make up less than 30% of the

biomass. The soil characteristics are relatively uniform and the primary soil type is loam. The average annual precipitation is 1226 mm and the average air temperature is 11.1 °C. The Mediterranean-type climate is characterized by wet winter and a long dry summer. Precipitation mainly occurs from October through May and there are very few rainfall events from June to September. During the dry summer, plants are primarily sustained by water stored in the unsaturated and saturated zones. So in the later period of the summer, plants will be under water-limited conditions. In this circumstance the biological and hydrological processes included in the VIC+ model (e.g., HR, groundwater dynamics and plant water storage) will play important roles in the water, energy and carbon cycles. Therefore it is convenient to investigate and demonstrate the impacts of these processes on the water, energy and carbon cycles. In addition, the wet season in winter at this site can facilitate evaluating the impact of frozen soil on downward HR.

This site is situated in a region where vegetation is known to have deep roots. In order to investigate the function of deep roots, in this modeling study the maximum root depth is set as 8 m, which is similar to the root depths adopted by previous studies at this site [e.g., *Quijano et al.*, 2012]. The soil depth is set to be larger than 8 m to allow for fluctuation of the groundwater table in the soil. In the trial model simulations using the forcing data of year 2004, the modeled groundwater table depths are always smaller than 11 m. Therefore the soil depth of 12 m is adopted. The whole soil column is evenly discretized into 600 sublayers, each of which is 2 cm thick, in the numerical simulations. Values of soil parameters are obtained from the database of ROSETTA model developed by USDA. The LAI data is from the MODIS Land Product Subsets developed by the Oak Ridge National Laboratory. The climatic data of year 2004 from the website of the AmeriFlux network are used. The annual precipitation and mean air temperature are 1025 mm and 11.6 °C, respectively. The annual precipitation is lower than the average annual

value by 16.4%. Similar to the application at the Duke site, a few parameters are adjusted in the model simulation. Values of some model parameters for this site are listed in Table 3.1. The modeled results are compared with the observed data in the following section.

3.3.2 Comparison to Observations

The HR process is considered in the simulation of the “HR” scenario. The modeled soil moisture results of the “HR” scenario are compared to the observations at the depth of 10 cm and 30 cm, respectively (Figure 3.5). The R^2 between modeled and observed soil moisture for 10 cm depth and 30 cm depth are 0.94 and 0.96, respectively. The RMSEs for 10 cm depth and 30 cm depth are 0.036 and 0.020, respectively. At a depth of 10 cm, the modeled results are close to the observations during most of the wet season, but are obviously higher than the observations in the dry season (Figure 3.5a). Some previous studies at the Blodgett site found similar results [e.g., Quijano *et al.*, 2012]. One possible reason may be that the model does not properly simulate the

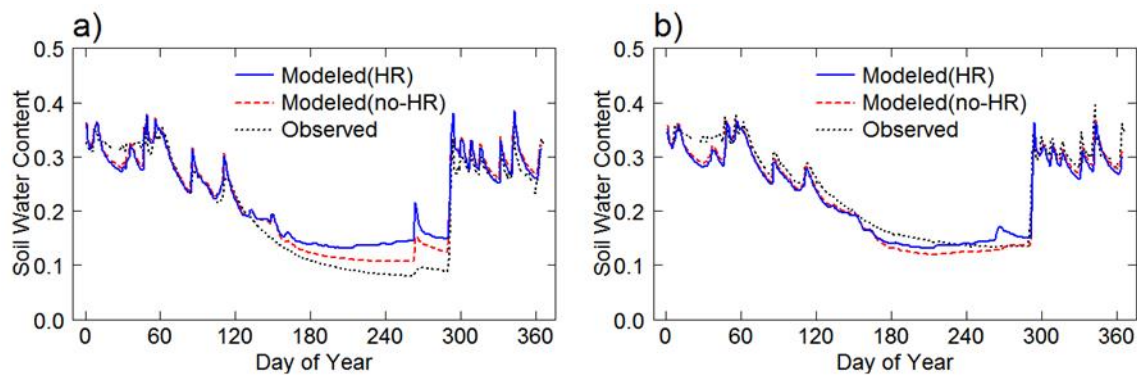


Figure 3.5 Comparison of modeled soil moisture results with the observed data at the Blodgett site for the year 2004. a) At the depth of 10 cm; b) At the depth of 30 cm. Hydraulic redistribution (HR) is considered in the “HR” scenario simulation and not considered in the “no-HR” scenario simulation.

distribution of root uptake in the vertical direction, namely roots absorb less water in the shallow soil and absorb more water in the deep soil, as compared to the actual root uptake. Another reason may be that the modeled amount of soil evaporation at the ground surface is lower than the real amount. At the depth of 30 cm, in the dry season the modeled results are closer to the observations (Figure 3.5b) than at the depth of 10 cm.

Results of the “no-HR” scenario are also shown in Figure 3.5. In the “no-HR” scenario, the HR process is shut down, namely roots cannot release water to the soil. It is demonstrated that during the dry season HR has evident impacts on soil moisture of the shallow soil layer. Soil moisture results of the “HR” scenario are higher than that of the “no-HR” scenario because water in the deep soil is pumped up to the shallow layer through the HR process. On the other hand, during the wet season the soil moisture results of the “HR” scenario are sometimes slightly lower than that of the “no-HR” scenario. This is the consequence of the downward HR process, namely water is transferred from the shallow soil to the deep soil through roots.

The modeled latent heat flux results of the “HR” scenario are compared to the observed data at the daily scale (Figure 3.6a). The R^2 and RMSE between modeled and observed latent heat flux are 0.90 and 12.7 W/m^2 , respectively. In the later period of the dry season (i.e., August and September), the observed latent heat flux drops down dramatically as the result of water limitation. This decline of latent heat flux is also captured by the model. The latent heat flux results of the “no-HR” scenario are also included in Figure 3.6a. It is shown that HR promotes latent heat flux during the dry season and does not have visible impacts on latent heat flux in the wet season. The HR process leads to an increase of the average latent heat flux of three months (July, August and September) by 11.7 W/m^2 (relative increase of 15.9%).

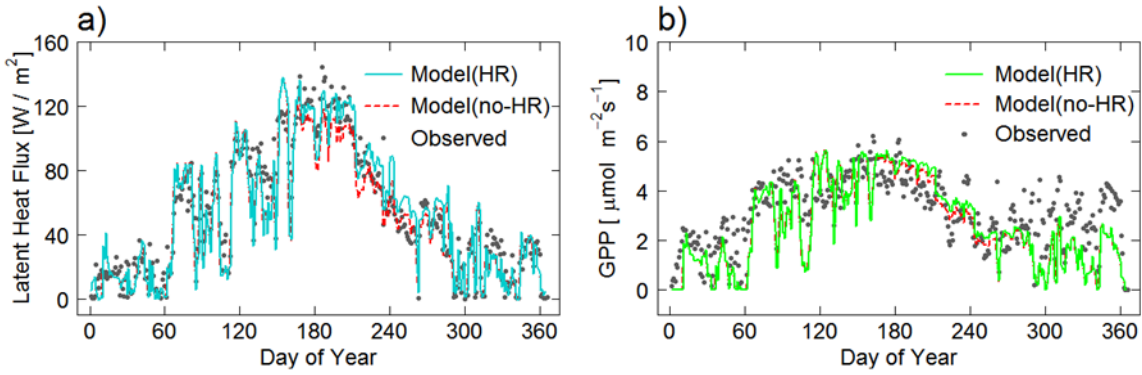


Figure 3.6 Comparison of modeled results with the observations at the Blodgett site for the year 2004. a) Latent heat flux; b) Gross primary productivity (GPP). The modeled results of both the “HR” scenario and the “no-HR” scenario are shown.

The daily GPP results of the “HR” scenario are compared to the observations (Figure 3.6b). The R^2 and RMSE between modeled and observed GPP are 0.55 and $1.27 \mu\text{mol} \cdot \text{m}^{-2} \cdot \text{s}^{-1}$, respectively. Figure 3.6b also shows the GPP results of the “no-HR” scenario. It is shown that the HR process promotes GPP during the dry season. The increase of the average GPP of three months (July, August and September) is $0.27 \mu\text{mol} \cdot \text{m}^{-2} \cdot \text{s}^{-1}$ and the relative increase is 8.0%.

4.0 IMPACTS OF BIOLOGICAL/HYDROLOGICAL PROCESSES ON WATER, ENERGY AND CARBON BUDGETS

4.1 SCENARIO SIMULATIONS AT DUKE SITE

For the purpose of evaluating the effects of hydraulic redistribution (HR), which plays a more important role under a drier climatic condition, on water, energy and carbon budgets, two scenarios (i.e. Case A and Case R) are simulated and compared to each other. HR is considered in Case R. In Case A the HR process is shut down, namely roots cannot release water to the soil. The parameter values for soil and vegetation are same as that of Section 3.2 in both scenarios. The depths of the soil domain and the root zone are 7 m and 5 m, respectively. The initial soil saturation value is set to be 0.4 for the unsaturated zone and the initial groundwater table depth is assumed to be 6 m.

Due to limited available measurements at the Duke site, hypothetical forcing data based on the data of year 2005 are constructed for dry conditions for conducting the scenario simulations. For the precipitation, the hourly precipitation values of 2005 are multiplied by 0.6 to scale down the annual precipitation of 2005 to an annual amount of 561 mm which is close to the annual precipitation of year 1941 (498 mm), the driest in 80 years (1931-2010). The mean annual precipitation of the 80 years is 1001 mm. Since the annual mean air temperature of 1941 is similar to that in 2005, the hourly air temperature time series of 2005 is used. There is no

information for other variables, such as the wind speed, humidity, pressure, etc., thus, the hourly data from 2005 for these variables are used. These forcing data may not be as dry as those the scaled precipitation (i.e. 561 mm per year) suggested. Such a time series of the constructed hypothetical forcing data would introduce inconsistencies among the forcing variables. However, it is the differences between the two cases rather than the absolute values that are investigated in the sensitivity analyses. Thus, the simulated results of the constructed forcing data are adequate. In addition, this treatment on the forcing data for the sensitivity analysis has also been used by previous studies [e.g., *Maxwell and Kollet, 2008*].

4.1.1 Impact of Hydraulic Redistribution on Root Uptake

Figure 4.1 shows the profiles of total daytime uptake in one year, starting from the prescribed initial condition, for Case A (without HR) and Case R (with HR) . When HR is considered, roots absorb more water in the shallow soil layer (about 0 - 0.35 m depth) and absorb less water within the range from about 0.35 m to 4.5 m depth during daytime. In Case R, water is transferred to the shallow soil layer via the HR process under dry conditions, thus, it makes it easier for roots to absorb water in the shallow layer during the daytime period, but at the same time it makes less water for roots to absorb in the deeper soil layer. Figure 4.2 shows differences between the two daytime uptake profiles of Case A and Case R.

Figure 4.3 shows the profile of total nighttime uptake in one year for Case R (with HR). It is clearly illustrated that during the nighttime water flows from the deep soil (about 1–5 m depth) to the shallower layer (about 0.1–1 m depth) through roots. In this way the shallow layer obtains water during nighttime, which facilitates transpiration of the next day.

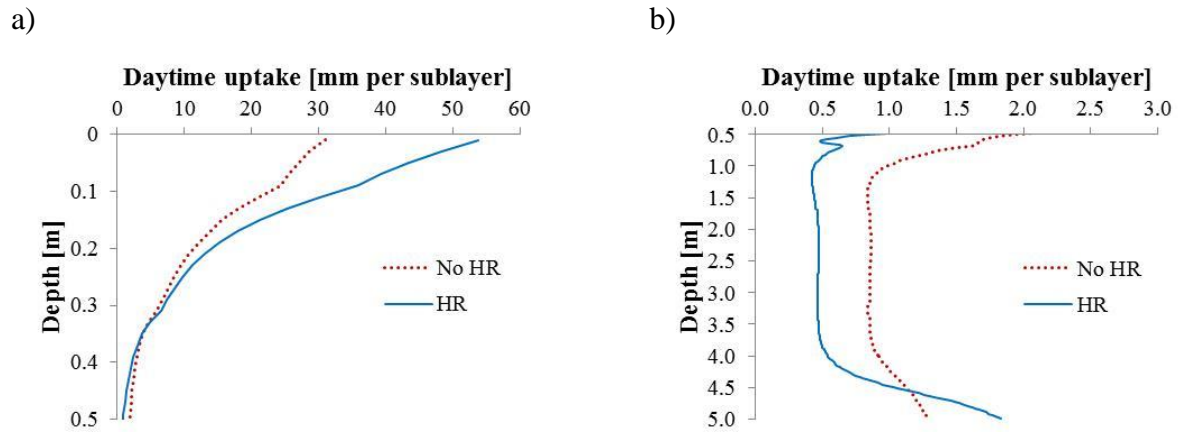


Figure 4.1 Profiles of total daytime uptake in one year for Case A (without HR) and Case R (with HR): a) From ground surface to 0.5 m depth; b) From 0.5 m to 5 m depth.

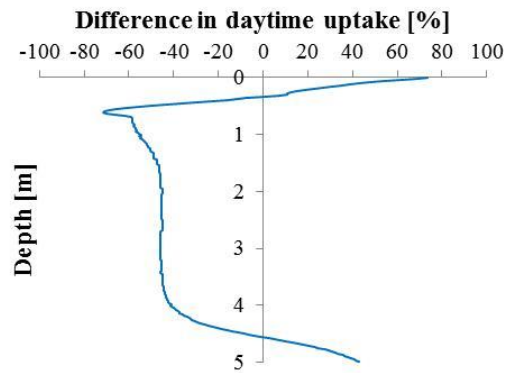


Figure 4.2 Relative differences between daytime uptake profiles of Case A and Case R. Positive values mean that uptake of Case R is larger than that of Case A and the vice versa.

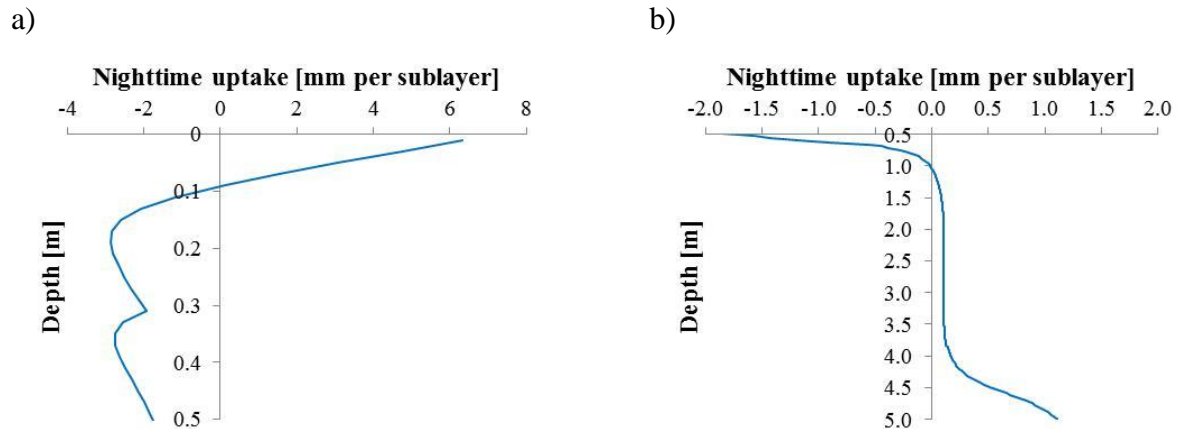


Figure 4.3 Profile of total nighttime uptake in one year for Case R (with HR): a) From ground surface to 0.5 m depth; b) From 0.5 m to 5 m depth. (Negative values mean that roots release water into the soil.)

4.1.2 Impact of Hydraulic Redistribution on Soil Moisture

The HR process redistributes soil water and consequently alters the status of soil wetness in the root zone. Figure 4.4 shows average simulated SWC of the top soil layer (0-30 cm) for Case A (without HR) and Case R (with HR). The comparison shows that SWC of the top layer can be decreased (e.g., 20 ~ 120 day) as a result of downward HR process (i.e., water is transferred from the top layer to deeper soil through roots) when the top layer is wet. On the other hand, SWC of the top layer could be evidently increased (e.g., 160 ~ 280 day) as a result of upward HR process (i.e., water is transferred from deeper soil to the top layer through roots) when the top layer is dry.

The annual mean SWC profile of Case A is compared to that of Case R in Figure 4.5a. The abrupt changes on the SWC profiles are due to heterogeneous soil properties. The differences between the two SWC profiles are shown in Figure 4.5b. It is evident that the HR process changes the SWC profile in the vertical direction. From ground surface to about 0.35 m

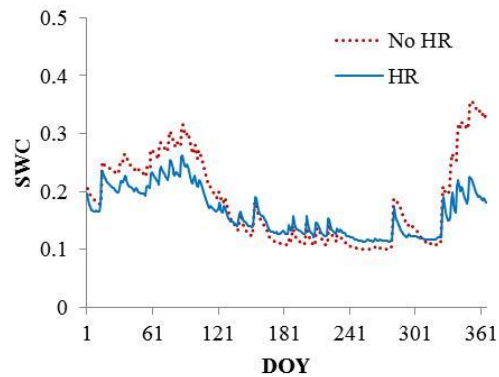


Figure 4.4 Average volumetric soil water content (SWC) of the top layer (0-30 cm) for Case A (without HR) and Case R (with HR).

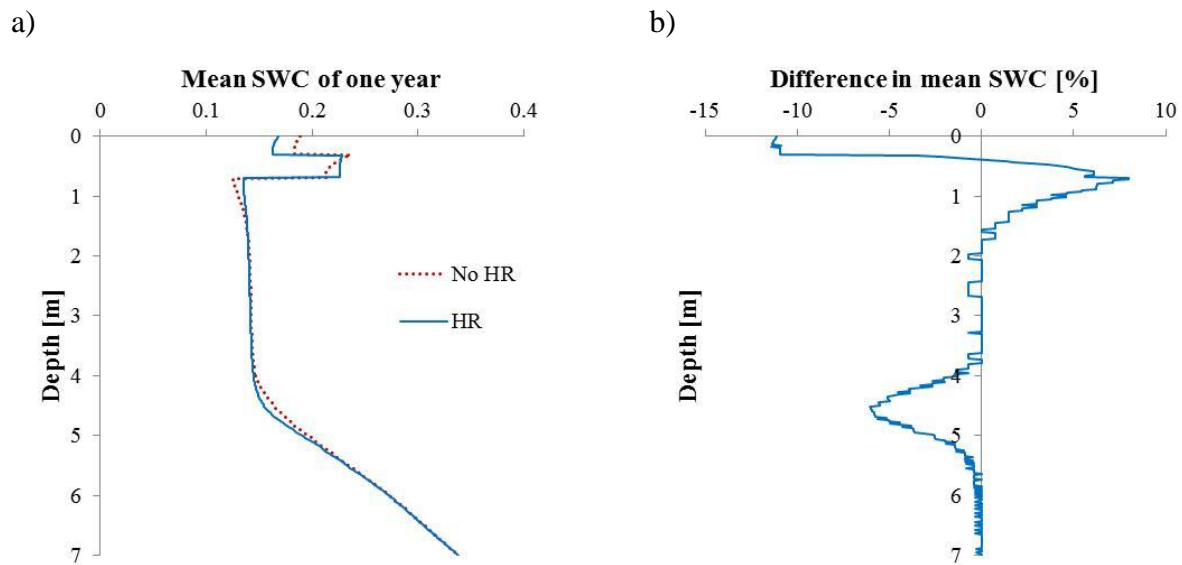


Figure 4.5 Comparison of SWC profiles between Case A (without HR) and Case R (with HR): a) Mean SWC profiles of one year for Case A and Case R; b) Relative differences between the mean SWC profile of Case R and that of Case A (Positive values mean that SWC of Case R is higher than that of Case A and the vice versa). The abrupt changes on the SWC profiles are due to heterogeneous soil properties.

depth the HR process decreases SWC by up to 12 %. From about 0.35 m to 1.5 m depth SWC is increased by up to 8%. Around the bottom of the root zone (about 3.9 ~ 5.5 m depth) SWC is reduced by up to 6%.

Figure 4.6 shows the comparison of SWC profiles between Case A and Case R for a short wet period and a short dry period, respectively. The short wet period consists of three days (from 9 to 11 March) after March 8 when rain events occurred. It is evident that the HR process decreases SWC of the shallow layer and increases SWC of the deep soil. The short dry period consists of 11 days (from August 23 to September 2) when potential evapotranspiration overwhelms precipitation. The comparison shows that the HR process promotes soil moisture in the shallow layer and makes the deep soil drier.

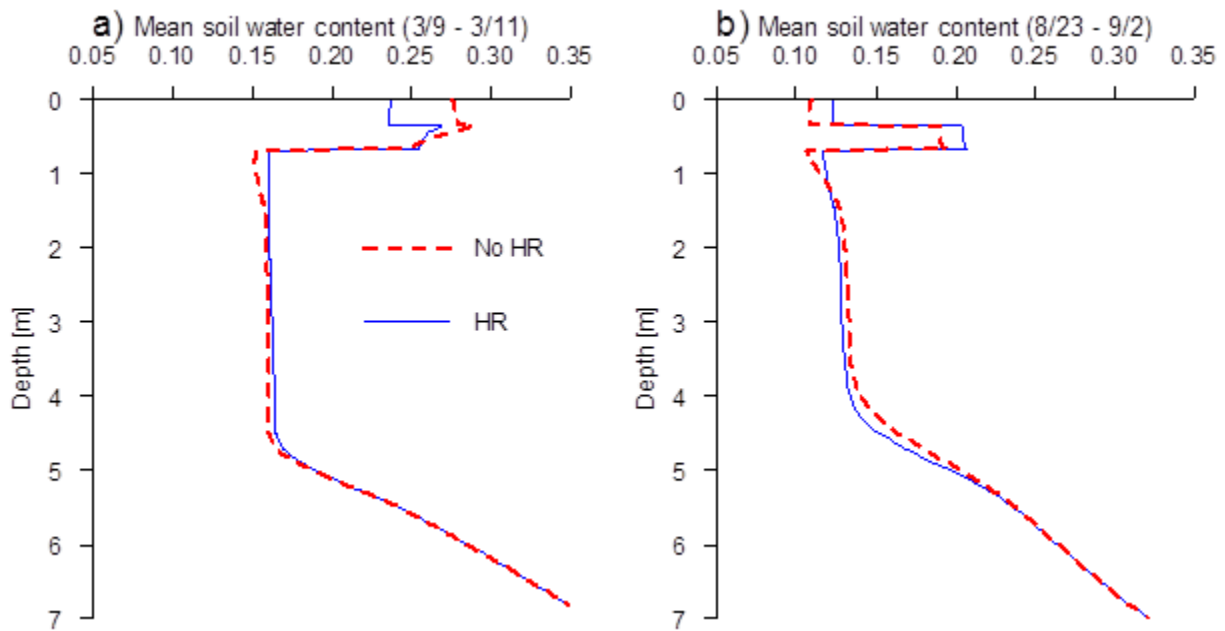


Figure 4.6 Comparison of SWC profiles between Case A (without HR) and Case R (with HR) for a) a wet period (from 3/9 to 3/11, the three days after a rain event on 3/8) and b) a dry period (from 8/23 to 9/2, when potential evapotranspiration overwhelms precipitation).

Figure 4.7 shows the comparison of SWC profiles between Case A and Case R at the end of a long wet or dry period. Precipitation is compared to potential transpiration at the monthly time scale in Figure 4.8. Potential transpiration overwhelms precipitation from April to September. So this period of six months is treated as the dry period. The remaining six months are treated as two wet periods (January ~ March and October ~ December) as precipitation is much higher than potential transpiration (except October when the difference is small). During the wet period, soil water is transferred from the wetter shallow layer to the drier deep soil through the downward HR process. Therefore on March 31 (the approximate end of the wet period) SWC of the HR case is lower than SWC of the no-HR case in the shallow layer and the contrary is true in the deep soil (Figure 4.7a). During the dry period, deep-soil water is pumped to the shallow layer via the upward HR process. Consequently, on September 30 (the approximate end of the dry period) the relationship between SWC of the HR case and SWC of

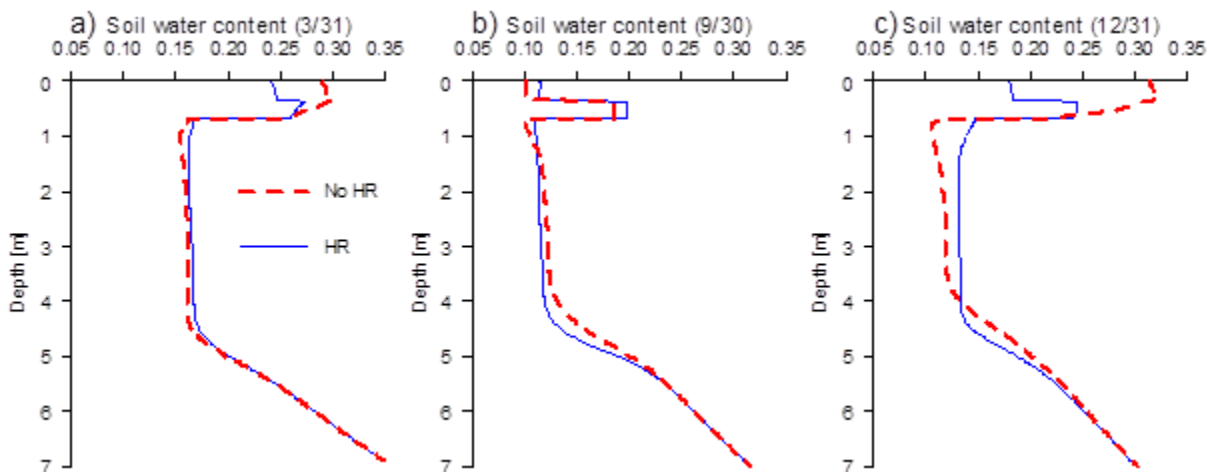


Figure 4.7 Comparison of SWC profiles between Case A (without HR) and Case R (with HR) for three days: a) March 31, approximate the end of the wet period; b) September 30, approximate the end of the dry period; c) December 31, the end of three wet months.

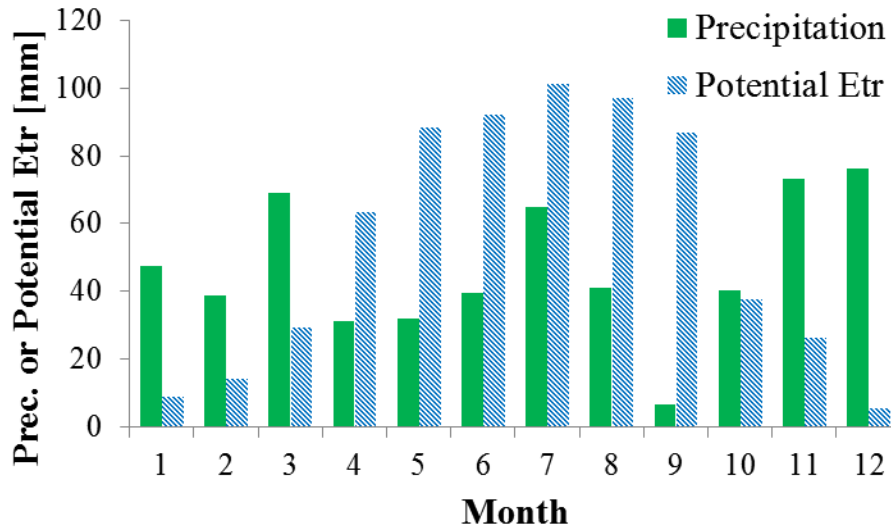


Figure 4.8 Comparison of precipitation to potential transpiration at the monthly time scale.

the no-HR case is contrary to that of March 31 (Figure 4.7b). Figure 4.7c indicates that during the second wet period (October ~ December) shallow-soil water is transferred to the deep soil via the downward HR process.

4.1.3 Impact of Hydraulic Redistribution on Transpiration, Latent Heat, Sensible Heat and GPP

Besides soil moisture, other land surface processes are also affected by HR. Effects of HR on transpiration, latent heat flux, sensible heat flux and GPP are investigated by comparing the modeled results of Case R with those of Case A as shown in Table 4.1. Over the one year simulation period, HR promotes transpiration, latent heat flux, and GPP by 6.9 %, 6.1 % and

5.2%, respectively, and reduces sensible heat flux by 5.7 %. These results are in accordance with the qualitative analysis. Transpiration can be limited by available soil water under dry conditions. However, during nighttime through the upward HR process water flows from deeper soil to the shallow layer, which facilitates root uptake and promotes transpiration in the next day. Latent heat flux is increased to a similar extent by the HR process since transpiration accounts for the majority of the total latent heat flux in a heavily vegetated area. An increase of the latent heat flux is accompanied by a decrease of the sensible heat flux. HR also increases the GPP results due to the coupling feedback effects between the photosynthesis process and the transpiration process.

Table 4.1 Comparison of the modeled results of the two scenarios.

Scenarios	12 Months				September			
	Transpiration [mm]	Latent Heat Flux [W/m ²]	Sensible Heat Flux [W/m ²]	GPP [mol/m ²]	Transpiration [mm]	Latent Heat Flux [W/m ²]	Sensible Heat Flux [W/m ²]	GPP [mol/m ²]
Case A	511.6	44.1	40.8	151.4	52.6	51.9	49.4	13.0
Case R	546.7	46.8	38.5	159.2	64.9	63.4	39.2	15.9
Difference between Case R and Case A	35.1	2.7	-2.3	7.8	12.3	11.5	-10.1	3.0
Relative difference between Case R and Case A [%]	6.9	6.1	-5.7	5.2	23.3	22.3	-20.5	22.8

Figure 4.8 indicates that September is the driest month in the one year simulation. In September the precipitation amount is only 6.7 mm and the ratio of precipitation to potential transpiration (86.8 mm) is 0.08. Both of these two values (i.e., the precipitation and the ratio) are the lowest among all the months. The modeled results of September for Case R and Case A are separately listed in Table 4.1. The Effects of HR in September are more significant than the

average effects of HR over the one year period. This result implies that HR could exert larger impact on land surface processes under drier climatic conditions.

4.1.4 Summary

Scenario simulations are conducted at the Duke site to investigate the effects of HR on water, energy and carbon budgets in the soil-plant-atmosphere continuum under water-limited conditions. The profile of total nighttime uptake over a one year period shows that water is “pumped” from the deep soil layer to the shallow soil layer via the HR process during the nighttime. As a consequence more water is “deposited” in the shallow soil layer, which causes the changes in the profile of daytime uptakes by roots. Simulated soil moisture results indicate that HR has an evident impact on SWC of the shallow soil layer and also affects the SWC vertical profile. The modeled results of one dry year show that HR generally promotes the transpiration, latent heat flux and GPP, and reduces sensible heat flux. These effects in September, the driest month, are much more significant than those in other months.

4.2 SCENARIO SIMULATIONS AT BLODGETT SITE

In this section, the impacts of hydraulic redistribution (HR), groundwater, root depth and plant water storage on the water and energy cycles in the soil-plant-atmosphere continuum, as well as the interactions among these factors, are demonstrated through the results of a few scenario simulations. In addition, the effect of frozen soil on HR is also revealed with scenario simulations. These simulations are conducted at the Blodgett site. This site has a long dry

summer when the four factors (i.e., HR, groundwater, root depth and plant storage) are expected to have evident impacts on the water and energy processes. The wet winter of this site is favorable to evaluate the effect of frozen soil on downward HR.

4.2.1 Impacts of Hydraulic Redistribution, Groundwater and Plant Storage on Latent Heat Flux

For the purpose of studying the individual impacts exerted by HR, groundwater dynamics, and plant storage, respectively, on the water and energy processes, several scenario simulations are carried out. These simulations are divided into two groups which differ in the maximum root depth (2 m for one group and 8 m for the other group). Each group consists of five scenarios. The setup of the five scenarios is shown in Table 4.2. In the first scenario (benchmark), the groundwater table is comparatively deep and neither HR nor plant storage is considered in the simulation. Depth of the groundwater table is controlled by changing one parameter (i.e., the maximum daily subsurface runoff) of the ARNO algorithm through which to determine the

Table 4.2 Setup of scenarios for studying impacts of HR, groundwater depth and plant water storage on water and energy cycles ^a

Scenarios	Considering hydraulic redistribution	Groundwater table	Considering plant water storage
1 (Benchmark)	No	Deep	No
2	Yes	Deep	No
3	No	Shallow	No
4	No	Deep	Yes
5 (HRGWC)	Yes	Shallow	Yes

^a This table shows scenarios of one group. Two groups of scenario simulations are conducted. The

maximum root depth is 2 m for one group and 8 m for the other group.

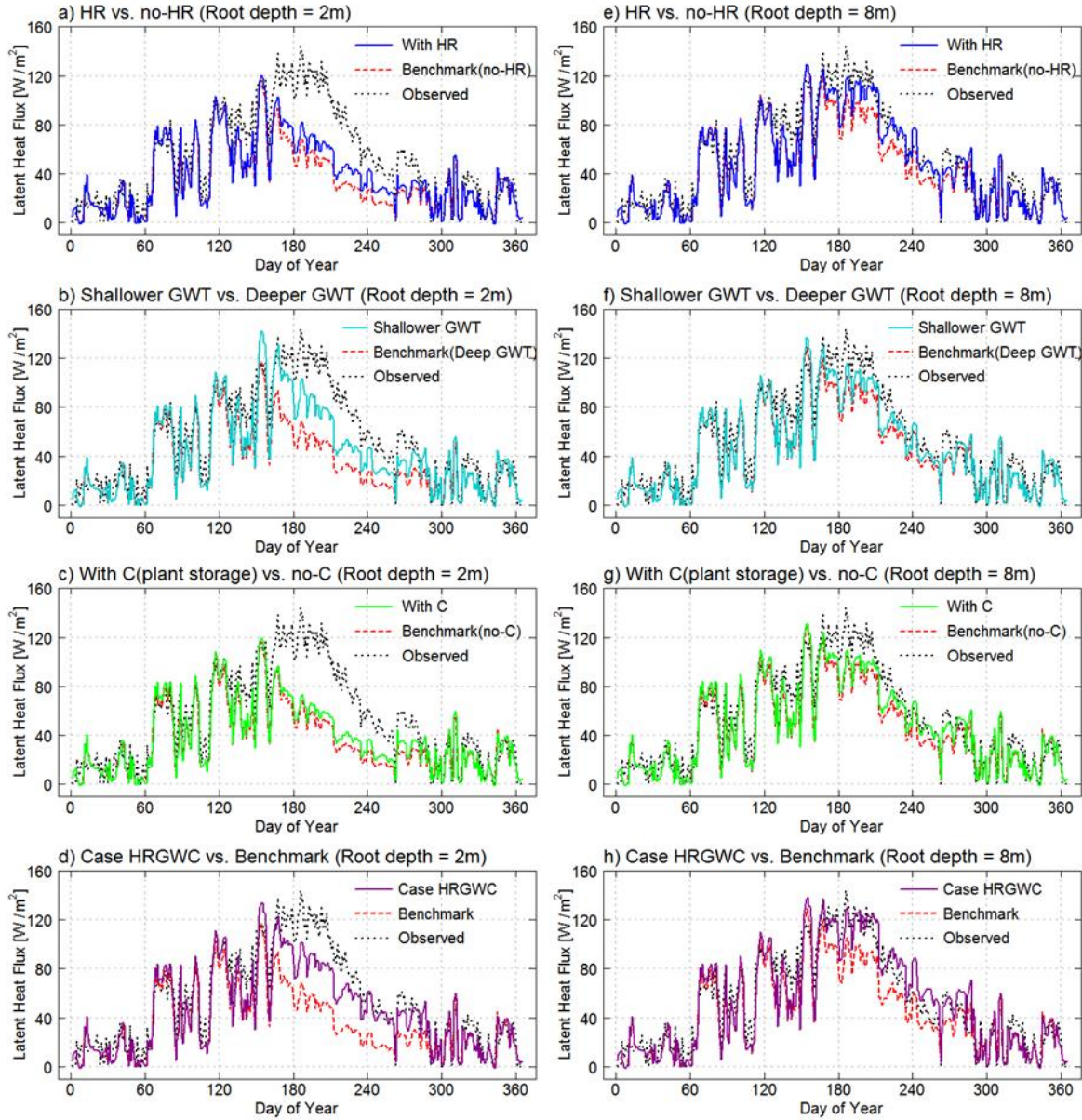


Figure 4.9 Comparison of latent heat flux between the benchmark scenario and other scenarios when the maximum root depth is 2 m (a, b, c and d) or 8 m (e, f, g and h). a) and e): Scenario 2 vs. Benchmark Scenario (HR vs. no-HR); b) and f): Scenario 3 vs. Benchmark Scenario (Shallower groundwater table vs. Deeper groundwater table); c) and g): Scenario 4 vs. Benchmark Scenario (With plant storage vs. Without plant storage); d) and h): Scenario HRGWC vs. Benchmark Scenario.

amount of the subsurface runoff. In scenarios 2, 3 and 4, the three factors (i.e., HR, groundwater table depth and plant storage) are changed one by one. In the last scenario (HRGWC), the groundwater table is comparatively shallow and both HR and plant storage are included in the simulation. The simulated latent heat flux results of the other four scenarios are compared with that of the benchmark scenario (see Figure 4.9 and Table 4.3).

Table 4.3 Comparison of dry-season latent heat flux among different scenarios

Max root depth [m]	Scenarios	Average latent heat flux of Jul., Aug. and Sep. [W/m ²]	Increase from the benchmark [W/m ²]	Relative increase from the benchmark [%]
2	1(Benchmark)	33.3	--	--
	2	44.1	10.9	32.7
	3	51.7	18.4	55.3
	4	40.1	6.8	20.5
	5(HRGWC)	60.7	27.4	82.3
8	1(Benchmark)	59.8	--	--
	2	73.6	13.8	23.0
	3	66.7	6.9	11.6
	4	67.6	7.8	13.1
	5(HRGWC)	84.3	24.5	40.9

Figure 4.9a shows that HR evidently promotes latent heat flux during the dry season and does not have obvious impact on latent heat flux during the remaining period of the year. HR increases the average latent heat flux of three months (abbreviated as LE3Mo hereinafter; the three months are July, August and September) by 10.9 W/m² and the relative increase is 32.7%. When the root depth is 8 m, HR increases LE3Mo by 13.8 W/m² and the relative increase is 23.0% (Figure 4.9e).

HR can increase dry-season latent heat flux. The main reason is that at nighttime the HR process transfers water from the deep soil to the shallow soil where most roots concentrate. This process is favorable for plant transpiration and hence promotes latent heat flux. Figure 4.10 shows profiles of annual total root uptake at daytime and nighttime, respectively. When HR is considered in the simulation, it is clear that at nighttime roots absorb water in the deep soil and release water in the shallow soil. During the daytime, the root uptake of “HR” scenario is much higher than that of “no-HR” scenario in the shallow soil. The root uptake profiles in the shallow

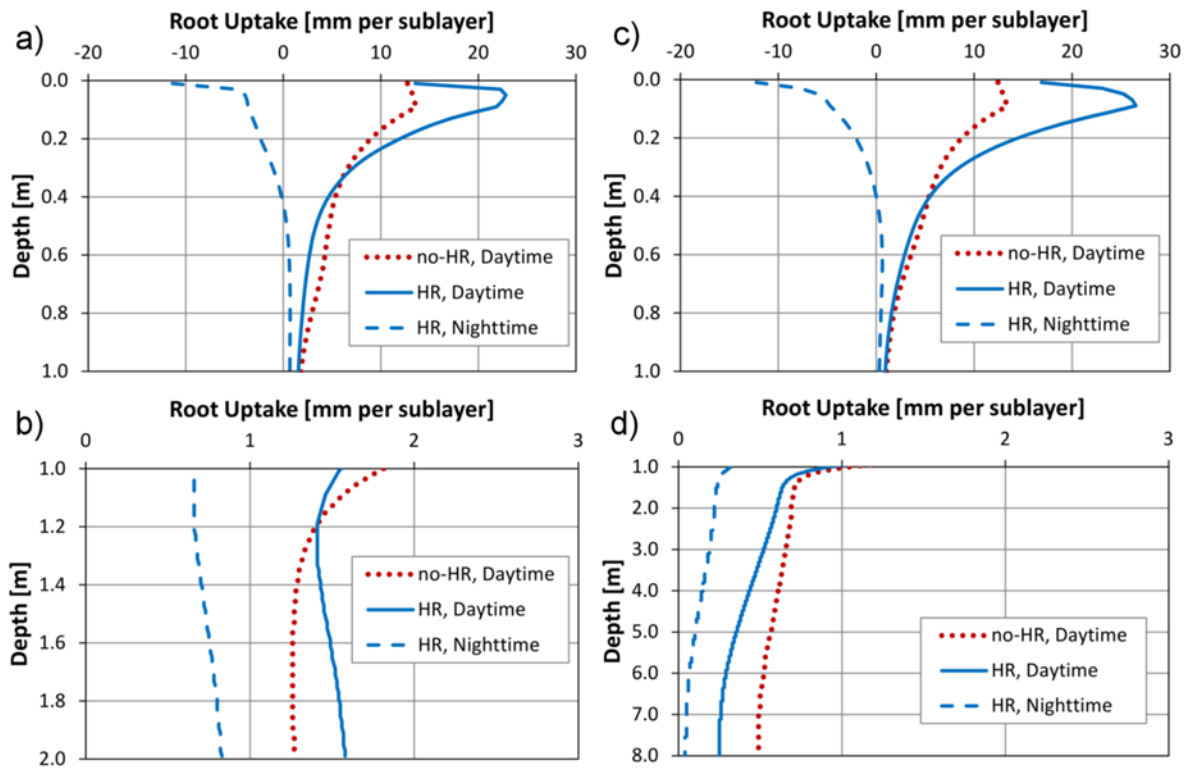


Figure 4.10 Comparison of root uptake profiles between the Benchmark Scenario (no-HR) and the Scenario 1 (HR). The profiles show annual total root uptake at daytime and nighttime, respectively. Negative values mean that roots release water into the soil. When the maximum root depth is 2 m, results are shown in a) (from ground surface to 1 m depth) and b) (from 1 m to 2 m depth). When the maximum root depth is 8 m, results are shown in c) (from ground surface to 1 m depth) and d) (from 1 m to 8 m depth).

layer (0 – 1 m) are similar for the scenarios of different root depths (i.e., 2 m versus 8 m). One important reason is that the distributions of the live fine roots in the shallow layer are assumed to be identical for these different scenarios. Therefore the total mass of live fine roots is larger for the scenarios with deeper maximum root depths.

When the root depth is 2 m, the rise of groundwater table (the mean annual groundwater table depth decreases from 7.2 m to 2.8 m) promotes latent heat flux of the dry season dramatically (Figure 4.9b). The LE3Mo is increased by 18.4 W/m^2 and the relative increase is 55.3%. The main reason is that the rise of groundwater table makes the root zone wetter and increases the amount of soil water available to plant transpiration. However, when the root depth is 8 m, the rise of groundwater table (the mean annual groundwater table depth decreases from 8.3 m to 4.1 m) does not have such a large impact on latent heat flux of the dry season. The LE3Mo is increased by 6.9 W/m^2 and the relative increase is 11.6%. The deep roots can access water from the deep wet layer even though the groundwater table is comparatively deep [Caldwell *et al.*, 1998; Jackson *et al.*, 2000]. In this case the rise of groundwater increases soil-water amount available to plant transpiration but to a lesser extent as compared with the shallow-root case.

Figure 4.9c and Figure 4.9g demonstrate that plant storage can increase latent heat flux and that the effect is more obvious during the dry season. Plant storage can store water absorbed by roots at nighttime and supply water to transpiration during the daytime if root uptake cannot satisfy the transpiration requirement. The LE3Mo is promoted by plant storage to the similar extent for the shallow root and deep root cases (6.8 W/m^2 and 7.8 W/m^2 , respectively).

If both HR and plant storage are considered in the simulation, and at the same time there is an evident rise of the groundwater table, latent heat flux of the dry season will be promoted to

a large extent (Figure 4.9d and Figure 4.9h). When the root depth is 2 m, the LE3Mo is increased by 27.4 W/m² and the relative increase is 82.3%, and the primary contributing factor is the rise of groundwater table. When the root depth is 8 m, the LE3Mo is increased by 24.5 W/m² and the relative increase is 40.9%, and the primary contributing factor is HR.

4.2.2 Interactions among the Impacts of Root Depth, Hydraulic Redistribution and Groundwater

Roots, groundwater and the HR process are linked with each other, thus there are interactions among them. For example, in the above section it is shown that the impacts of HR or groundwater on latent heat flux can be sensitive to the root depth. The interactions among roots, groundwater and HR are investigated through a few scenario simulations. These scenarios are divided into four groups as shown in Table 4.4. Each group consists of four scenarios with different root depths (i.e., 2 m, 4 m, 6 m and 8 m). The plant storage is not considered in these scenarios. The LE3Mo values (the average latent heat flux of July, August and September) of these scenarios are shown in Figure 4.11a. Data points of the four scenarios belonging to the

Table 4.4 Setup of groups for studying interactions among HR, groundwater and root depth ^a

Group No.	With hydraulic redistribution	Groundwater table
1	Yes	Shallow
2	Yes	Deep
3	No	Shallow
4	No	Deep

^a Each group consists of four scenarios with different root depths (i.e., 2 m, 4 m, 6 m and 8 m).

same group are connected by line segments, and the corresponding group number is labeled beside the line. The mean annual groundwater table depths of the 16 scenarios are shown in Figure 4.11b.

4.2.2.1 Impact of Root Depth

For each of the four groups, it is clear that the dry-season latent heat flux (LE3Mo) rises as the root depth increases (Figure 4.11a). For example, when HR is considered and the groundwater table is shallow, dry-season latent heat flux rises from 58.1 W/m² to 78.1 W/m² as the root depth increases from 2 m to 8 m (Line 1 in Figure 4.11a). During the dry season, plant transpiration is mainly sustained by water stored in the soil. The increase of root depth makes more soil water

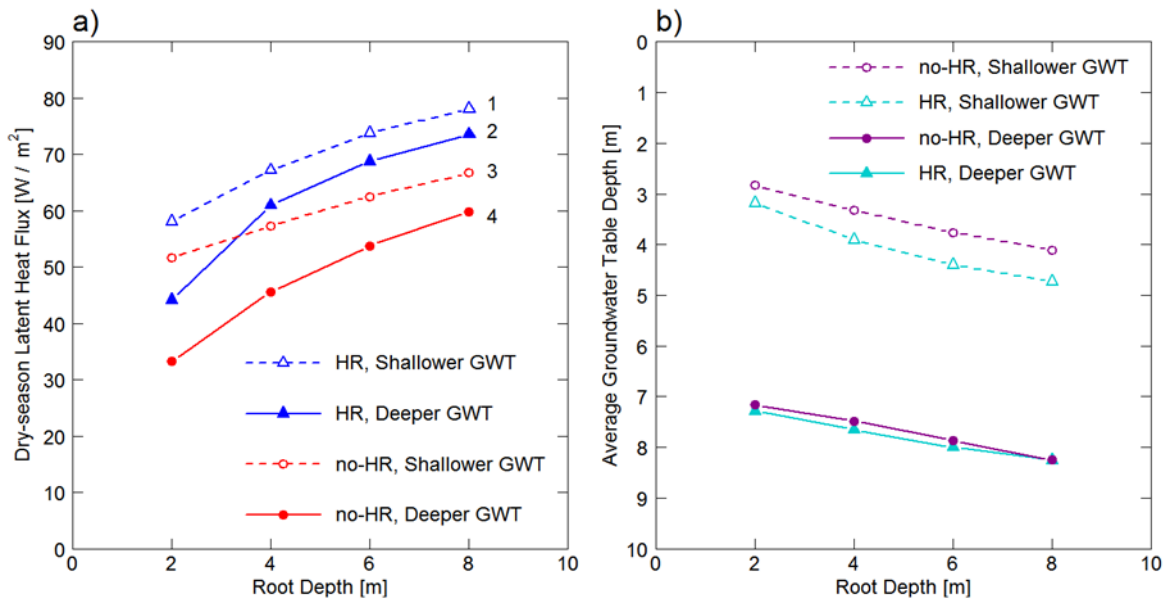


Figure 4.11 (a) Relationships between dry-season latent heat fluxes and root depths for the four groups of scenarios in Table 3; (b) Relationships between average groundwater table depths and root depths for the four groups of scenarios. “GWT” is the abbreviation of “groundwater table”.

available to plant transpiration. So the plant transpiration and hence the latent heat flux are higher when roots are deeper. This result demonstrates that deep roots are significant for plant growth during the dry season.

Figure 4.11a also shows that the influence of root depth on the dry-season latent heat flux is larger when the groundwater table is deeper, no matter whether HR is considered (Line 1 versus Line 2) or not (Line 3 versus Line 4). For example, when HR is not considered and the root depth increases from 2 m to 8 m, the latent heat flux increase is 26.5 W/m^2 (the relative increase is 79.7%) for deep groundwater table condition (Line 4) and 15.1 W/m^2 (29.1%) for shallow groundwater table condition (Line 3). The corresponding mean annual groundwater table depths are from 7.2 m to 8.3 m for the deep groundwater table condition and from 2.8 m to 4.1 m for the shallow groundwater table condition (Figure 4.11b). This result indicates that, in the water-limited circumstance, deep roots play a more important role when the groundwater table is deep, as compared with the shallower groundwater table condition.

4.2.2.2 Impact of Hydraulic Redistribution

Under the shallow groundwater table condition, impacts of HR on the dry-season latent heat flux become larger as the root depth increases from 2 m to 8 m (Line 1 versus Line 3). The HR induced-increase of the latent heat flux is comparatively small (6.4 W/m^2) when the root depth is 2 m. There is an evident growth in such an increase (from 6.4 W/m^2 to 9.9 W/m^2) as the root depth increases from 2 m to 4 m. However, as the root depth increases from 4 m to 8 m, the increase in latent heat flux slows down (from 9.9 W/m^2 to 11.4 W/m^2). Similar phenomenon is observed under the deep groundwater table condition (Line 2 versus Line 4). This result indicates that shallow rooting depths limit the impact/role of HR in promoting the latent heat flux. Impacts

of HR on water and energy processes become significant as the root depth increases within a certain range (e.g., from 2 m to 4 m in the above cases).

By comparing the differences between Line 1 and Line 3 with the differences between Line 2 and Line 4, it is demonstrated that, for all of the four root depths cases, the HR induced-increase of the dry-season latent heat flux is higher under the deep groundwater table conditions, as compared with the shallower groundwater table conditions. When the groundwater table is deep, groundwater cannot be effectively utilized by plants to satisfy the transpiration demand during the daytime. However, the HR process can pump the deep groundwater to the shallow layer at nighttime and facilitate the transpiration process in the next day. Therefore, under the water-limited condition, the impact of HR on latent heat flux is more significant when the groundwater table is deeper.

4.2.2.3 Impact of Groundwater

Figure 4.11a shows that the rise of the groundwater table evidently promotes dry-season latent heat flux no matter whether HR is included (Line 1 versus Line 2) or not (Line 3 versus Line 4). However, this promotion is smaller when HR is included, as compared to no-HR scenarios. The main reason is that HR can enhance the utilization of groundwater by plants, even though the groundwater table is deep. This makes the plant transpiration and hence latent heat flux less sensitive to the fluctuations of the groundwater table.

When HR is not considered, the increase of the dry-season latent heat flux caused by the rise of groundwater table (differences between Line 3 and Line 4) declines from 18.4 W/m^2 to 6.9 W/m^2 as the root depth increases from 2 m to 8 m. Similar phenomenon is observed when HR is considered (Line 1 versus Line 2). The reason is that deep roots enhance the capability of

plants to utilize groundwater and reduce the impact of groundwater table fluctuation on the plant transpiration.

4.2.3 Impact of Plant Storage on Hydraulic Redistribution

Connection between the plant storage flow (i.e., flow into/out of plant storage) and the HR process is explicitly represented in the VIC+ model. Therefore the interaction between plant storage and HR is modeled in the simulations. This interaction is demonstrated by some of the modeled results. For example, variation of the amount of hydraulically redistributed water (HRW) can reveal the impact of plant storage on HR.

Hydraulically redistributed water refers to water flow from roots into the soil. Figure 4.12a shows daily HRW amounts from ground surface to 30 cm depth for two scenarios (considering and not considering plant storage) when the root depth is 2 m. Positive HRW amount means that soil water is redistributed from the deeper soil to the surface layer (0 – 30 cm)

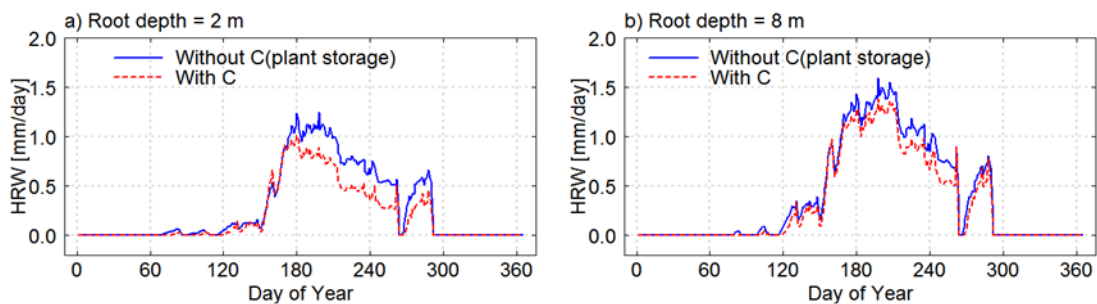


Figure 4.12 Comparison of amounts of hydraulically redistributed water in the shallow soil layer between the scenario with plant storage and the scenario without plant storage. a) The maximum root depth is 2 m; b) The maximum root depth is 8 m.

through the HR process. Higher HRW amount implies larger impact of HR on the water and energy processes. It is shown that the HRW is evident during the dry season, which indicates that HR plays a more important role during the dry season than during other periods of the year.

It is interesting to note that the HRW amounts decrease significantly for most of the dry season while plant storage is considered in the simulation. In other words, this phenomenon demonstrates that plant storage can weaken the intensity of the HR process. Table 4.5 shows annual total HRW amounts in the surface soil layer (0 – 30 cm) for different scenarios. When the maximum root depth is 2 m, including plant storage reduces the HRW amount by 28.9 mm and the relative decrease is 28.0%. Water stored in plant storage is depleted by transpiration during the daytime. At nighttime plant storage is replenished by water coming from root uptake. On the other hand, the HR process also occurs at nighttime under the dry climatic conditions. Usually water from the deeper soil is pumped up and released into the shallow layer. Therefore both plant storage and the shallow soil layer obtain water transferred from the deeper soil. The inclusion of plant storage into the simulation reduces the water amount redistributed to the shallow layer.

Table 4.5 Comparison of hydraulically redistributed water (HRW) amounts ^a

Max root depth [m]	Without plant storage [mm]	With plant storage [mm]	Difference [mm]	Relative difference [%]
2	103.2	74.3	28.9	28.0
8	140.7	119.2	21.5	15.3

^a The values are annual total HRW amounts in the surface soil layer (0 – 30 cm).

Comparison between Figure 4.12a and Figure 4.12b shows that the HRW amounts increase when the root depth is increased; at the same time the effect of plant storage on the HRW amounts decreases. This phenomenon is also demonstrated in Table 4.5. As roots extend

into deeper soil, more soil water can be utilized by plants [e.g., *Jackson et al.*, 2000; *Amenu and Kumar*, 2008]. At nighttime, the increase of root uptake in the deep soil is favorable to water release by roots in the shallow layer. At the same time, more water is provided to replenish plant storage and the impact of plant storage on HR is weakened.

4.2.4 Impact of Frozen Soil on Hydraulic Redistribution

For general simulations, the freezing process of soil water is represented, namely partial soil water turns into ice when soil temperature is lower than the freezing point. These general simulations are also referred to as “Frozen soil” scenario simulations hereinafter. For evaluating the effect of frozen soil on HR, we conducted a few special simulations where soil water does not turn into ice when soil temperature is below the freezing point. These special simulations are also referred to as “No frozen soil” scenario simulations hereinafter.

These simulations are conducted at the Blodgett site which has the Mediterranean-type climate. During the wet winter, the frozen soil may have impact on the downward HR. At first, the observed forcing data of year 2004 are used. Figure 4.13 shows the comparison of daily downward HRW (Hydraulically Redistributed Water) for the “Frozen soil” scenario and the “No frozen soil” scenario. We can see the downward HRW of “Frozen soil” scenario is slightly lower than that of “No frozen soil” scenario in the winter. The annual total amounts of downward HRW for the “Frozen soil” scenario and the “No frozen soil” scenario are 131.1 mm and 135.7 mm, respectively. Figure 4.14 shows the comparison of profiles of total root uptake in the winter for the “Frozen soil” scenario and the “No frozen soil” scenario. It is shown that root uptake is restricted by frozen soil in the surface layer (0 – 10 cm depth). Examination of the forcing data shows that the weather of year 2004 is not very cold at the Blodgett site. For 526 hours out of

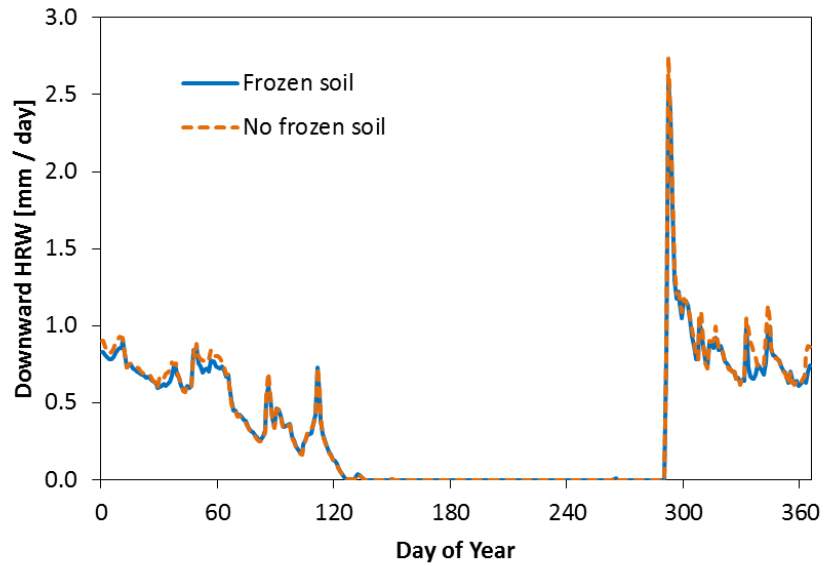


Figure 4.13 Comparison of daily downward HRW (Hydraulically Redistributed Water) for the “Frozen soil” scenario and the “No frozen soil” scenario in the year 2004 at the Blodgett site.

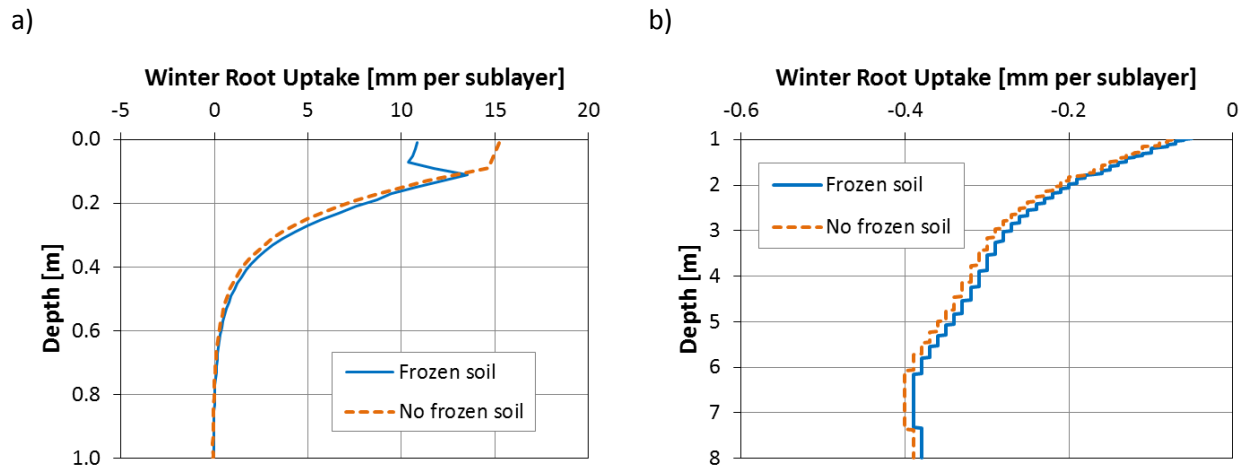


Figure 4.14 Comparison of profiles of total root uptake in the winter for the “Frozen soil” scenario and the “No frozen soil” scenario: (a) 0 – 1 m root zone; (b) 1 – 8 m root zone. Negative values mean that roots release water into the soil. Root uptake values of each 2 cm sublayer are shown.

8784 hours in this year (6.0% of the time steps in simulations), the average air temperature values are below zero degree Celsius. The comparatively warm weather is one important reason why the results do not show evident impact of frozen soil on HR.

The “Frozen soil” and “No frozen soil” scenario simulations are repeated with modified forcing data of year 2004 where air temperature values are lowered by 3 degrees Celsius. The results exhibit obvious impact of frozen soil on HR. The annual total amounts of downward HRW for the “Frozen soil” scenario and the “No frozen soil” scenario are 107.3 mm and 125.3

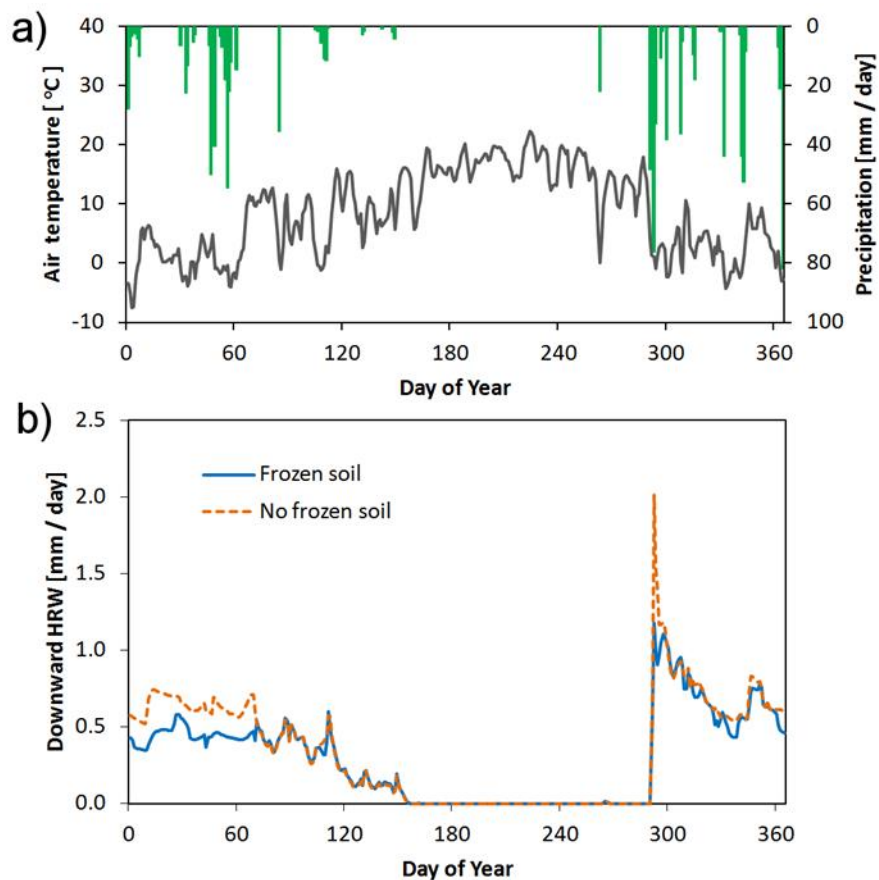


Figure 4.15 Comparison of daily downward HRW (Hydraulically Redistributed Water) for the “Frozen soil” scenario and the “No frozen soil” scenario (the lower panel) when the air temperature is lowered by 3 degrees Celsius for each hour of year 2004. The adjusted daily air temperature and daily precipitation are shown in the upper panel.

mm, respectively. Figure 4.15 shows the daily downward-HRW amounts of the two scenarios and the corresponding daily air temperature and precipitation. The figure demonstrates that the downward-HRW amount of the “Frozen soil” scenario is lower than that of the “No frozen soil” scenario when the air temperature is around zero degree Celsius. Figure 4.16 shows the profiles of total root uptake during the cold periods (Day 1 – Day 69 and Day 292 – Day 366) for the two scenarios. This figure demonstrates that root uptake is restricted in the shallow layer and at the same time roots release less water in the deep soil when the freezing process is considered in the simulation.

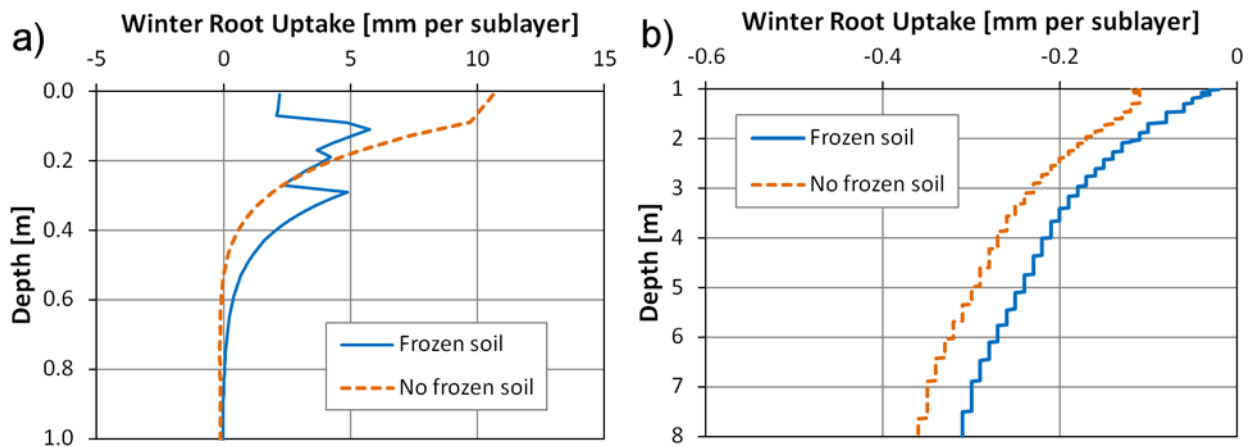


Figure 4.16 Comparison of profiles of total root uptake in the winter for the “Frozen soil” scenario and the “No frozen soil” scenario when the air temperature is lowered by 3 degrees Celsius. (a) 0 – 1 m root zone; (b) 1 – 8 m root zone. Negative values mean that roots release water into the soil. Root uptake values of each 2 cm sublayer are shown.

4.2.5 Summary

A group of scenario simulations are performed at the Blodgett site to investigate the impacts of HR, groundwater dynamics, plant storage and root depth on the water and energy cycles (Table 4.2). The modeled results demonstrate that each of the three factors (i.e., HR, groundwater dynamics and plant storage) can evidently increase latent heat flux in the dry season, while they do not have obvious impacts on the latent heat flux in the wet season, no matter whether the maximum root depth is small (2 m) or large (8 m) (Figure 4.9 and Table 4.3). The combined effects of the three factors can exert larger impacts on the dry-season latent heat flux than each of the three factors alone and can increase the latent heat flux by 82.3% and 40.9%, when the maximum root depth is 2 m and 8 m, respectively.

As the new biological and hydrological processes in the VIC+ model are closely coupled with each other, it enables an investigation of the interactions among these processes. The interactions among roots, groundwater table and HR are investigated through a series of scenario simulations. The modeled results reveal that the impact of one factor (i.e., maximum root depth, groundwater table depth or HR) on dry-season latent heat flux may be influenced by the other two factors (Figure 4.11): (1) The increase of root depth is favorable for dry-season latent heat flux, which is more sensitive to root depth when the groundwater table is deeper; (2) The dry-season latent heat flux is promoted by HR more obviously when either the groundwater table or the root depth is deeper ; (3) The rise of groundwater table will increase the dry-season latent heat flux and the effect is more evident when there is no HR or when the root depth is shallow. In addition, the interaction between plant storage and HR is demonstrated by comparing two

scenarios in terms of the amount of hydraulically redistributed water in the shallow soil layer (Figure 4.12). It is found that plant storage can weaken the intensity of the upward HR in the dry summer (Figure 4.12 and Table 4.5).

In the wet season, soil water of the shallow layer may be transferred to the deep soil via downward HR. However, downward HR may be restricted by frozen soil in the shallow layer if the wet season is in winter. The effect of frozen soil on the downward HR is investigated with scenario simulations and the results show that frozen soil can evidently reduce the downward HR in winter (Figure 4.15 and Figure 4.16), which decreases water amount stored in the deep soil and hence can reduce transpiration during the dry season.

5.0 RELATIONSHIPS BETWEEN PLANT TRANSPIRATION AND GROUNDWATER DYNAMICS

5.1 INTRODUCTION

Groundwater can have significant impacts on the subsurface, land surface and atmospheric processes by way of mechanisms such as exerting influence on soil moisture of the root zone. The impact of groundwater on plant transpiration is one important aspect of the interactions between groundwater and the land surface, vegetation and atmosphere in vegetated territory. Groundwater could play an important role in sustaining the plant transpiration, especially under the dry climate conditions. When groundwater is shallow and the groundwater table is higher than the bottom of the root zone, groundwater in the saturated zone can be absorbed by plant roots and directly utilized by plants. When the groundwater table is below the root zone bottom, groundwater can also diffuse upward into the root zone and partially sustain the plant transpiration.

The impact of groundwater on plant transpiration is influenced by many factors such as precipitation, vegetation type and soil type. In general, plant transpiration is sustained by both precipitation and groundwater. So plant transpiration is affected by groundwater more evidently under the dry climate conditions. On the other hand, the actual transpiration is also related to the transpiration capability which partially determined by the vegetation characteristics and varies

for different vegetation types. In addition, groundwater interacts with plants via the soil medium and hence the interaction is influenced by the soil characteristics.

The interaction between groundwater and plants is also influenced by some subsurface processes such as the hydraulic redistribution process. Hydraulic redistribution (HR) means that soil water can move from the position of higher water potential to the position of lower water potential by way of plant roots. Here “water potential” means the total water potential, which includes the gravitational potential and the matrix potential (or pressure potential). The HR process influences the distribution of soil moisture and could enhance the impact of groundwater on plant transpiration. Experiments also revealed that existence of groundwater, together with the effect of HR, could provide more potential transpirational water to plants [Dawson, 1996]. It has been verified by field experiments that the HR process exists for many plant species living under different climate conditions around the world [e.g., Caldwell *et al.*, 1998]. So it is significant to consider the HR process while studying the interaction between groundwater and plants.

The effects of groundwater on the land surface and atmospheric processes have received attention in the land surface and climate studies and the groundwater dynamics has been represented in some land surface models. In earlier land surface models, usually free drainage is adopted as the lower boundary condition for the soil domain and the saturated zone and the groundwater table are not represented. This method does not fully reflect the role of groundwater in the subsurface processes and the impacts of groundwater on the land surface and atmospheric processes. In the past decade, explicit consideration of groundwater (or the saturated zone) has been incorporated into some land surface models and the interactions between groundwater dynamics and the land surface processes have been demonstrated [e.g., Liang *et al.*, 2003; Kollet and Maxwell, 2008].

In this study, the interaction between groundwater and plant transpiration is investigated by employing the extended Three-layer Variable Infiltration Capacity (VIC-3L) land surface model (referred to as VIC+ model) which has included the representations of groundwater dynamics and the HR process. The VIC+ model is used to perform a series of numerical experiments involving different combinations of precipitation conditions, vegetation types, soil types and the treatment of the HR process (i.e., include or does not include the HR process in the model simulation).

The impact of groundwater dynamics on plant transpiration is demonstrated by the curve of the relationship between transpiration and the groundwater table depth (GWTD), which is generated based on the simulated results of the numerical experiments. The characteristics of the transpiration–GWTD relationship curves are analyzed. The impacts of other factors (e.g., precipitation condition, vegetation type and soil type) on this relationship are investigated. The role of HR in the interaction between groundwater and plant transpiration is examined. In order to understand the relationship between groundwater dynamics and plant transpiration and the impacts of other factors on this relationship, some subsurface processes (i.e., upward diffusion of groundwater, the HR process and daytime uptake by roots) in different scenarios are examined. Forcing data from two sites are used. For the two sets of forcing data, the temporal distribution of precipitation is quite different. The impacts of forcing conditions on Transpiration – GWTD relationships and subsurface processes are analyzed and discussed.

5.2 MODEL DESCRIPTION

The VIC land surface model solves a full energy and water balance for the land surface and subsurface. In the early versions of the VIC land surface model, the saturated zone is not explicitly represented and the subsurface runoff (base flow) is estimated following the ARNO method [Franchini and Pacciani, 1991]. Later the groundwater dynamics is explicitly represented and the surface and groundwater interactions are implemented into the VIC model [Liang *et al.*, 2003].

In the VIC+ model employed in this study, another method is adopted to represent the groundwater dynamics for the convenience of coupling the HR process with the unsaturated flow and the groundwater dynamics. In this method, the Richards equation is used to describe soil water movement in both the unsaturated zone and the saturated zone. So the groundwater table, namely the interface between the unsaturated and saturated zones, is explicitly represented.

The Richards equation is widely used to describe variably saturated flow in the soil. It can also be used to simulate water movement in the saturated zone [e.g., van Dam and Feddes, 2000; Kollet and Maxwell, 2008]. The three forms of the Richards equation are the volumetric water content-based form (also abbreviated as θ -based form), the pressure-based form and the mixed form. The θ -based form can conserve the mass balance well but cannot be used for the saturated soil. The pressure-based form can be used for both the unsaturated soil and the saturated soil but cannot conserve the mass balance well. The mixed form combines the merits of the θ -based form and the pressure-based form. The mixed form, unlike the θ -based form, can be used in the saturated zone and at the same time can conserve the mass balance better than the pressure-based form. Therefore the mixed-form Richards equation is used in the VIC+ model to describe the water movement in both the unsaturated zone and the saturated zone.

The HR process is explicitly represented and coupled with the soil water dynamics in the VIC+ model. The Poiseuille law is used to approximate the axial water transport along roots. The water movement in roots is connected with soil water via the water exchange at the interface between roots and the soil and the water exchange is represented with one equation. The flow direction at the interface depends on the comparison between the root water potential and the soil water potential. Roots absorb water when the root water potential is lower than the soil water potential. On the contrary, roots release water into the soil as the root water potential is higher than the soil water potential. This unique phenomenon is the key component of the HR process.

The axial water transport along roots is represented by one differential equation which is coupled with the Richards equation via the equation for the water exchange between roots and the soil. The three equations are solved simultaneously to obtain the distribution of soil moisture and the water exchange between roots and the soil.

Plant transpiration is calculated by combining the method of Ohm's law analogy with the Penman-Monteith method, where the stomatal conductance is linked with the photosynthesis process. Therefore plant transpiration is confined by both the soil moisture status and the meteorological condition. The interactions between plant transpiration and subsurface processes are explicitly represented.

5.3 DESIGN OF NUMERICAL EXPERIMENTS

The VIC+ land surface model is employed to conduct a series of numerical experiments involving different combinations of precipitation conditions, vegetation types, soil types and the treatment of the HR process. In each numerical experiment, the model is used to simulate

hydrological and energy cycles at a spot with the homogenous vegetation type. The simulation lasts for several years (typically 5 – 8 years) until a dynamic equilibrium is reached. Then the simulated results of the equilibrium state are used for the analysis purpose.

5.3.1 Description of One Numerical Experiment

In each numerical experiment, hydrological and energy cycles of a homogeneously vegetated spot are simulated by using the VIC+ land surface model. It is assumed that there is one soil type at the spot and the soil characteristics are uniformly distributed.

In order to reduce the impact of initial soil moisture conditions on the results and properly compare different experiments with different groundwater table depth (GWTD), all numerical experiments are performed following the same procedure described here. The initial GWTD is set as 0.5m and the simulation lasts for several years until a dynamic equilibrium is achieved. Here the dynamic equilibrium is judged based on annual plant transpiration and the annual average GWTD. When both the difference of annual plant transpiration and the difference of the average GWTD between two successive years are small, it is deemed that the dynamic equilibrium is reached. For most experiments of this study, the groundwater table declines during the simulation course since the depletion is larger than the recharge due to the dry climate conditions. When the precipitation amount is comparatively high, the GWTD will be stable at a certain value and the dynamic equilibrium is achieved after the simulation lasts for a few years. When the precipitation amount is comparatively low, the groundwater table will ceaselessly decline and the dynamic equilibrium cannot be achieved. In order to obtain the results of dynamic equilibrium state at different GWTD values and investigate the impact of the GWTD on plant transpiration, a maximum GWTD is set for each experiment, namely the GWTD cannot

exceed the maximum GWTD. This phenomenon occurs in the real world when groundwater is replenished by neighbor water source. For different experiments the maximum GWTD values are set to be from 1m to 10m with the increment of 1m. Besides these 10 experiments with the maximum GWTD values, there is another experiment which does not constrain the decline of the groundwater table.

In all the numerical experiments, the simulation lasts for 15 years. It is found that the dynamic equilibrium is achieved before the 15th year for all cases. The observed forcing data of year 2004 at the Blodgett Forest (US-Blo) site or the Duke Forest (US-Dk3) site are repeated to generate the artificial forcing input of 15 years to drive the simulations.

At the boundaries of the soil domain, it is assumed that there is no outward subsurface runoff or deep seepage. Therefore groundwater is only depleted by plant transpiration and it is more straightforward to compare the transpiration–GWTD relationships of different experiments since the effects of outward subsurface runoff or deep seepage on the GWTD need not to be considered. Sometime inward subsurface runoff could occur in order to prevent the GWTD from exceeding the maximum GWTD. Surface runoff is always taken into account.

The soil domain is set to be 15m thick. In order to solve the coupled root transport equation and Richards equation with the finite difference method, the soil domain is evenly discretized to 750 sub-layers of which each is 2 cm thick. One advantage of the even discretization is that the groundwater table can move up and down smoothly.

For all the numerical experiments the time step size is hour.

5.3.2 Differences among Numerical Experiments

The numerical experiments involves three precipitation conditions, three vegetation types, three soil types, and both HR and no-HR scenarios. For most numerical experiments, the forcing data of the Blodgett Forest (US-Blo) site are used. For a few numerical experiments, the forcing data of the Duke Forest (US-Dk3) site are used. These conditions are described as follows.

The three precipitation conditions mean that the annual precipitation is equal to 50%, 70% and 100% of the potential transpiration of tree in year 2004 at the Blodgett site. The three precipitation conditions are represented by P50, P70 and P100. Here the tree type is the ponderosa pine which dominates at the Blodgett site. The potential transpiration is calculated under the condition that the transpiration is not constrained by soil moisture and is estimated to be 740 mm per year. Consequently, for precipitation conditions P50, P70 and P100, the annual precipitation is 370 mm, 518 mm and 740 mm, respectively. The time series of precipitation used for the simulations are obtained by scaling the observed hourly precipitation of year 2004 at the Blodgett site.

For other forcing variables such as air temperature, wind speed, humidity, pressure, etc., the observed hourly data of year 2004 are used in these numerical experiments. This treatment of the forcing input brings some inconsistencies among the forcing variables. But these inconsistencies will not have much impact on the results of the numerical experiments since it is the differences among different experiments are analyzed in this study. Moreover, this treatment of forcing data has also been used by other studies [e.g., *Maxwell and Kollet, 2008*].

The vegetation types used in these numerical experiments include tree, shrub and grass. For all the three vegetation types, the vertical distribution of roots is represented by an asymptotic equation following Gale and Grigal [1987]. The coefficients of the asymptotic

equation are based on the work of Jackson et al. [1996, 1997]. The maximum root depths of tree, shrub and grass are assumed to be 5m, 4m and 2m, respectively. The root hydraulic conductivities are estimated by using the method described in the previous Chapter 2. The related root parameters (such as surface area of live fine roots and root mass) of the three vegetation types are obtained from Jackson et al. [1996, 1997].

The three soil types used in the numerical experiments are clay, loam and sand. But in each experiment, only one soil type is used. The values of soil parameters, including saturated hydraulic conductivity, porosity, residual soil water content and the van Genuchten parameters, are obtained from the database of ROSETTA model developed by Agricultural Research Service of USDA. The soil water content–soil water potential relationship and the soil hydraulic conductivity–soil water potential relationship are represented by the van Genuchten model [*van Genuchten*, 1980].

The numerical experiments include both HR scenarios and no-HR scenarios. In the HR scenarios, the HR process is considered and coupled with other hydrological processes in the soil-plant-atmosphere continuum. In the no-HR scenarios, the HR process is shut down and roots cannot release water into the soil.

In order to investigate how the Transpiration – GWTD relationship is affected by the factors such as precipitation, soil type, vegetation type, HR and forcing type, several groups of numerical experiments are conducted.

(1) Numerical experiments for studying the impact of precipitation on Transpiration – GWTD relationship

For numerical experiments of this group, the vegetation type is tree and the soil type is loam. This group includes 6 subgroups as a result of combinations of three precipitation

conditions (P50, P70 and P100) and different treatment of HR (with HR or without HR). Each subgroup includes 11 numerical experiments. The 11 experiments only differ in the prescription of the maximum GWTD. For 10 experiments, the maximum GWTD values are set to be from 1m to 10m with the increment of 1m. For the remaining experiment, the decline of the groundwater table is not constrained.

(2) Numerical experiments for studying the impact of soil type on Transpiration – GWTD relationship

For numerical experiments of this group, the vegetation type is tree and precipitation condition is P50. This group includes 6 subgroups as a result of combinations of three soil types (clay, loam and sand) and different treatment of HR (with HR or without HR). Each subgroup includes 11 numerical experiments differ in the maximum GWTDs as described above.

(3) Numerical experiments for studying the impact of vegetation type on Transpiration – GWTD relationship

For numerical experiments of this group, the soil type is loam and precipitation condition is P50. This group includes 6 subgroups as a result of combinations of three vegetation types (tree, shrub and grass) and different treatment of HR (with HR or without HR). Each subgroup includes 11 numerical experiments differ in the maximum GWTDs.

(4) Numerical experiment for studying the impact of forcing type on Transpiration – GWTD relationship

For numerical experiments of the above groups, the forcing data of the Blodgett site are used. At the Blodgett site, the temporal distribution of rainfall is not even in one year. Precipitation mainly occurs from October through May and there are very few rainfall events from June to September. At the Duke Forest (US-Dk3) site, the temporal distribution of rainfall

in one year is more even than that of the Blodgett site. In this group, the forcing data of the Duke site is used. The vegetation type is tree, the soil type is loam and the precipitation condition is P50. This group consists of two subgroups (with HR and without HR). Each subgroup includes 11 numerical experiments differ in the maximum GWTDs as described above.

5.4 SIMULATION RESULTS AND DISCUSSION

For all the numerical experiments, the hydrological cycle in the soil-plant- atmosphere continuum reaches a state of dynamic equilibrium at the late stage of the simulation period of 15 years. The last year (i.e., the 15th year) is chosen as the representative year when the dynamic equilibrium state is maintained. The results of the last year are analyzed and discussed in this section.

5.4.1 Transpiration–GWTD Relationships

The impacts of precipitation, vegetation type, soil type or HR on transpiration–GWTD relationships are demonstrated in the following sections.

5.4.1.1 Impact of Precipitation on Transpiration–GWTD Relationships

Transpiration–GWTD relationships under three precipitation conditions (P50, P70 and P100) are compared in Figure 5.1 for both HR scenarios and no-HR scenarios. In these scenario simulations, the vegetation type is tree and the soil type is loam.

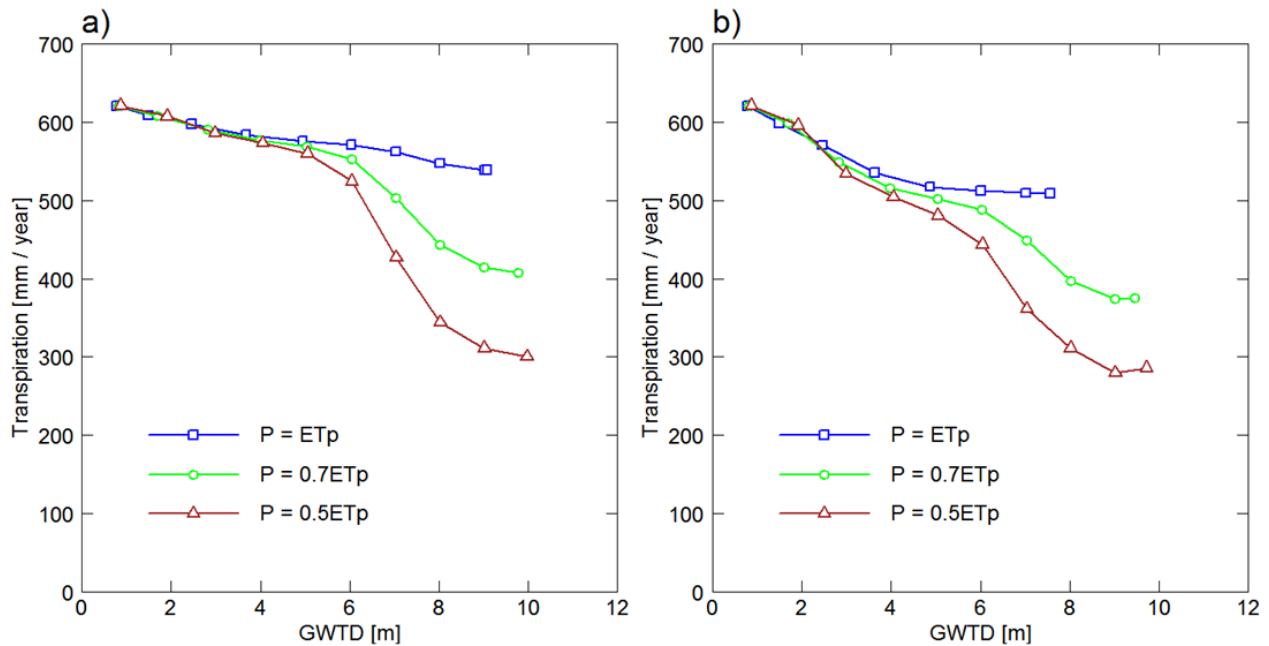


Figure 5.1 Comparisons of Transpiration – GWTD relationships under three precipitation conditions: (a) When HR is considered; (b) When HR is not considered. The vegetation type is tree and the soil type is loam.

Figure 5.1a shows the results of the HR scenarios (i.e., HR is considered in the simulations). Under the precipitation condition P50 (i.e., the annual precipitation equals 50% of the potential transpiration of tree), we can see transpiration is sensitive to the GWTD, namely transpiration decreases abruptly as the groundwater table drops, as the GWTD is within a certain range (from about 5 to 8 m for this case, named as “transitional range” hereinafter). Transpiration is less sensitive to the GWTD as the latter is out of the transitional range. When the groundwater table is within the root zone, which is 5 m thick in this case, transpiration is sustained by soil water which is replenished by both infiltration and groundwater. Transpiration is mainly determined by meteorological conditions since soil water is sufficient. When the groundwater table is far below the root zone bottom, soil water of the root zone is hardly

replenished by groundwater. Therefore transpiration is primarily sustained and controlled by precipitation under dry climate condition.

Figure 5.1a also shows that transpiration is not much sensitive to precipitation when the groundwater table is higher than the root zone bottom. However, the impact of precipitation on transpiration becomes obvious as the groundwater table is lower than the root zone bottom.

While HR is not considered in the scenario simulations, transpiration–GWTD relationships under three precipitation conditions (P50, P70 and P100) are compared in Figure 5.1b. We can see that for these no-HR scenarios, transpiration is more sensitive to both GWTD and precipitation amount when the groundwater table is within the root zone, as compared with HR scenarios. This phenomenon suggests that the HR process can enhance the utilization of groundwater by plants.

5.4.1.2 Comparisons among Different Vegetation Types

Transpiration capabilities of different vegetation types differ a lot from each other. Therefore the transpiration–GWTD relationship is related to vegetation type. In Figure 5.2 we compare the transpiration–GWTD relationships of three vegetation types (tree, shrub and grass) under the precipitation condition of P50. The soil type is loam and the comparisons are for both HR and no-HR scenarios.

Figure 5.2 shows that when HR is considered, the transpiration–GWTD relationships of three vegetation types show different characteristics. As the vegetation type is tree, transpiration is sensitive to GWTD when the groundwater table is within the transitional range, as elaborated in the previous section. As the vegetation type is shrub, the transitional range is less obvious than that of tree. The transitional range is obscure on the transpiration–GWTD relationship curve for the vegetation type of grass. The reason is that the transpiration capabilities of shrub and grass

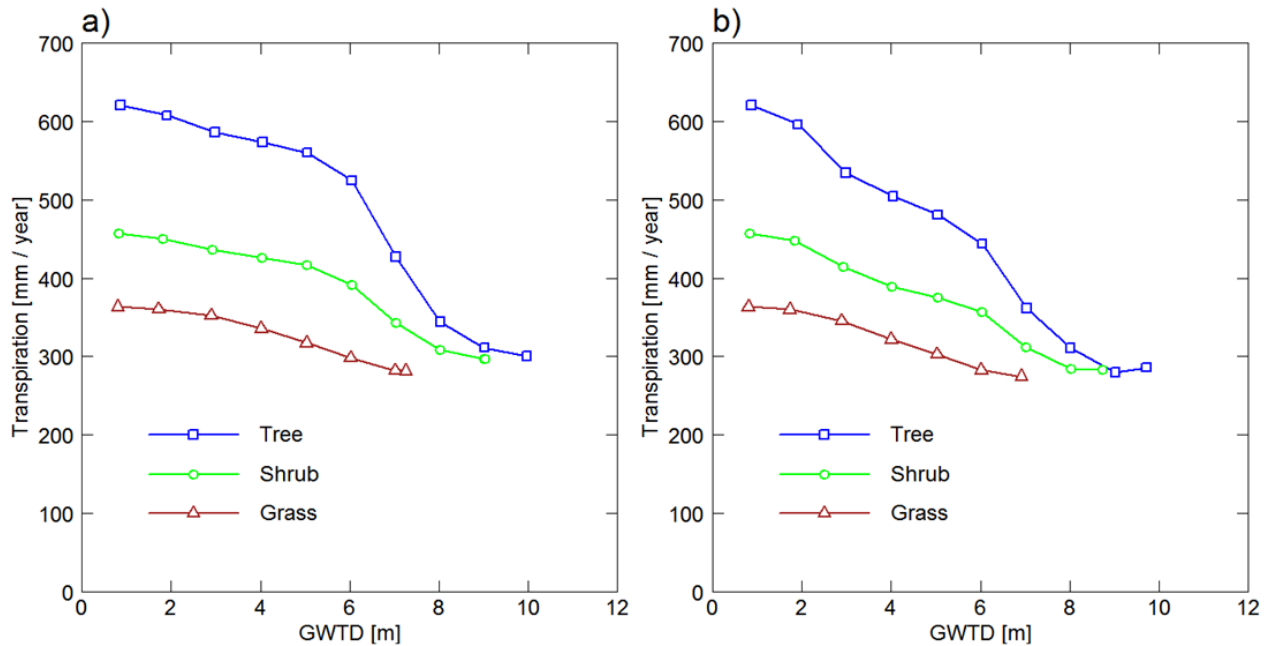


Figure 5.2 Comparisons of Transpiration – GWTD relationships of three vegetation types: (a) When HR is considered; (b) When HR is not considered. The soil type is loam and the precipitation condition is P50.

are lower than that of tree and can primarily be sustained by precipitation. Transpiration of shrub and grass is less dependent on groundwater than that of tree. Therefore transpiration of shrub and grass decreases mildly as the groundwater table declines.

In Figure 5.2a it is shown that transpiration amounts of three vegetation types are quite different when the GWTD is less than about 7 m, and tend to the similar amount when the groundwater table is deep. Transpiration differences are mainly caused by discrepancies in transpiration capabilities of different vegetation types as the groundwater table is comparatively shallow and considerable amount of groundwater is utilized by plants. When the groundwater table is deep and groundwater utilization by plants is small, transpiration is sustained and controlled by precipitation under dry climate conditions. Hence transpiration amounts of different vegetation types are similar.

Figure 5.2b shows that the transitional range, where transpiration is much sensitive to GWTD, is not evident in the transpiration–GWTD relationship curves for the no-HR scenarios of all the three vegetation types.

5.4.1.3 Impact of Soil Type on Transpiration–GWTD Relationships

Transpiration–GWTD relationships of three soil types (clay, loam and sand) under the precipitation condition of P50 are compared in Figure 5.3. The vegetation type is tree and the comparisons are for both HR and no-HR scenarios.

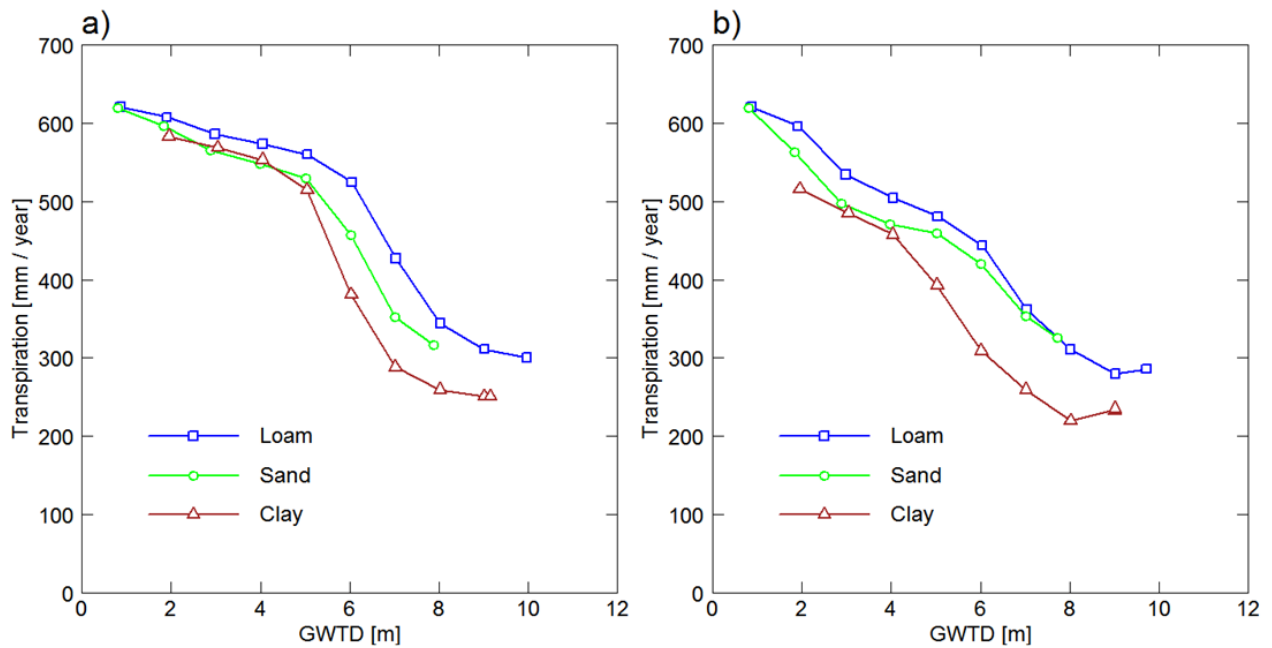


Figure 5.3 Comparisons of Transpiration – GWTD relationships of three soil types: (a) When HR is considered; (b) When HR is not considered. The vegetation type is tree and the precipitation condition is P50.

When HR is considered, the transpiration–GWTD relationship curves of the three soil types have the similar shape and transitional range. Figure 5.3a shows that the transitional range of GWTD is from about 5 ~ 8 m for all the three soil types. However, transpiration of the three

soil types differs obviously as the GWTD is within the transitional range. In Figure 5.3a, when the GWTD is 6 m, transpiration values are about 530 mm, 450 mm and 380 mm for the loam, sand and clay scenarios, respectively. The transpiration differences are caused by discrepancies in the diffusion of soil water for the three soil types. The groundwater table is below the root zone bottom and groundwater cannot be directly utilized by plants. But groundwater can diffuse upward into the root zone and hence be used for transpiration. So the upward diffusion of soil water can have impact on plant transpiration. The upward diffusion of soil water will be further analyzed later based on the modeled results.

When the groundwater table is within the root zone, transpiration of loam scenario is obviously higher than those of sand and clay scenarios as the HR process is not considered in those simulations. But the transpiration differences among scenarios of three soil types are small as the HR process is considered. Therefore it is concluded that the impact of HR on transpiration is larger for sand and clay scenarios, as compared with the loam scenario, when the groundwater table is comparatively shallow.

5.4.1.4 Impact of HR on Transpiration–GWTD Relationships

Transpiration–GWTD relationships of HR scenarios are compared with those of no-HR scenarios for different situations. Figure 5.4 shows comparisons for three precipitation conditions (P50, P70 and P100). The vegetation type is tree and the soil type is loam.

Under the precipitation condition of P50 (Figure 5.4a), the shape of the transpiration–GWTD relationship curve of the HR scenario is different from that of the no-HR scenario. When the groundwater table declines within the range of the root zone, the transpiration descent of the HR scenario is smaller than that of the no-HR scenario. In the curve of the HR scenario, the transitional range is more evident and the transpiration descent within the transitional range is

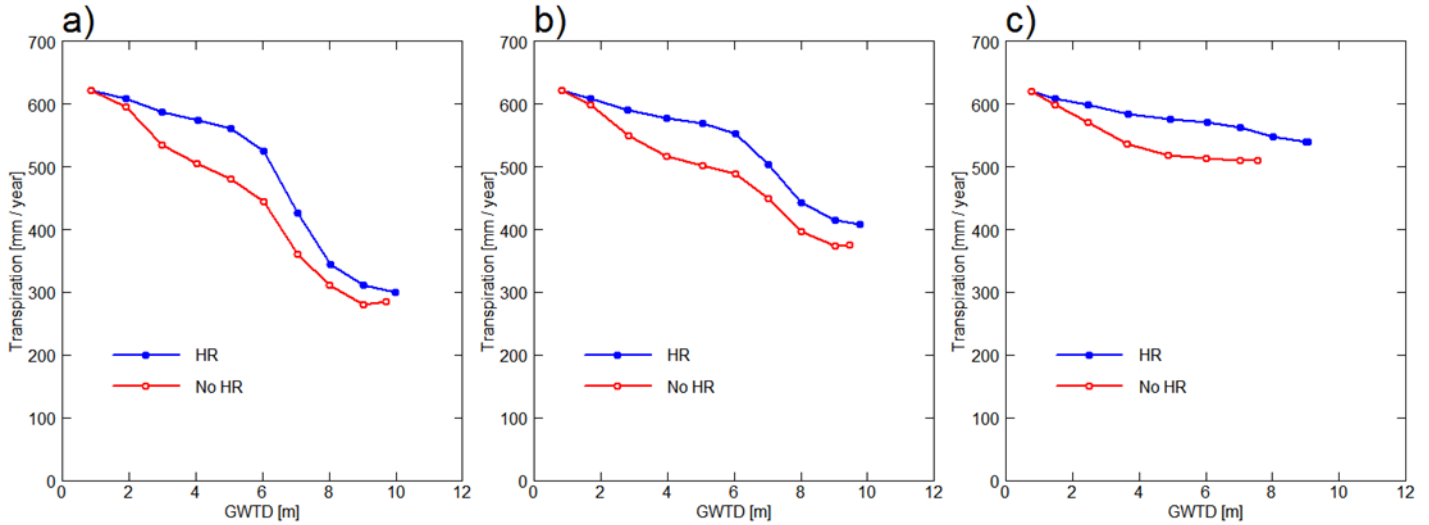


Figure 5.4 Comparisons of Transpiration – GWTD relationships between HR and no-HR scenarios under three precipitation conditions: (a) P50; (b) P70; (c) P100. The vegetation type is tree and the soil type is loam.

more abrupt. The comparison of the curve of the HR scenario with that of the no-HR scenario shows that the promotion of transpiration by HR is very small as the groundwater table is very shallow and increases as the groundwater table declines. The promotion by HR reaches the maximum value as the groundwater table is around the root zone bottom. But when the groundwater table further declines, the impact of HR on transpiration will decrease.

Under the precipitation condition of P70 (Figure 5.4b), the shape of the transpiration–GWTD relationship curves is similar to that of the precipitation condition P50. The transpiration promotion by HR is slightly smaller than that of the precipitation condition P50. This result demonstrates that the impact of HR on transpiration becomes weaker under comparatively wetter climatic conditions.

Under the precipitation condition of P100 (Figure 5.4c), transpiration decreases mildly as groundwater table declines. Transpiration is still promoted by HR when the GWTD is greater than about 1 m.

Transpiration–GWTD relationships of HR scenarios are compared with those of no-HR scenarios for three soil types (i.e., loam, sand and clay) in Figure 5.5. The vegetation type is tree and the precipitation condition is P50.

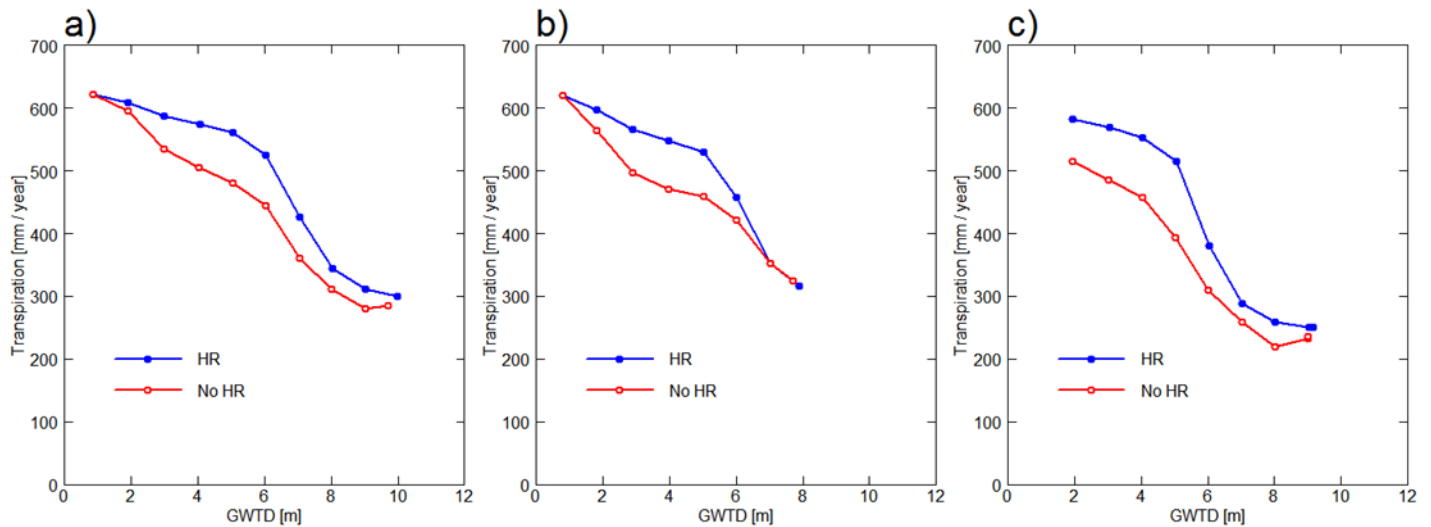


Figure 5.5 Comparisons of Transpiration – GWTD relationships between HR and no-HR scenarios for three soil types: (a) Loam; (b) Sand; (c) Clay. The vegetation type is tree and the precipitation condition is P50.

Transpiration–GWTD relationship curves of both HR scenarios and no-HR scenarios for different soil types show similar characteristics. In the transpiration – GWTD curve of HR scenarios there is a transition range where transpiration is sensitive to GWTD. The transpiration promotion caused by HR is larger when the groundwater table is around the root zone bottom and is smaller when the groundwater table is shallow or below the root zone.

Transpiration–GWTD curves of HR scenarios are compared with those of no-HR scenarios for three vegetation types (i.e., tree, shrub and grass) in Figure 5.6. The soil type is loam and the precipitation condition is P50.

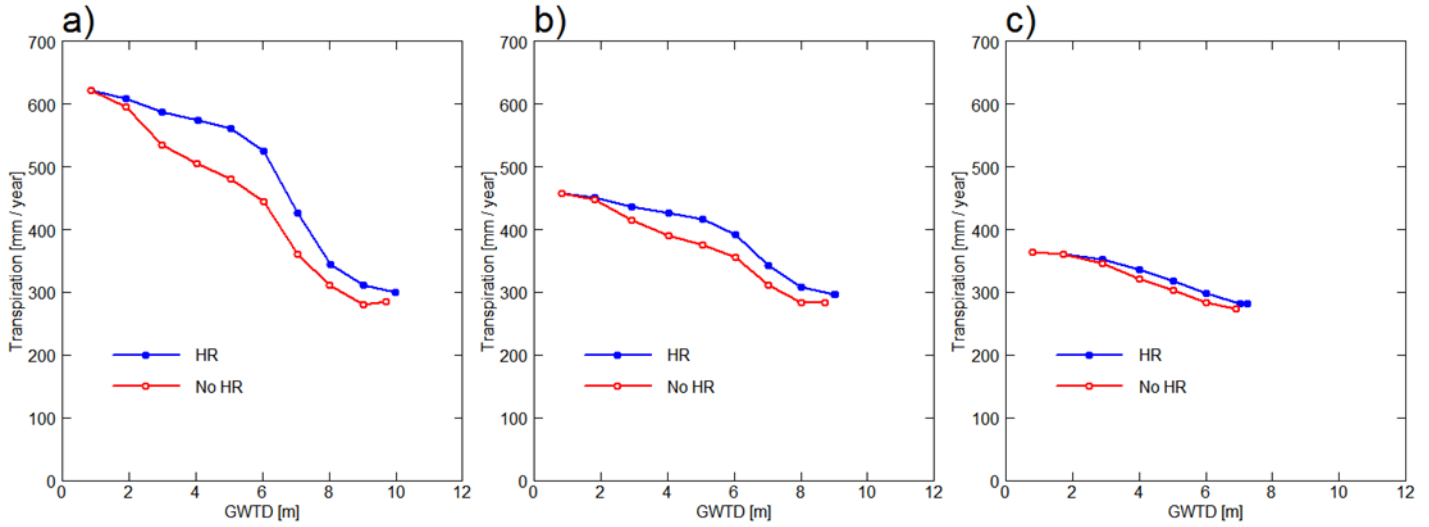


Figure 5.6 Comparisons of Transpiration – GWTD relationships between HR and no-HR scenarios for three vegetation types: (a) Tree; (b) Shrub; (c) Grass. The soil type is loam and the precipitation condition is P50.

Figure 5.6 shows that the transpiration promotion by HR for shrub or grass scenarios is much lower than that of the tree scenario. The main reason is that the transpiration capability of shrub or grass is lower than that of tree, hence the root zone of the shrub scenario or the grass scenario is wetter than that of the tree scenario. Under wet conditions, the effect of HR on transpiration will be comparatively weak.

5.4.2 Upward Diffusion of Soil Water

In the soil domain, the distribution of soil water potential is not uniform due to many factors such as the uneven distribution of soil moisture and the heterogeneous soil characteristics. Soil water will diffuse in the soil along the gradient of soil water potential, namely from the location of higher soil water potential to the location of lower soil water potential. If the climate condition is dry and the groundwater table is below the root zone, groundwater of the saturated zone could

diffuse upward into the root zone and be utilized by plants. The amount of upward diffusion of groundwater is affected by the GWTD. This is one important cause for the impact of the GWTD on plant transpiration.

The impacts of precipitation, soil type or HR on upward diffusion of groundwater will be investigated in the following sections. The upward diffusion of soil water through the horizontal plane 0.5 m below the root zone bottom is summed to represent the amount of upward diffusion of groundwater. The depths of the horizontal plane are 5.5 m, 4.5 m and 2.5 m for the vegetation type of tree, shrub and grass, respectively.

5.4.2.1 Impact of Precipitation on Upward Diffusion of Soil Water

Figure 5.7 shows the comparisons of upward diffusion of soil water under three precipitation conditions (P50, P70 and P100) for both HR and no-HR scenarios. The soil type is loam and the vegetation type is tree.

It is shown that the amount of upward diffusion of soil water drops quickly (from about 290 mm per year to about 20 mm per year for the precipitation condition of P50) as the groundwater table declines from the depth of 6 m to the depth of 10 m. When the groundwater table is close to the root zone bottom, the upward diffusion amounts of the three precipitation conditions differ a lot from each other. The upward diffusion increases as precipitation decreases. The upward diffusion amounts are about 120, 220 and 290 mm per year for the P100, P70 and P50 precipitation conditions, respectively. The upward diffusion increases as a result of steeper gradient of soil water potential which is caused by the drier root zone due to lower precipitation. However, when the groundwater table is far below the root zone bottom, the upward diffusion

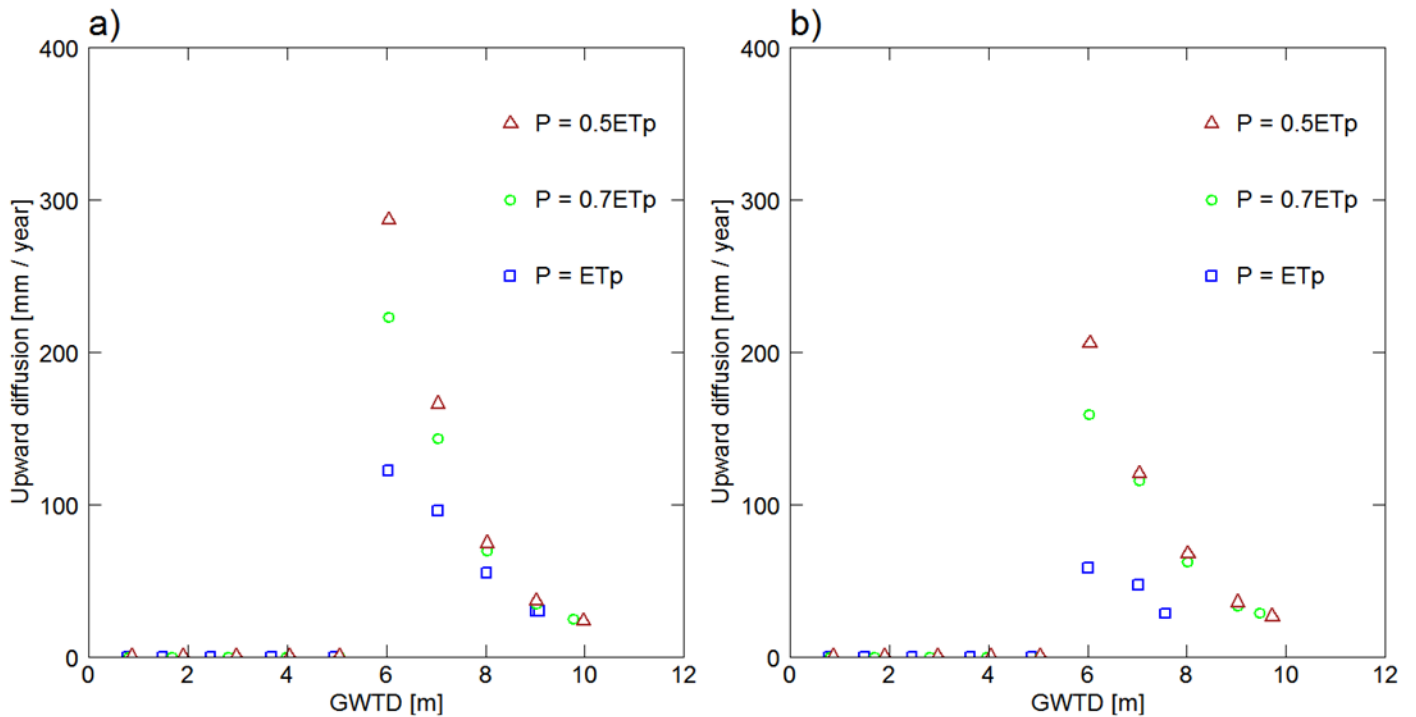


Figure 5.7 Comparisons of upward diffusion of soil water under three precipitation conditions (P50, P70 and P100) for (a) HR scenarios and (b) no-HR scenarios. The soil type is loam and the vegetation type is tree. The upward diffusion occurs at the depth of 5.5m (i.e., 0.5 m below the root zone bottom).

amounts of the three precipitation conditions are similar and very small. For example, the upward diffusion amount is about 20 mm per year as the groundwater table is at the depth of 10 m (i.e., 5 m below the root zone bottom). This result indicates that the link between groundwater and the hydrological processes at surface or shallow subsurface is weak when the groundwater table is deep (i.e., far below the root zone bottom).

Comparing the results of HR scenarios (Figure 5.7a) with those of no-HR scenarios (Figure 5.7b), we can see that the discrepancies in the upward diffusion of different precipitation conditions are smaller when the HR process is not considered in the simulations. This result

indicates that the impacts of HR on the hydrological processes of the subsurface are influenced by the soil moisture of the root zone (or the precipitation condition).

5.4.2.2 Impact of Soil Type on Upward Diffusion of Soil Water

Figure 5.8 shows the comparisons of upward diffusion of soil water among three soil types (i.e., clay, loam and sand) for both HR and no-HR scenarios. The vegetation type is tree and the precipitation condition is P50.

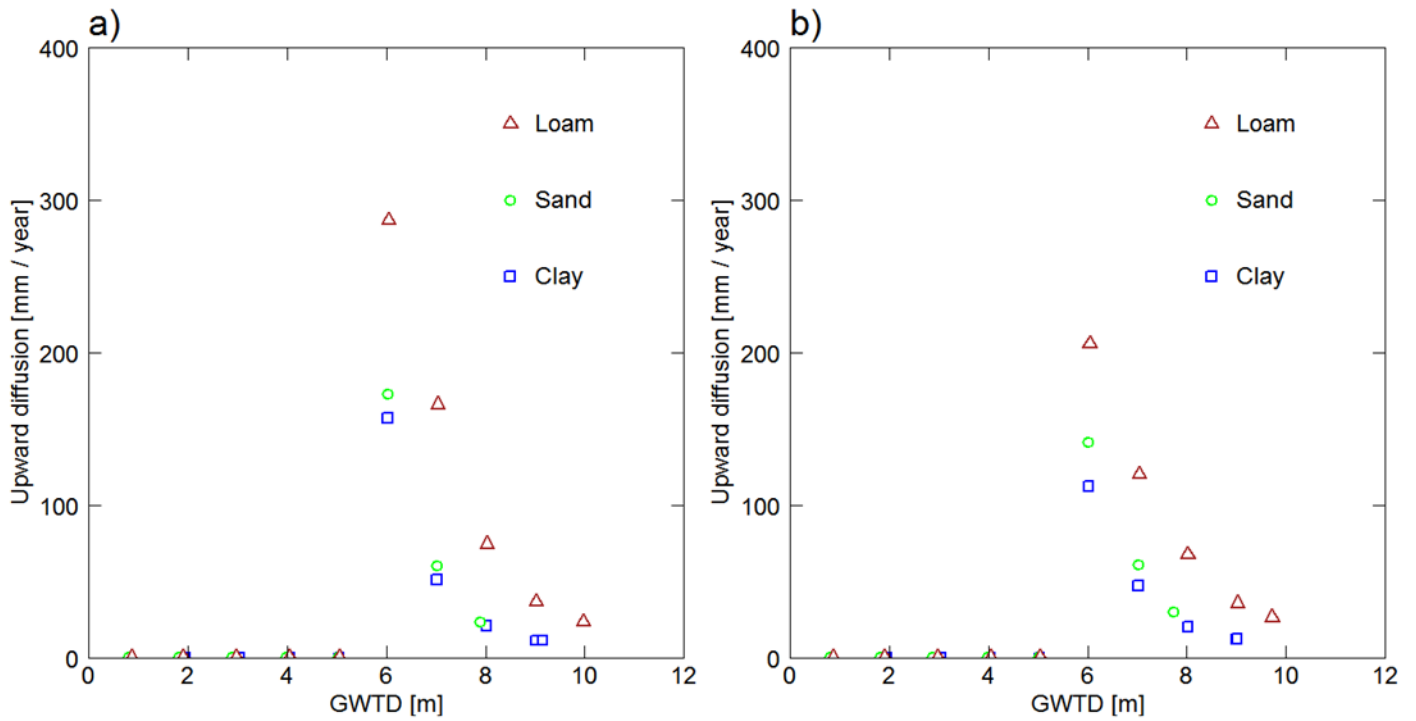


Figure 5.8 Comparisons of upward diffusion of soil water for three soil types (loam, sand and clay): (a) When HR is considered; (b) When HR is not considered. The precipitation condition is P50 and the vegetation type is tree. The upward diffusion occurs at the depth of 5.5m (i.e., 0.5m below the root zone bottom).

Figure 5.8a shows that upward diffusion of the loam scenario is higher than that of the sand scenario, and upward diffusion of the clay scenario is the lowest. The impact of soil

characteristic on upward diffusion of soil water is more evident as the groundwater table is close to the root zone bottom. The upward diffusion amounts are about 290, 170, and 150 mm per year for loam, sand, and clay scenarios, respectively, when the groundwater table is at the depth of 6 m (i.e., 1 m below the root zone bottom). The impact of soil characteristic on upward diffusion of soil water will decrease along with the decline of the groundwater table.

Comparing the results of no-HR scenarios with those of HR scenarios, we can see that the discrepancies in the upward diffusion among the three soil scenarios are smaller when the HR process is not considered. This result indicates that the impacts of HR on the hydrological processes of the subsurface are influenced by the soil characteristics.

5.4.2.3 Impact of HR on Upward Diffusion of Soil Water

Figure 5.9 shows the comparisons of upward diffusion of soil water between HR and no-HR scenarios for three soil types (i.e., clay, loam and sand). The precipitation condition is P50 and the vegetation type is tree.

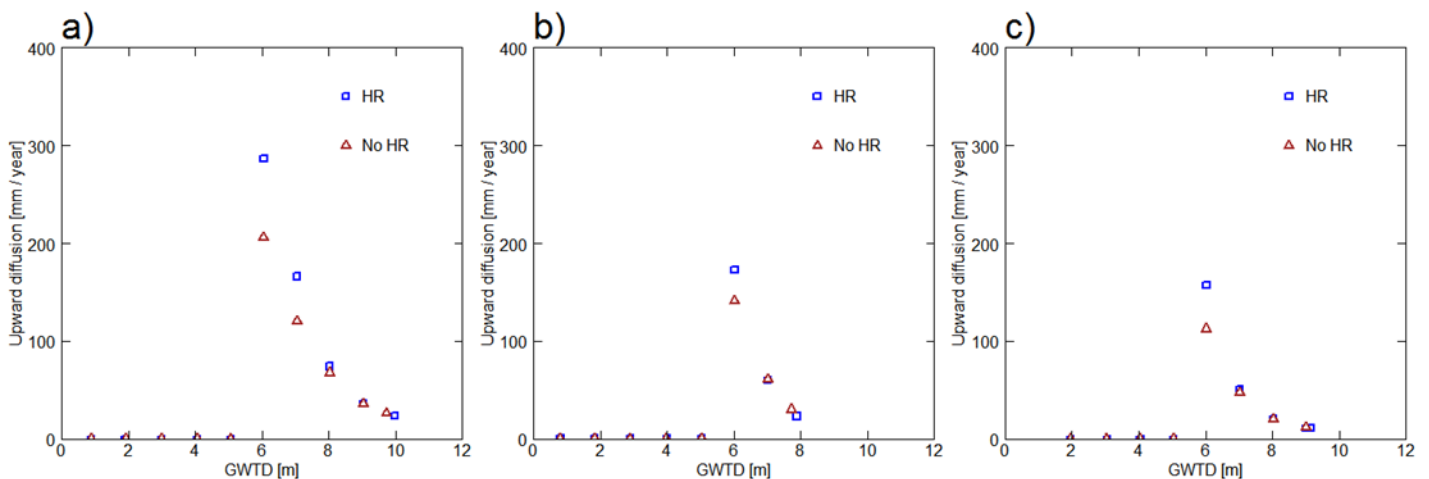


Figure 5.9 Comparisons of upward diffusion of soil water between HR scenarios and no-HR scenarios for three soil types: (a) Loam; (b) Sand; (c) Clay. The precipitation condition is P50 and the vegetation type is tree. The upward diffusion occurs at the depth of 5.5m (i.e. 0.5m below the root zone bottom).

Take Figure 5.9a as an example. The impact of HR on upward diffusion of soil water is evident when the groundwater table is close to the root zone bottom. The upward diffusion amount is increased by HR from about 200 mm/year to about 290 mm/year as the groundwater table is at the depth of 6 m (i.e., 1 m below the root zone bottom). The impact of HR on upward diffusion diminishes quickly as the groundwater table declines. The impact is hard to be observed when the groundwater table is 8 m deep.

The comparisons among Figure 5.9a, Figure 5.9b and Figure 5.9c demonstrate that the impact of HR on upward diffusion of soil water is influenced by soil characteristic. For example, the promotion of upward diffusion by HR is about 90 mm, 30 mm, and 40 mm for the loam scenarios, sand scenarios, and clay scenarios, respectively, when the groundwater table is at the depth of 6 m.

5.4.3 Hydraulically Redistributed Water

Hydraulically redistributed water (HRW) means the water amount released into the soil by roots. The water movement from roots into the soil is one important component of the HR process. The phenomenon of releasing water by roots makes it possible for the HR process to change the distribution of soil water in the subsurface, including the root zone and even the area below the root zone, and thereby exert impacts on the surface and subsurface hydrological processes. Previous discussions demonstrate that the HR process can have impact on the transpiration–GWTD relationships. HRW is one direct and important index for quantifying the HR process. Analyses of HRW are helpful for us to gain more insight into the HR process and understand the effects of HR on other processes.

The impacts of GWTD, precipitation, soil type, or vegetation type on HRW are investigated in the following sections.

5.4.3.1 Impact of Precipitation on Hydraulically Redistributed Water

Figure 5.10 shows the comparisons of HRW – GWTD relationships under three precipitation conditions (i.e., P50, P70, and P100). The comparisons are for HRW of both the shallow root zone (0-1m depth) and the deep root zone (1-5m depth). The vegetation type is tree and the soil type is loam. The impacts of GWTD and precipitation on HRW are illustrated in this figure.

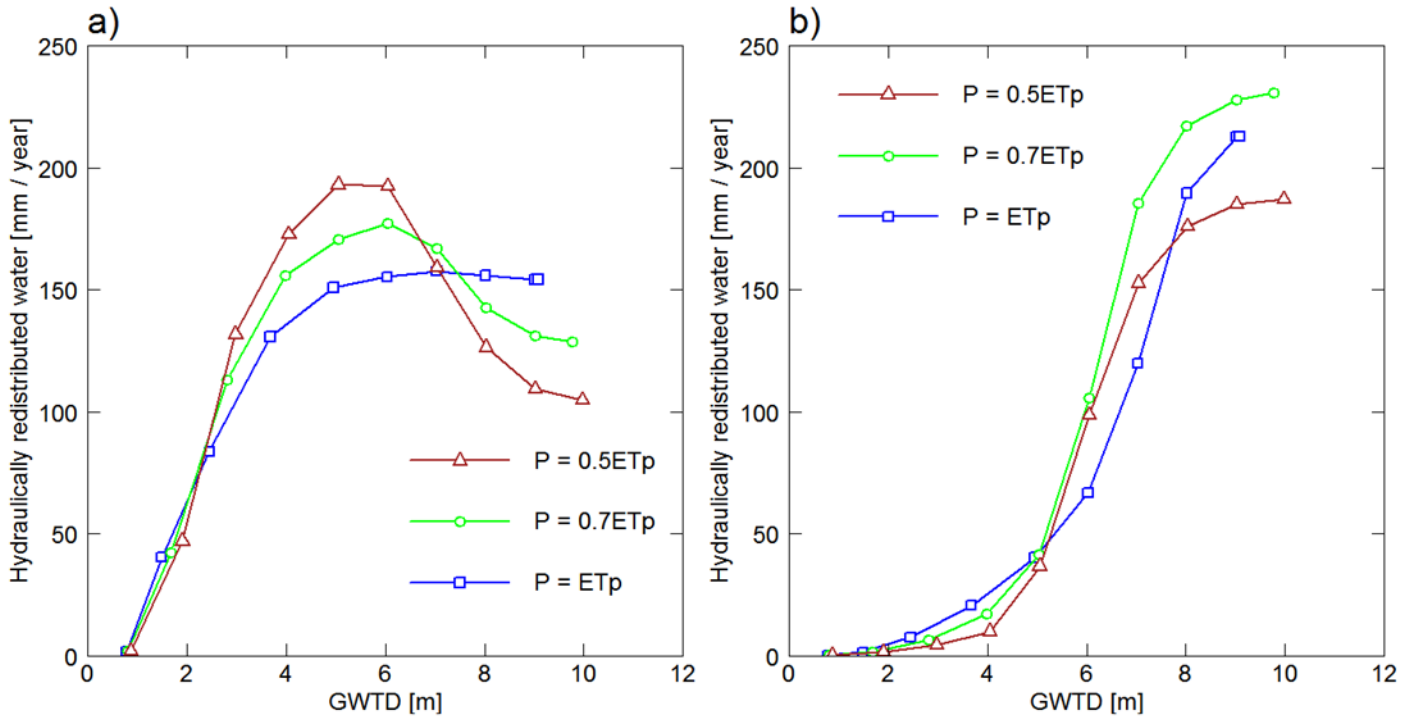


Figure 5.10 Comparisons of hydraulically redistributed water (HRW) – GWTD relationships under three precipitation conditions (P50, P70 and P100) for both (a) the shallow root zone (0-1m depth) and (b) the deep root zone (1-5m depth). The vegetation type is tree and the soil type is loam.

Figure 5.10a shows HRW in the shallow root zone (0-1 m depth), which is the consequence of upward HR. Take the precipitation condition P50 in Figure 5.10a as an example. It is shown that the amount of HRW depends on the GWTD. The HRW amount is close to zero when the GWTD is 1 m. The HRW amount increases as the groundwater table declines and is around the maximum value (about 200 mm/year) when the groundwater table is close to the root zone bottom (i.e., from about 5 to 6 m deep). But as the groundwater table continues to decline, the HRW amount drops abruptly.

When precipitation increases from the condition P50 to the condition P70, the shape of the HRW–GWTD curve maintains similar although differences exist. When the GWTD is from about 3 to 7 m, the HRW amount is lower, as compared with that of the precipitation condition of P50. The main reason is that the shallow layer is wetter due to higher precipitation amount, which reduce the redistribution of groundwater into the shallow layer through roots. When precipitation further increases to be the condition P100 and the GWTD is from about 3 to 7 m, the HRW amount further decreases.

In summary, the above results demonstrate that the upward hydraulic redistribution (HR) is more evident, when the groundwater table is around the root zone bottom. In addition, the upward HRW amount is greater under drier conditions when the groundwater table is around the root zone bottom.

Figure 5.10b shows HRW in the deep root zone (1-5 m depth), which is the consequence of downward HR. Take the precipitation condition P50 in Figure 5.10b as an example. We can see HRW in the deep root zone is affected by the GWTD. The HRW amount is close to zero when the GWTD is smaller than 2 m and increases as the groundwater table declines. The HRW amount increases more quickly as the groundwater table is right below the root zone bottom (i.e.,

from about 5 – 7 m deep) and tends to be stable as the GWTD is larger than 8 m. The amount of HRW in the deep root zone increases as precipitation increases from the condition P50 to the condition P70. The HRW amount in the deep root zone decreases unexpectedly when precipitation increases from the condition P70 to the condition P100 and the GWTD is greater than 5 m.

5.4.3.2 Impact of Soil Type on Hydraulically Redistributed Water

Figure 5.11 shows the comparisons of HRW – GWTD relationships among three soil types (clay, loam and sand) for both the shallow root zone (0 – 1 m depth) and the deep root zone (1 – 5 m depth). The vegetation type is tree and the precipitation condition is P50.

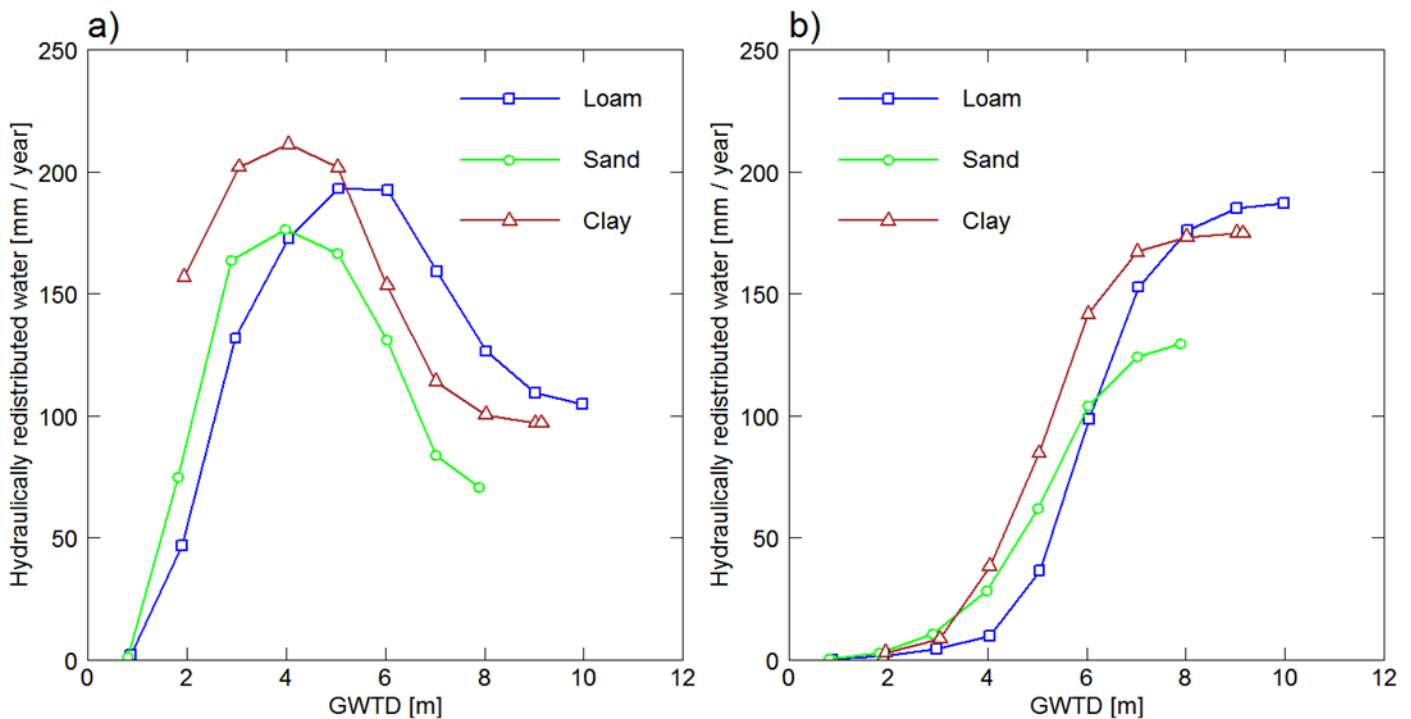


Figure 5.11 Comparisons of HRW – GWTD relationships among three soil types (loam, sand and clay) for both (a) the shallow root zone (0-1m depth) and (b) the deep root zone (1-5m depth). The vegetation type is tree and the precipitation condition is P50.

Figure 5.11a shows that the shape of the HRW–GWTD curves is similar for the three soil types. However, there exist distinct differences among the HRW–GWTD curves of the three soil types. For the soil types of clay and sand, the HRW amount reaches the maximum value when the GWTD is around 4 m. For the soil type of loam, the HRW amount reaches the maximum value when the GWTD is around 6 m. The maximum HRW amounts are 210 mm/year, 190 mm/year and 170 mm/year, respectively, for the soil types of clay, loam and sand. These results illustrate that soil characteristics could distinctly affect the upward HR and thereby the HRW amount in the shallow root zone.

For the deep root zone, the shape of the HRW–GWTD curves of the three soil types is similar (see Figure 5.11b). The HRW amount is close to zero when the groundwater table is shallow and increases as the groundwater table declines. The increase is steeper when the groundwater table declines within a transitional zone. The HRW amount tends to be stable after the groundwater table falls below the transitional zone. However, there are evident differences among the HRW–GWTD curves of the three soil types. The transitional range is from about 5m to 8m for loam scenarios and from about 4m to 7m for sand and clay scenarios. The maximum HRW amounts are about 190 mm/year, 175 mm/year and 130 mm/year, respectively, for the soil types of loam, clay and sand.

5.4.4 Daytime Uptake by Roots

In this section, daytime uptake by roots in both the shallow root zone and the deep root zone will be investigated. Daytime uptake by roots is mainly used to supply transpiration since usually the daytime hydraulic redistribution is not evident. Therefore the analysis of daytime uptake by roots

is helpful for us to understand how the transpiration is affected by other factors (e.g., the GWTD). The impacts of GWTD, precipitation and HR on daytime uptake by roots are analyzed in the following paragraphs.

5.4.4.1 Impact of Precipitation on Daytime Uptake by Roots

Figure 5.12 shows comparisons of Daytime Root Uptake – GWTD relationships under three precipitation conditions (P40, P60 and P100) for both the shallow root zone (0-1m depth) and the deep root zone (1-5m depth). The vegetation type is tree, the soil type is loam and the HR process is considered.

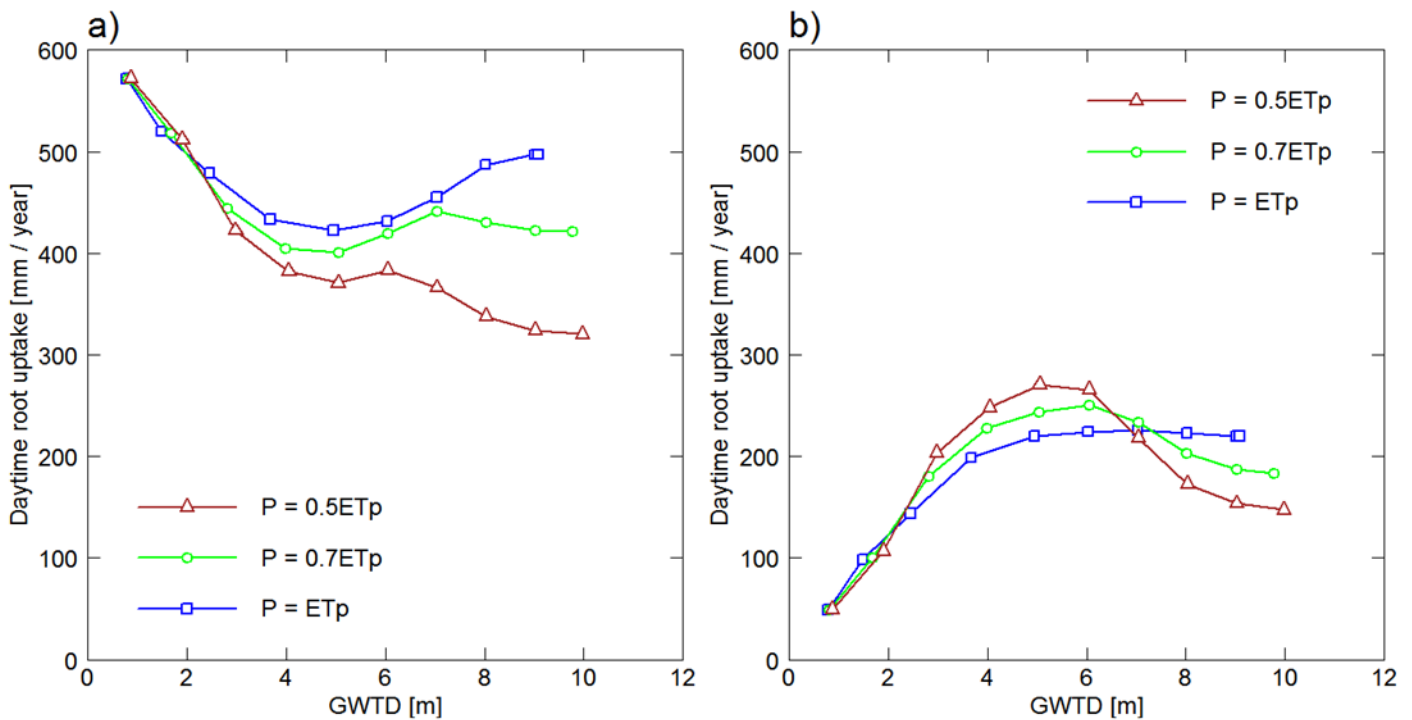


Figure 5.12 Comparisons of Daytime Root Uptake – GWTD relationships under three precipitation conditions (P50, P70 and P100) for both (a) the shallow root zone (0-1m depth) and (b) the deep root zone (1-5m depth). The vegetation type is tree, the soil type is loam and the HR process is considered.

Figure 5.12a shows that daytime root uptake in the shallow root zone becomes higher when precipitation increases and the GWTD is greater than about 2.5 m, especially when the GWTD is greater than 6 m (i.e., more than 1 m below the root zone bottom). The result reveals that plant transpiration is more dependent on precipitation when the groundwater table is comparatively deep. It is also shown in Figure 5.12a that daytime root uptake in the shallow root zone is obviously affected by the GWTD under all the three precipitation conditions (P50, P70 and P100).

Figure 5.12b shows that daytime root uptake in the deep root zone first increases then decreases as the groundwater table declines. This uptake amount is greater when the groundwater table is around the root zone bottom (i.e., the GWTD is from about 3 – 7 m), as compared with conditions of shallower or deeper groundwater table. It is also shown that this uptake amount is higher under drier climatic conditions when the GWTD is from about 3 – 7 m. This result reveals that deep roots play an important role to support plant transpiration under dry climatic conditions when the groundwater table is around the root zone bottom.

The comparison between Figure 5.12a and Figure 5.12b demonstrates that major daytime uptake by roots occurs in the shallow root zone for the three precipitation conditions (P50, P70 and P100).

5.4.4.2 Impact of HR on Daytime Uptake by Roots

Figure 5.13 shows the comparisons of daytime root uptake between HR and no-HR scenarios for both the shallow root zone (0 – 1 m depth) and the deep root zone (1 – 5 m depth). The vegetation type is tree, the soil type is loam and the precipitation condition is P50.

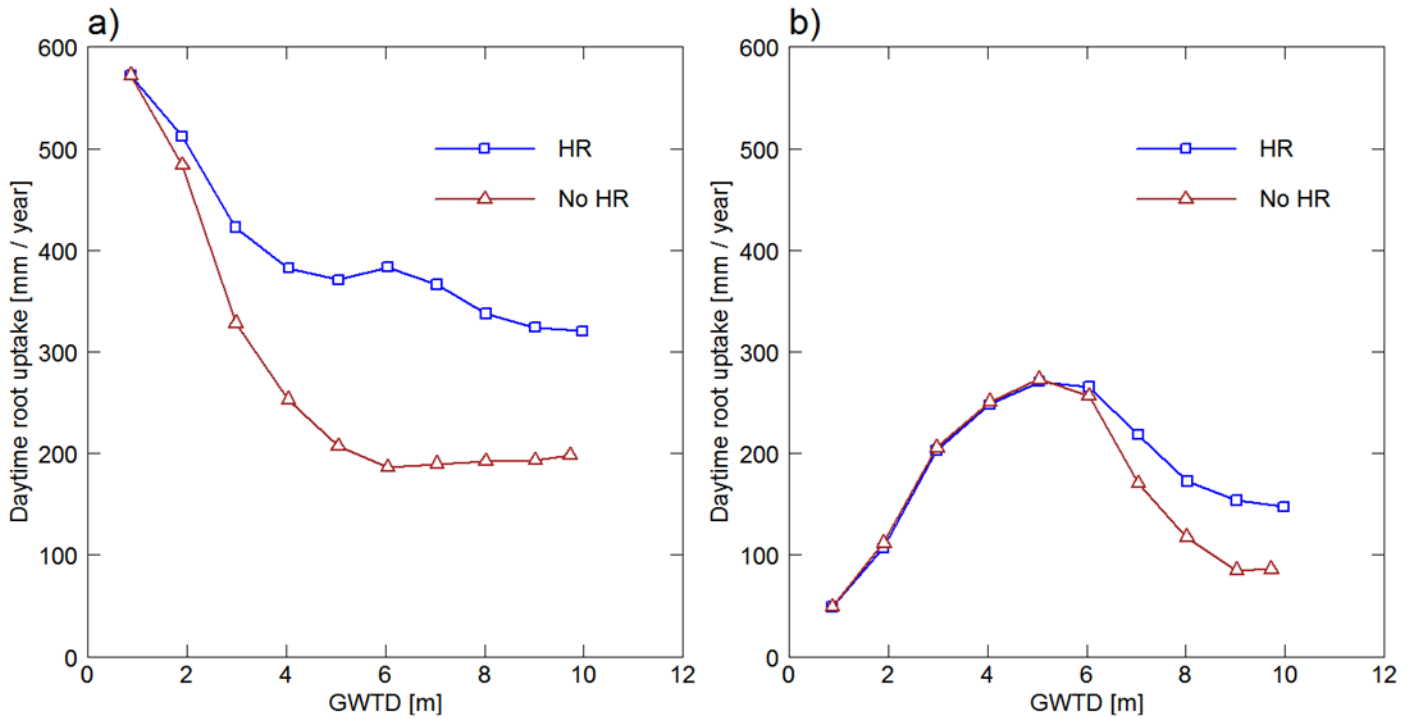


Figure 5.13 Comparisons of daytime root uptake between HR and no-HR scenarios for both (a) the shallow root zone (0-1m depth) and (b) the deep root zone (1-5m depth). The vegetation type is tree, the soil type is loam and the precipitation condition is P50.

In the shallow root zone, the daytime root uptake of HR scenarios is higher than that of no-HR scenarios when the GWTD is greater than about 1 m (Figure 5.13a). The reason is that in HR scenarios soil water is transferred from the deep soil to the shallow soil layer during the nighttime, which facilitates the root uptake in the next day. This is one main reason for the transpiration promotion by HR.

Figure 5.13b shows that the daytime root uptake in the deep root zone of HR scenarios is almost the same as that of no-HR scenarios when the groundwater table is within the root zone (i.e., the GWTD is smaller than 5 m). It is also shown that the daytime uptake by deep roots in

HR scenarios is higher than that of no-HR scenarios, namely the daytime uptake by deep roots is promoted by HR, when the groundwater table falls below the root zone (i.e., the GWTD is greater than 5 m).

5.4.5 Effects of Forcing Type on Transpiration – GWTD Relationship

The Transpiration – GWTD Relationships may be affected by forcing type, for example temporal distribution of precipitation in one year. In order to gain more understanding on the Transpiration – GWTD relationship, the forcing data of the year 2004 at the Duke Forest (US-Dk3) site are used in a group of simulations. Results of this group are compared with results of previous simulations using the forcing data of the Blodgett Forest (US-Blo) site.

For different forcing data, the same vegetation and soil data are used. The precipitation condition P50 is used, namely the annual precipitation is set as 50% of the potential evapotranspiration (ET). For Blodgett forcing data, the potential ET is 740 mm/year and the annual precipitation is set as 370 mm/year. For Duke forcing data, the potential ET is 670 mm/year and the annual precipitation is set as 335 mm/year.

5.4.5.1 Transpiration – GWTD Relationships

Figure 5.14 shows comparisons of Transpiration – GWTD relationships between HR and no-HR scenarios for both the Blodgett forcing data and the Duke forcing data. The vegetation type is tree, the soil type is loam and the precipitation condition is P50.

For different forcing data, the Transpiration – GWTD relationship curves have similar shape, but distinct differences exist. When the groundwater table is comparatively shallow,

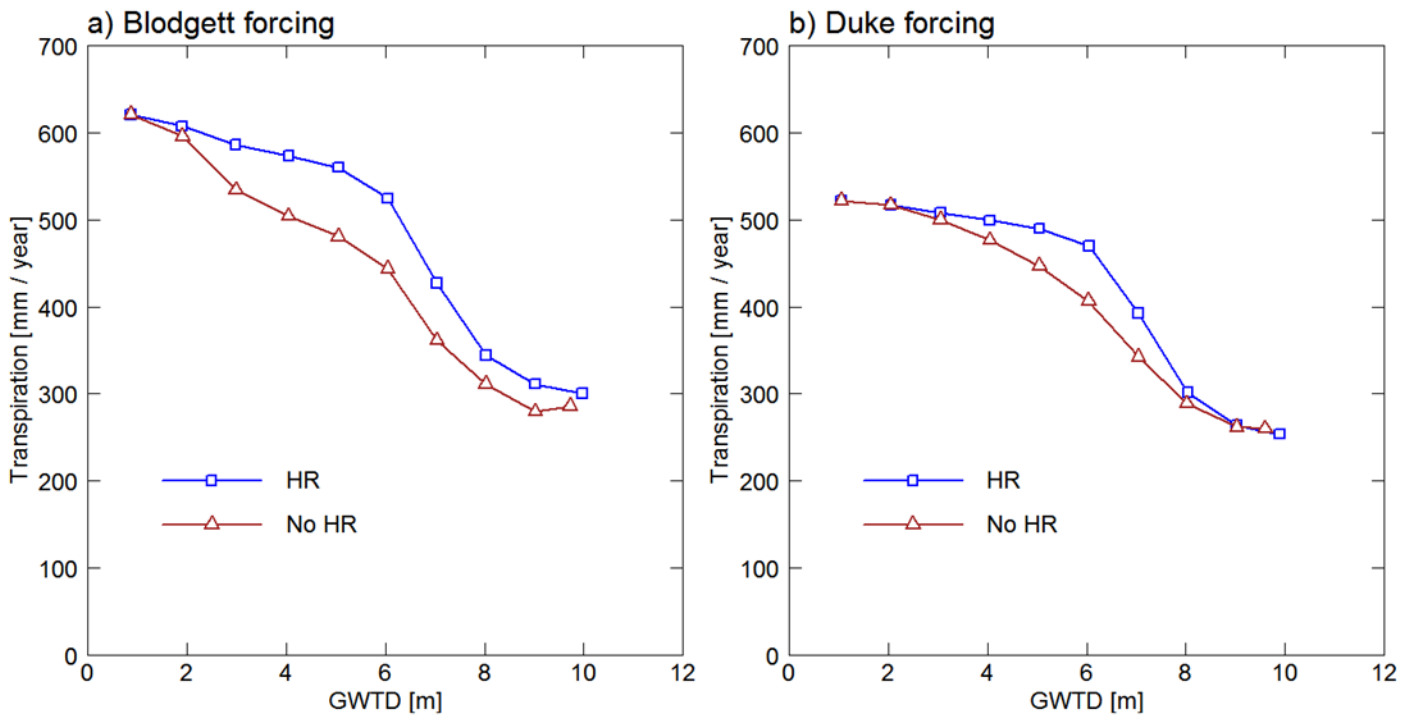


Figure 5.14 Comparisons of Transpiration – GWTD relationships between HR and no-HR scenarios for different forcing data: (a) Blodgett forcing data; (b) Duke forcing data. The vegetation type is tree, the soil type is loam and the precipitation condition is P50.

transpiration is primarily determined by atmospheric conditions and hence transpiration of the Blodgett forcing condition is higher than that of the Duke forcing condition. When the groundwater table is far below the root zone, transpiration is primarily sustained and determined by precipitation. Therefore transpiration of the Blodgett forcing condition is higher than that of the Duke forcing condition.

The comparison between Figure 5.14a and Figure 5.14b shows that the transpiration promotion caused by HR is greater when using Blodgett forcing data, as compared with the results when using Duke forcing data. The reason is analyzed in the following paragraph.

The daily transpiration of HR scenarios is compared with that of no-HR scenarios for both the Blodgett forcing data and the Duke forcing data in Figure 5.15. Figure 5.15a shows that transpiration is promoted by HR during a long period (i.e., from day 170 – day 285). The reason is that there is a long dry summer at the Blodgett site and HR plays a more important role under drier conditions. Figure 5.15b shows that transpiration is promoted by HR in a few short periods since there are only a few short dry periods in one year at the Duke site.

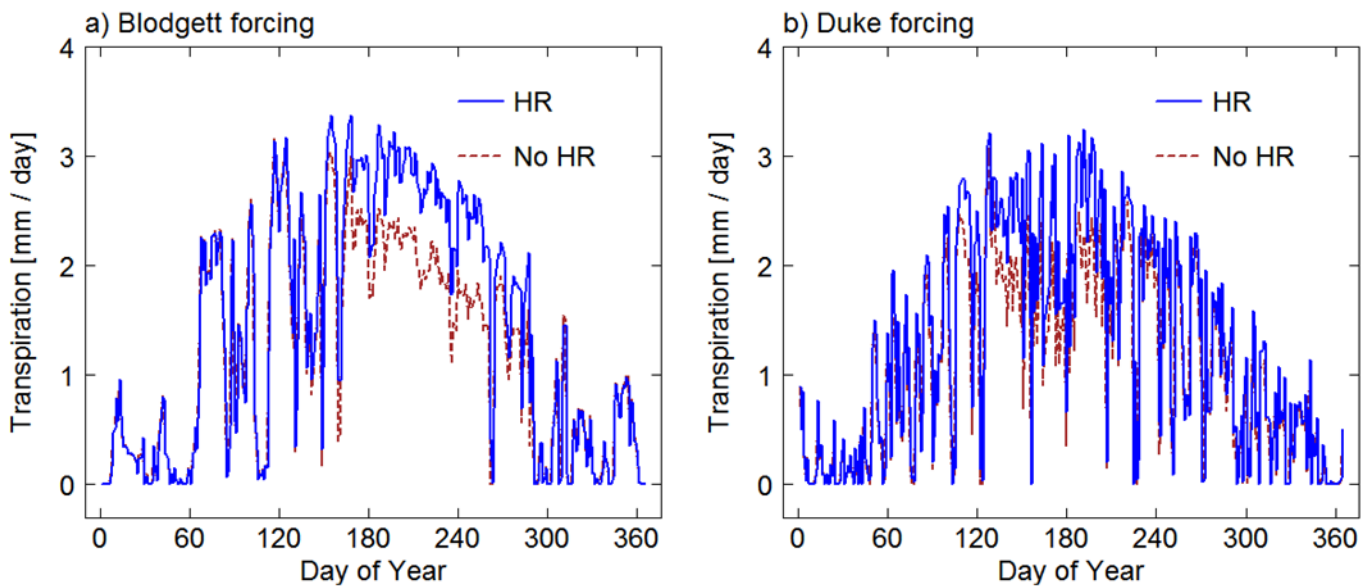


Figure 5.15 Comparisons of daily transpiration between HR and no-HR scenarios for different forcing data: (a) Blodgett forcing data; (b) Duke forcing data. The vegetation type is tree and the soil type is loam. The precipitation condition is P50 and the groundwater table depth is 6 meters.

5.4.5.2 Hydraulically Redistributed Water

Figure 5.16 shows HRW – GWTD relationships for the shallow root zone (0 – 1 m depth) and the deep root zone (1 – 5 m depth) under both the Blodgett forcing condition and the Duke forcing condition.

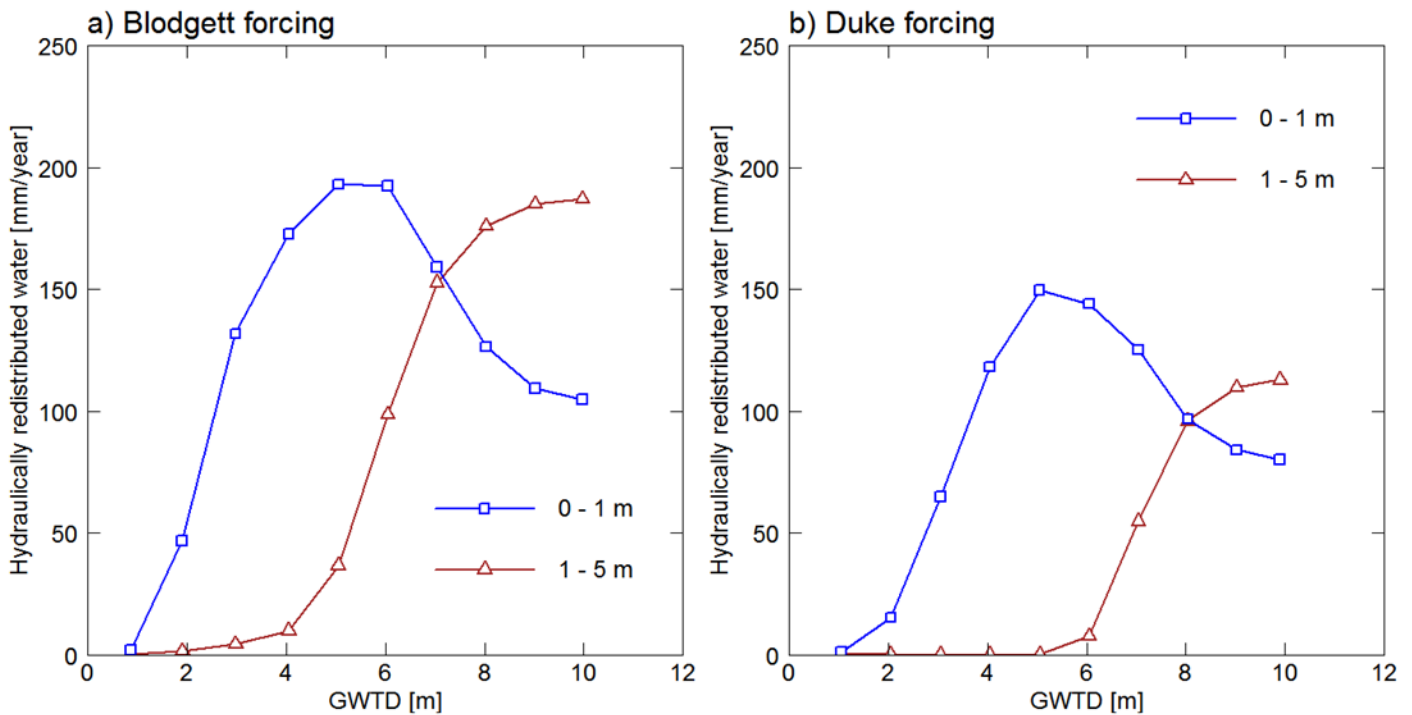


Figure 5.16 HRW – GWTD relationships for the shallow root zone (0-1m depth) and the deep root zone (1-5m depth) under different forcing conditions: (a) Blodgett forcing data; (b) Duke forcing data. The vegetation type is tree, the soil type is loam and the precipitation condition is P50.

For the two forcing conditions, the shape of the HRW – GWTD relationship curves is similar. Large amounts of HRW in the shallow root zone appear as the groundwater table is around the root zone bottom (i.e., the GWTD is from about 5 – 6 m). HRW in the deep root zone reaches large values as the groundwater table is comparatively deep. However, forcing condition has obvious impact on magnitude of HRW. For the Blodgett forcing condition and the Duke forcing condition, the maximum HRW amounts in the shallow root zone are about 190 mm/year and 150 mm/year, respectively; and the maximum HRW amounts in the deep root zone are about 185 mm/year and 120 mm/year, respectively.

Figure 5.17 demonstrates daily values of HRW in the shallow root zone (0-1m depth) and the deep root zone (1-5m depth) under the Blodgett forcing condition and the Duke forcing condition. In both the shallow root zone and the deep root zone, HRW shows different temporal distributions for the two forcing conditions. HRW in the shallow root zone concentrates in the dry summer for the Blodgett forcing condition, and appears in each month for the Duke forcing condition. HRW in the deep root zone concentrates in the wet winter for the Blodgett forcing condition, and appears in several months for the Duke forcing condition. This result shows that forcing condition has significant impact on temporal distribution of HRW in both the shallow root zone and the deep root zone.

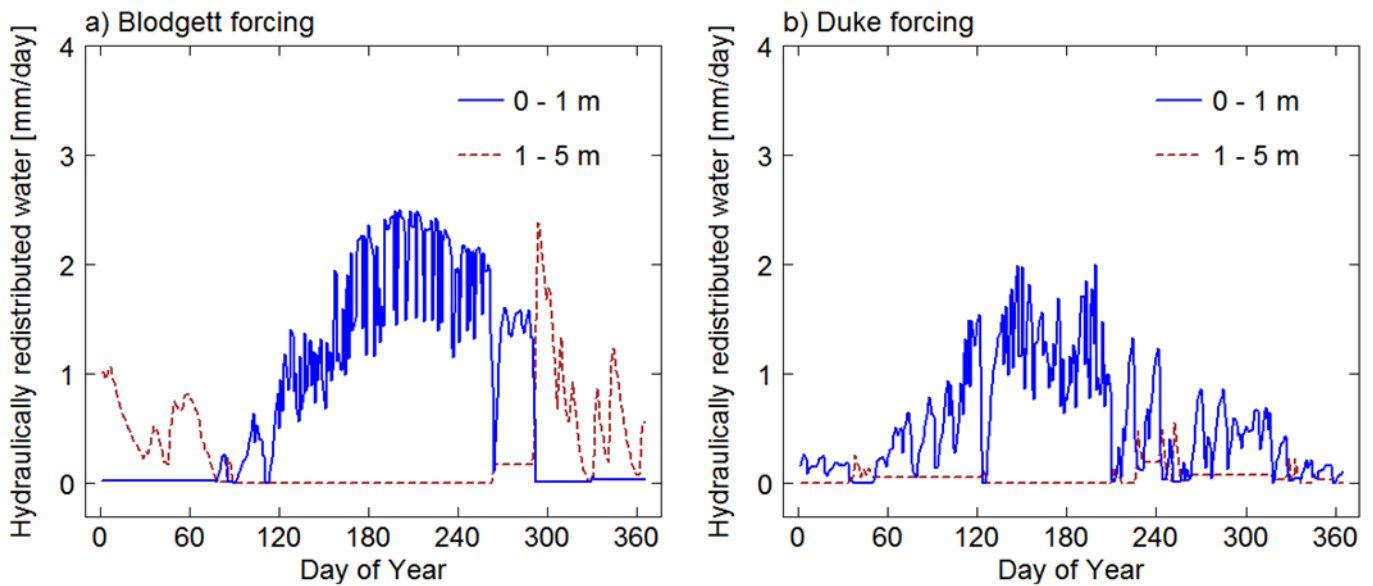


Figure 5.17 Daily HRW of the shallow root zone (0-1m depth) and the deep root zone (1-5m depth) under different forcing conditions: (a) Blodgett forcing data; (b) Duke forcing data. The vegetation type is tree and the soil type is loam. The precipitation condition is P50 and the groundwater table depth is 6 meters.

5.4.5.3 Upward Diffusion of Soil Water

Figure 5.18 shows comparisons of Upward Diffusion – GWTD relationships between HR scenarios and no-HR scenarios for the Blodgett forcing condition and the Duke forcing condition.

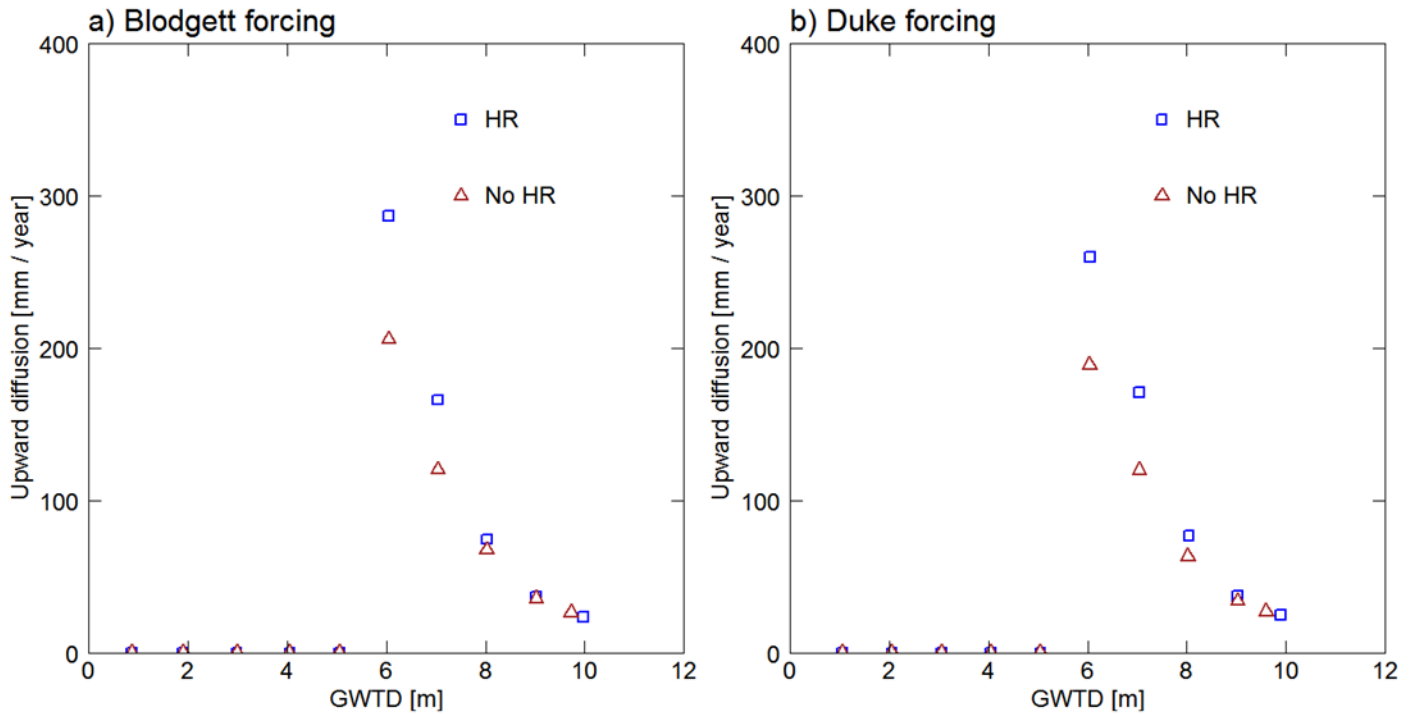


Figure 5.18 Comparisons of Upward Diffusion – GWTD relationships between HR scenarios and no-HR scenarios for different forcing conditions: (a) Blodgett forcing data; (b) Duke forcing data. The vegetation type is tree, the soil type is loam and the precipitation condition is P50. The upward diffusion occurs at the depth of 5.5m (i.e. 0.5m below the root zone bottom).

Comparison between Figure 5.18a and Figure 5.18b reveals that upward diffusion of soil water under the Blodgett forcing condition is slightly higher than that of the Duke forcing condition for both HR scenarios and no-HR scenarios. The increase of upward diffusion caused

by HR under the Blodgett forcing condition is similar to that of the Duke forcing condition. These results reveal that forcing condition does not have significant impact on upward diffusion of soil water.

Figure 5.19 shows daily upward diffusion of soil water for HR scenarios and no-HR scenarios under the Blodgett forcing condition and the Duke forcing condition. Upward diffusion of soil water fluctuates in one year and tends to be higher during the dry season. Comparison between Figure 5.19a and Figure 5.19b shows that forcing condition does not obviously affect upward diffusion of soil water at the daily scale for both HR and no-HR scenarios.

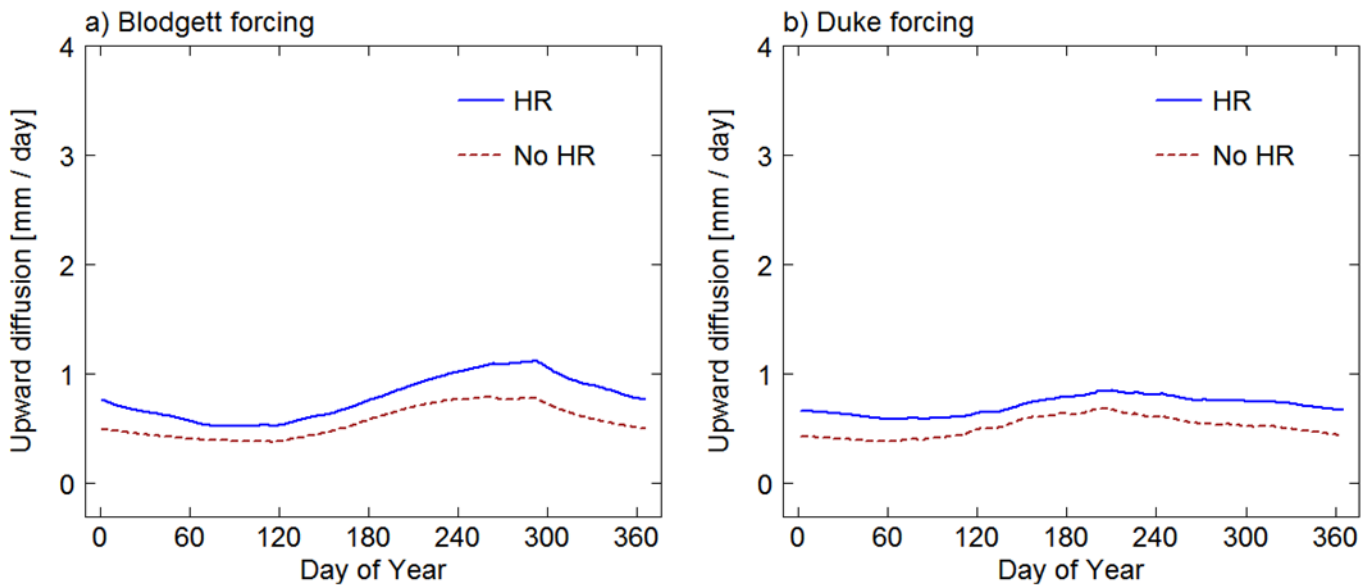


Figure 5.19 Comparisons of daily upward diffusion of soil water between HR scenarios and no-HR scenarios for different forcing conditions: (a) Blodgett forcing data; (b) Duke forcing data. The vegetation type is tree and the soil type is loam. The precipitation condition is P50 and the groundwater table depth is 6 meters. The upward diffusion occurs at the depth of 5.5m (i.e. 0.5m below the root zone bottom).

5.4.5.4 Daytime Uptake by Roots

Figure 5.20 shows Daytime Root Uptake – GWTD relationships for the shallow root zone (0-1m depth) and the deep root zone (1-5m depth) under the Blodgett forcing condition and the Duke forcing condition.

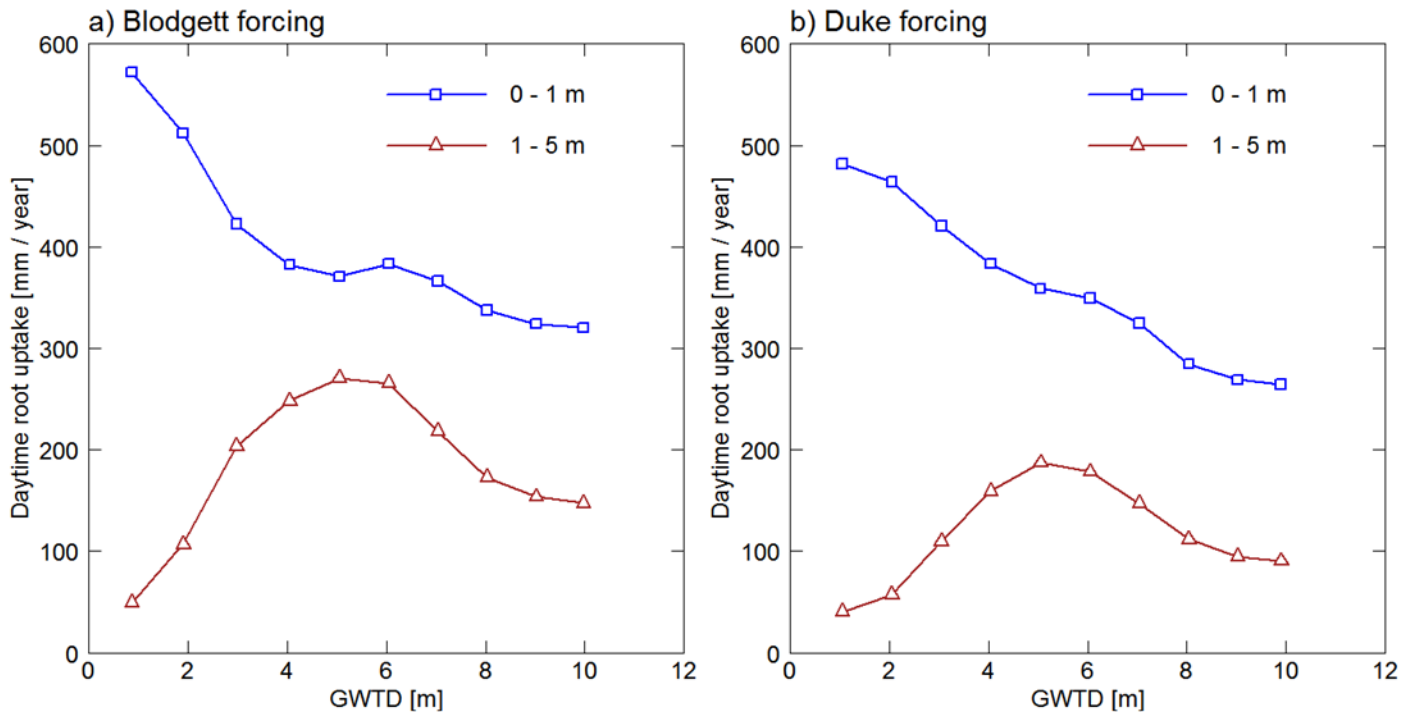


Figure 5.20 Daytime Root Uptake – GWTD relationships for the shallow root zone (0-1m depth) and the deep root zone (1-5m depth) under different forcing conditions: (a) Blodgett forcing data; (b) Duke forcing data. The vegetation type is tree and the soil type is loam. The precipitation condition is P50 and the HR process is considered.

For both the shallow root zone and the deep root zone, Daytime Root Uptake – GWTD relationship curves of the two forcing conditions have the similar shape. In general, daytime root uptake of the Blodgett forcing condition is higher than that of the Duke forcing condition due to the higher transpiration of the former case.

Figure 5.21 demonstrates daily daytime uptake by roots in the shallow root zone (0-1m depth) and the deep root zone (1-5m depth) under the Blodgett forcing condition and the Duke forcing condition. Daytime root uptake in the deep root zone shows different temporal distribution for the two forcing conditions. Under the Blodgett forcing condition, daytime uptake by deep roots is prominent in the dry summer and almost does not appear in the wet winter. For about three months of the dry summer, daytime uptake by deep roots is higher than that by shallow roots. This result demonstrates that deep roots can play a significant role in the dry season. Under the Duke forcing condition, daytime uptake by deep roots appears in each month of the year and is almost always lower than daytime uptake by shallow roots.

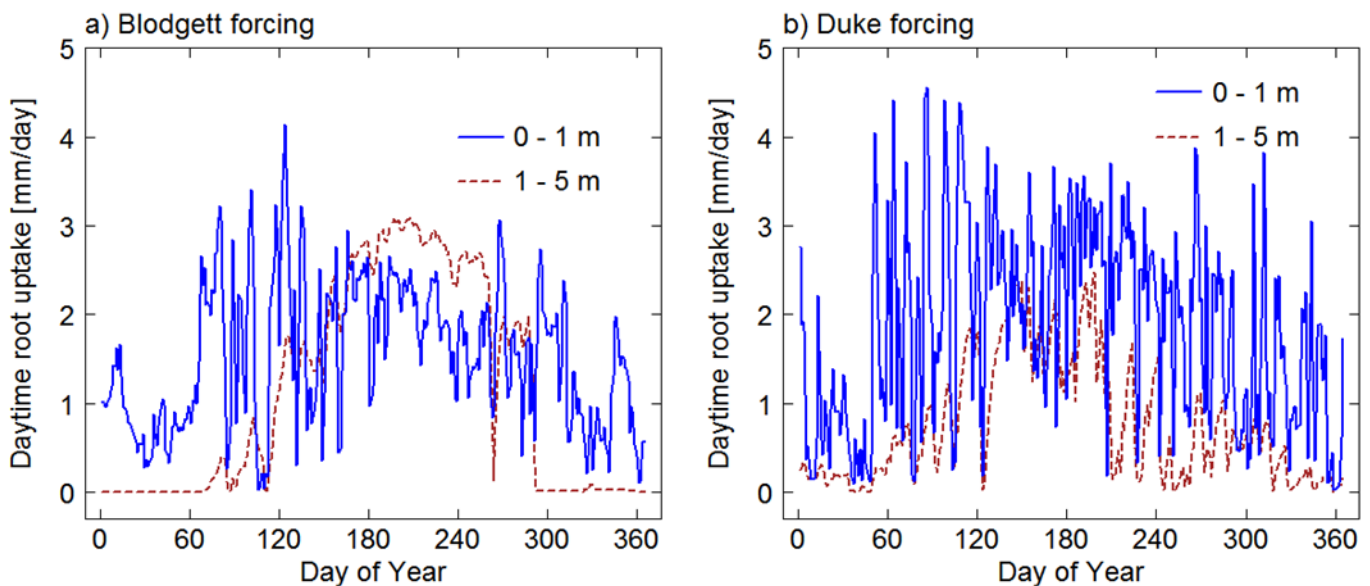


Figure 5.21 Daily daytime uptake by roots for the shallow root zone (0-1m depth) and the deep root zone (1-5m depth) under different forcing conditions: (a) Blodgett forcing data; (b) Duke forcing data. The vegetation type is tree and the soil type is loam. The precipitation condition is P50 and the groundwater table depth is 6 meters. The HR process is considered.

5.5 SUMMARY

Transpiration–GWTD relationships are investigated based on results of a series of scenario simulations which represent different combinations of precipitation conditions, vegetation types, soil types, GWTDs and the treatment of the HR process. The impacts of precipitation condition, vegetation type, soil type and the HR process on the transpiration–GWTD relationship are analyzed. Under the dry precipitation conditions, the impacts of vegetation type, soil type and the HR process on the transpiration–GWTD relationship are evident.

(1) Characteristics of the Transpiration–GWTD curves

The transpiration–GWTD curves of HR scenarios are different from those of no-HR scenarios (e.g., Figure 5.4a). For HR scenarios, the transpiration descent is small while the groundwater table declines within the root zone. In the curve there is a distinct transitional range where transpiration drops abruptly as the groundwater table declines. The location of the transitional range depends on the vegetation type and the soil type. When the groundwater table is lower than the transitional range, transpiration will descend slowly along with the decline of the groundwater table. At this stage, transpiration is mainly sustained and controlled by precipitation and receives less and less supply from groundwater as the groundwater table declines. Transpiration and groundwater tend to be disconnected.

For no-HR scenarios, transpiration descends more quickly while the groundwater table declines within the root zone. In the curve there is no distinct transitional range. However, transpiration and groundwater still tend to be disconnected as the groundwater table declines to be far below the root zone.

(2) Impact of vegetation type on the Transpiration–GWTD curves

The shape of the transpiration–GWTD curves for different vegetation types is similar (e.g., Figure 5.2). But there exist discrepancies among these curves. When the groundwater table is within the root zone, evident differences exist in transpiration of different vegetation types. These differences are mainly caused by discrepancies in transpiration capabilities of different vegetation types since plants can acquire sufficient water supply from groundwater and the actual transpiration is close to the potential transpiration. When the groundwater table declines away from the root zone, the transpiration differences among different vegetation types will decrease since transpiration is more constrained by available soil water. When the groundwater table is far below the root zone bottom, transpiration of different vegetation types is similar. This phenomenon suggests that groundwater utilization by plants is very small and transpiration and groundwater are almost disconnected. Transpiration is mainly sustained and hence controlled by precipitation.

(3) Impact of soil type on the Transpiration–GWTD curves

The impact of soil type on the transpiration–GWTD curves in HR scenarios are different from the impact in no-HR scenarios (Figure 5.3). When the groundwater table is within the root zone, the transpiration–GWTD curves of different soil types are close to each other for HR scenarios (Figure 5.3a); for no-HR scenarios, transpiration of loam scenarios is higher than that of sand and clay scenarios (Figure 5.3b).

When the groundwater table is within the transitional range of those transpiration–GWTD curves, the impact of soil type on transpiration is evident for HR scenarios (Figure 5.3a). The examination of subsurface hydrological processes shows that the upward diffusion of soil

water from groundwater to the root zone and the hydraulically redistributed water (HRW) in the shallow root zone are affected by soil characteristics, which helps to explain the differences in transpiration of different soil scenarios.

(4) Impact of HR on the Transpiration–GWTD curves

The promotion of transpiration caused by the HR process varies with the GWTD (e.g., Figure 5.4a). The promotion of transpiration by HR is very small as the groundwater table is close to the ground surface and increases as the groundwater table declines. The transpiration promotion by HR is most evident as the groundwater table is around the root zone bottom (i.e., the GWTD is about 5 m). But when the groundwater table further declines, the impact of HR on transpiration will decrease.

Transpiration is promoted by HR due to the mechanism that the upward HR process can transfer soil water from the deep soil to the shallow soil layer. So examining the amount of hydraulically redistributed water in the shallow root zone is helpful to understand the impact of HR on transpiration. The HRW amount in the shallow root zone follows the similar rule (e.g., Figure 5.10a). The HRW amount is comparatively small as the groundwater table is very shallow or far below the root zone, and reaches large values when the groundwater table is close to the root zone bottom.

The upward HR process increases the soil moisture in the shallow soil layer where most roots concentrated and facilitate the root uptake during the daytime. So the daytime uptake by roots in the shallow root zone also reflects the impact of HR on transpiration. The comparison of the daytime uptake between the HR and no-HR scenarios reveals that the impact of HR on transpiration is most prominent when the groundwater table is below and close to the root zone bottom (Figure 5.13a).

(5) Upward diffusion of groundwater

Under dry climate conditions, plant transpiration is more obviously affected and controlled by soil moisture in the root zone, which is influenced by subsurface hydrological processes, including water diffusion in the soil. When the groundwater table is below the root zone, groundwater could diffuse upward from the saturated zone into the root zone and be utilized by plants.

The simulation results show that the upward diffusion of groundwater (also abbreviated as “upward diffusion” hereinafter) is sensitive to the GWTD (e.g., Figure 5.7). When the groundwater table is close to the root zone bottom, the amount of upward diffusion is evident. In this situation, upward diffusion can also be advanced by HR obviously (Figure 5.9). This is one of the reasons why the transpiration can be promoted by HR. In addition, the climate condition also has impact on the amount of the upward diffusion. Lower the precipitation, higher the amount of the upward diffusion (Figure 5.7).

The amount of upward diffusion drops abruptly when the groundwater table declines away from the root zone (e.g., Figure 5.7). When the groundwater table is more than 3~5m away from the root zone bottom, the upward diffusion is weak and the root zone is almost disconnected from groundwater.

The impacts of precipitation and HR on the upward diffusion also diminish as the groundwater table declines (Figure 5.7 and Figure 5.9). When the groundwater table is more than 2~3m away from the root zone bottom, neither precipitation nor HR has notable impact on the upward diffusion of groundwater.

(6) Impacts of forcing condition on Transpiration – GWTD curves and subsurface processes

Comparisons of results of simulations using two sets of forcing data show the impacts of forcing condition on Transpiration – GWTD relationships and subsurface processes. For different forcing data, the Transpiration – GWTD relationship curves have similar shape (Figure 5.14). Transpiration amount is obviously affected by forcing condition. HR plays a more important role under forcing condition with longer dry period.

Forcing condition has evident impacts on amounts and temporal distribution of hydraulically redistributed water (HRW) in both the shallow root zone and the deep root zone (Figure 5.16 and Figure 5.17). However, forcing condition does not have significant impact on upward diffusion of soil water (Figure 5.18 and Figure 5.19).

Forcing condition also affects amounts and temporal distribution of daytime root uptake in both the shallow root zone and the deep root zone (Figure 5.20 and Figure 5.21). Deep roots can play a significant role under forcing condition with a long dry period (Figure 5.21a).

6.0 DYNAMIC REPRESENTATION OF VEGETATION

6.1 INTRODUCTION

Plants play an important role in water, energy and nutrient (e.g., C, N, etc.) cycles in the soil-plant-atmosphere continuum. On the other hand, the environment (e.g., climatic conditions, soil, etc.) exerts influence on plants and affects their growth. At the same time, dynamic variation of vegetation sends feedback to the environment. Therefore, it is significant to dynamically represent vegetation in some modeling studies, for example, to predict interactions between land surface and atmosphere in the future. In this study, dynamic growth of vegetation is represented in the CASACNP biogeochemical model. This biogeochemical model is weak in representations of water and energy cycles, which are strengths of land surface models. Coupling of a biogeochemical model and a land surface model is favorable to representing interactions between water, energy and biogeochemical cycles, as well as interactions between vegetation and the environment. Therefore the CASACNP biogeochemical model has been coupled with the VIC+ model. This coupled model is used to conduct scenario simulations to demonstrate impacts of vegetation on water and energy cycles when dynamic growth of vegetation is represented.

6.2 CASACNP BIOGEOCHEMICAL MODEL

The CASACNP biogeochemical model is used to describe the carbon (C), nitrogen (N) and phosphorus (P) cycles in terrestrial ecosystems. This model has been used to estimate carbon storage of terrestrial ecosystems under nitrogen and phosphorus limitations at the global scale [Wang *et al.*, 2010b]. The early version of the CASACNP model is the CASA model which is used to describe the terrestrial carbon cycle [Randerson *et al.*, 1997]. CASA is an offline model and uses satellite derived net primary productivity (NPP) as its input. Fung *et al.* [2005] developed the CASA' model based on the CASA model. The CASA' model is coupled with a land surface model, and uses net primary productivity produced by the land surface model as its input. The CASA' model has been used to study global carbon-climate feedback. The CASA' model has been coupled with the nitrogen and phosphorus cycle model developed by Wang *et al.* [2007] and Houlton *et al.* [2008] to form the CASACNP model [Wang *et al.*, 2010b].

In the CASACNP model, the terrestrial ecosystem consists of plants, litter and soil. Carbon, nitrogen and phosphorus are stored in different pools of plants, litter and soil, and can flow from one pool to another pool. Plant consists of leaf pool, root pool and wood pool. Litter consists of metabolic litter pool, structural litter pool and coarse woody debris pool. Soil consists of microbial biomass pool, slow pool and passive pool. In addition, in the soil there are one inorganic nitrogen pool and three phosphorus pools (i.e., labile phosphorus, sorbed phosphorus and occluded phosphorus).

The carbon cycle calculation is based on CASA' model [Fung *et al.*, 2005]. Change of carbon pool size depends on turnover rate, fractions of net primary productivity allocated to plant pools, transfer rates between different pools and nitrogen limitation on litter decomposition. The carbon cycle calculation needs input such as nutrient unlimited net primary productivity and

initial carbon pool size. This calculation produces nutrient limited net primary productivity, soil respiration, net ecosystem carbon exchange and model pool sizes.

The nitrogen (N) cycle calculation is based on the model developed by Wang et al. [2007]. Change of N pool size depends on coefficients for allocation of N uptake to different plant pools, root N uptake, the N resorption coefficient, the N:C ratio of the structural litter pool, the N-limiting factor of carbon decomposition, the N deposition rate, the N fixation rate, the fertilizer N addition rate, the net N mineralization rate and the N loss rate. The nitrogen cycle is coupled with the carbon cycle; carbon decomposition and gross N mineralization is coupled by the N:C ratios of the substrates. When the gross N mineralization rate is less than the N immobilization rate, the litter carbon decomposition rate is reduced. The N cycle calculation needs input such as atmospheric N deposition (both wet and dry), N fertilizer application, N fixation. Output of the calculation includes N leaching and gaseous loss.

The phosphorus (P) cycle calculation is based on the model of Wang et al. [2007] and Houlton et al. [2008]. Change of P pool size depends on coefficients for allocation of P uptake to different plant pools, plant P uptake, the P resorption coefficient, the maximum amount of sorbed P, the constant for the adsorption, the net biological P mineralization, dust P deposition, fertilizer P addition, the P weathering rate, the plant P uptake rate, P loss rates and the biochemical P mineralization rate. The P cycle calculation needs input such as weathering, deposition and fertilizer application. Output of the calculation includes leaching loss of labile P and loss of strongly sorbed P to the occluded P.

In the CASACNP model, net primary productivity (NPP) is limited by nutrient (i.e., N and P). Both nutrient concentration limiting and nutrient uptake limiting are considered. The nutrient concentration limiting factor is based on N:C and P:C ratios of leaf biomass. The

nutrient uptake limiting factor is based on the amount of mineral N in soil, the amount of labile P in soil and the minimal amounts of N and P uptake needed to sustain a given NPP. Therefore, NPP can be limited by nutrient when leaf N:C or P:C changes or soil nutrient supply cannot satisfy plant demand.

6.3 COUPLING CASACNP MODEL WITH VIC+ MODEL

In this study, the CASACNP model has been coupled with the VIC+ model. The simulated results of soil moisture, soil temperature and net primary productivity (NPP) produced by the VIC+ model are used as input by the CASACNP model. In addition, some forcing data (i.e., air temperature) used by the VIC+ model is also an input to the CASACNP model. The modeled leaf area index (LAI) results given by the CASACNP model are used by the VIC+ model.

The coupling between the CASACNP model and the VIC+ model reflects the interactions between the water cycle, the energy cycle and the biogeochemical cycle. For example, soil moisture and soil temperature results from the VIC+ model influence soil respiration, decomposition of organic carbon pools and plant growth in the CASACNP model. On the other hand, leaf area index (LAI) from the CASACNP model has impact on water, energy and carbon calculation in the VIC+ model. For example, LAI can affect interception of precipitation. LAI also affects photosynthesis, plant transpiration and hence latent heat flux.

6.4 SCENARIO SIMULATIONS

In this study, four scenario simulations have been conducted to demonstrate the interactions between the water cycle, the energy cycle and the biogeochemical cycle, as well as to show how the dynamic representation of vegetation affects the water and energy cycles.

The setup of the four scenarios is shown in the following table.

Table 6.1 Setup of scenarios for studying impacts of dynamic vegetation

Scenario No.	Model	Precipitation Condition
1	VIC+ model	Observed precipitation
2	VIC+ model + CASACNP model	Observed precipitation
3	VIC+ model	Observed precipitation * 60%
4	VIC+ model + CASACNP model	Observed precipitation * 60%

Two kinds of models are used: VIC+ model and the coupled model (i.e., the VIC+ model coupled with the CASACNP model). The observed leaf area index (LAI) data is used when using the VIC+ model alone (Figure 6.1). When using the coupled model, the modeled LAI results from the CASACNP model are used by the VIC+ model. Two kinds of precipitation conditions are used: observed precipitation data and decreased precipitation. The decreased precipitation condition means that observed precipitation values are reduced by 40% for each time step in the simulations.

The modeled transpiration results of the VIC+ model are compared to those of the coupled model under the observed precipitation condition and the decreased precipitation condition, respectively. The comparisons demonstrate impacts of dynamic vegetation on plant transpiration.

Under the observed precipitation condition, LAI values modeled by CASACNP are close to the observed data (Figure 6.1). The modeled LAI values are slightly lower or higher than the observed data for a few time periods. That is, LAI values used in Scenario 2 (where the coupled model is used) are close to those of Scenario 1 (where the VIC+ model is used). Figure 6.2 shows that transpiration results of Scenario 2 are also close to those of Scenario 1 although for most months the former is slightly lower than the latter. These results show that the coupled model can produce plant transpiration results similar to those of the VIC+ model.

Figure 6.3 shows that under the decreased precipitation condition, LAI values modeled by CASACNP are obviously lower than the observed LAI data during the latter part of the year. The observed LAI data is corresponding to the observed precipitation condition. Therefore it is shown that the CASACNP model can capture the response of vegetation to water-limited conditions. The dynamic variations of vegetation affect water and energy cycles in the soil-plant-atmosphere continuum. Figure 6.4 shows that the transpiration values produced by the coupled model (where the LAI values are provided by the CASACNP model) are obviously lower than those of the VIC+ model (where the observed LAI values are used) for most months of the year. The annual transpiration amount of the coupled model is 411 mm/year, which is 6.8% lower than that of the VIC+ model (441 mm/year). Decreases in plant transpiration can result in decreases of latent heat flux and thereby affect the energy cycle.

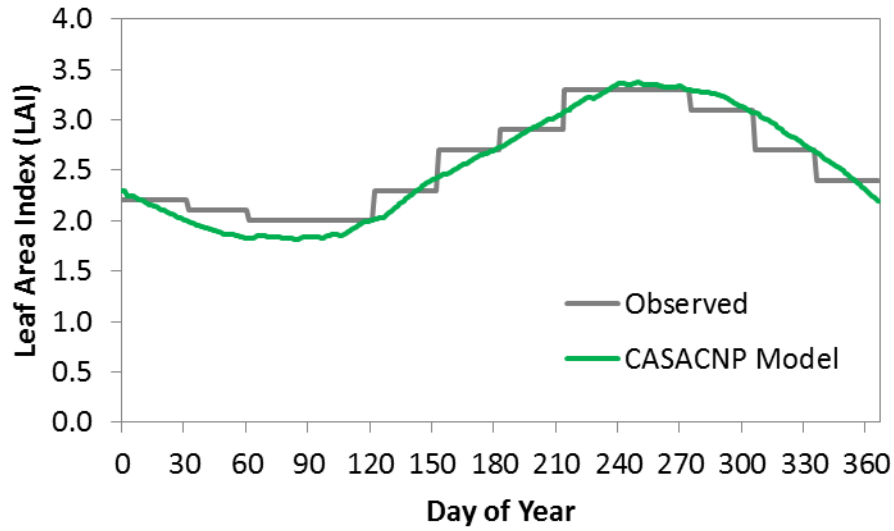


Figure 6.1 Comparison of observed leaf area index (LAI) to simulated results from the CASACNP model when using the observed precipitation data

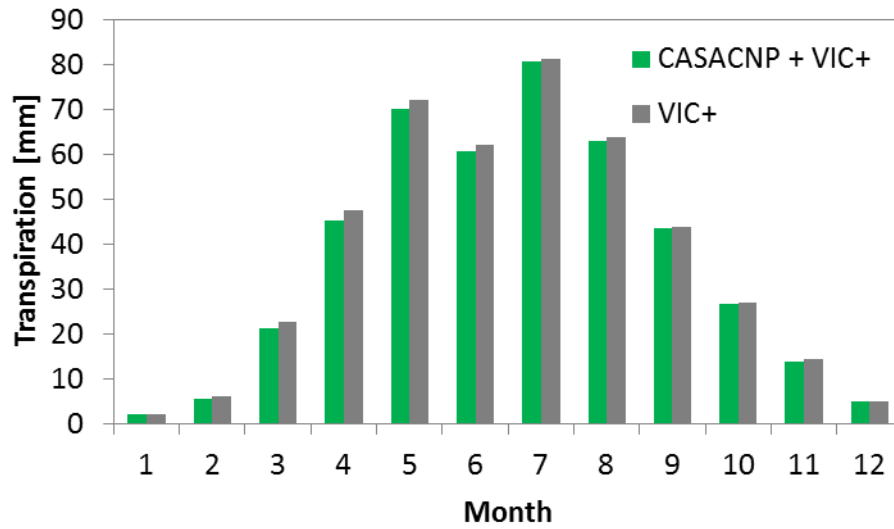


Figure 6.2 Comparison of transpiration modeled by VIC+ to that of the coupled model (CASACNP + VIC+) when using the observed precipitation data

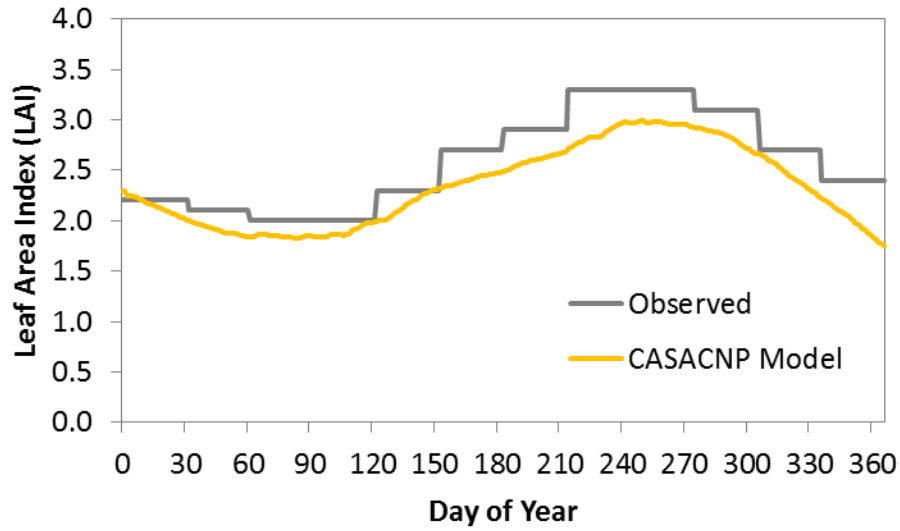


Figure 6.3 Comparison of observed leaf area index (LAI) to simulated results from the CASACNP model when using the decreased precipitation

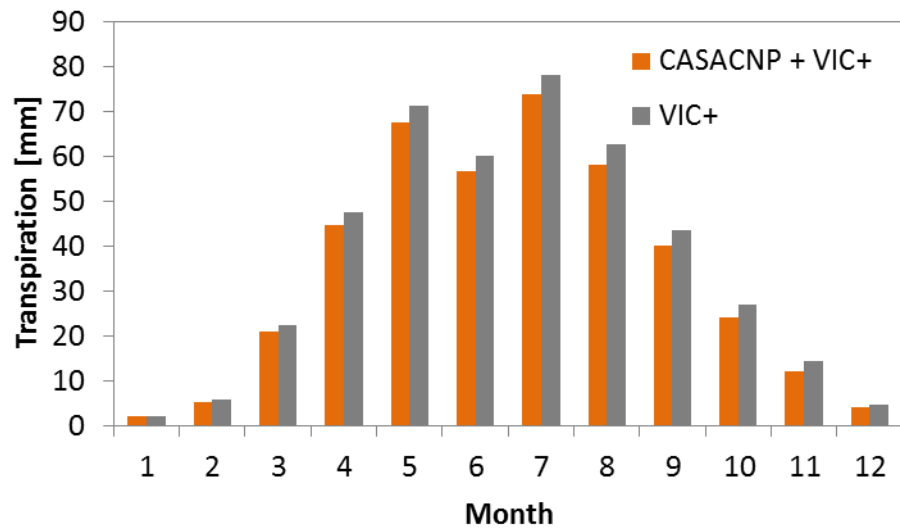


Figure 6.4 Comparison of transpiration modeled by VIC+ to that of the coupled model (CASACNP + VIC+) when using the decreased precipitation

7.0 SUMMARY AND CONCLUSIONS

7.1 VIC+ MODEL

In this study, the VIC-3L land surface model is extended by including representations of several important biological and hydrological processes under water-limited conditions, which are hydraulic redistribution (HR), groundwater dynamics, plant water storage and photosynthesis. HR is represented by a process-based scheme and its interaction with groundwater dynamics is explicitly considered. Plant transpiration is calculated by combining the Ohm's law analogy, where plant storage is considered, with the Penman-Monteith method which is coupled with the calculation of carbon assimilation. The new biological and hydrological processes are closely coupled and at the same time they interact with the other water and energy processes of the VIC-3L model.

7.2 MODEL VALITATION

The VIC+ model is first evaluated with an analytical solution under a simple condition for its modeling of water flow process in the soil and roots. The result, to some extent, verifies the reliability of the model for modeling water flows in roots, the unsaturated zone and the saturated zone.

The VIC+ model is also applied to two AmeriFlux sites. One is the “Duke Forest Loblolly Pine (US-Dk3)” site located in North Carolina, USA. The Duke site experienced some dry periods during the years of 2004 and 2005. The existence of HR in a loblolly pine plantation in a region close to the Duke site has been reported in previous studies. This application shows that the VIC+ model can reproduce the observed soil moisture, latent heat flux and gross primary productivity (GPP) at the daily time scale fairly well. There exist nighttime increases in the observed soil moisture data of this site; it is deduced that this phenomenon is primarily caused by HR. This phenomenon is also captured by the VIC+ model.

The other one is the “Blodgett Forest (US-Blo)” site located in California, USA. This site has a long dry summer each year. In the later period of the summer, plants are under water-limited conditions. In this circumstance the biological and hydrological processes investigated in this study are expected to play important roles in the water, energy and carbon cycles. Our results show that the observed soil moisture, latent heat flux and GPP are reproduced by the model reasonably well at the daily time scale. The modeled results are also compared with the results of the “no-HR” scenario, where the HR process is shut down. The comparison shows that soil moisture in the shallow layer is increased by HR in the dry season and decreased by HR in the wet season, while the impacts are more evident in the dry season. The comparison also shows that the latent heat flux and GPP are supported by HR in the dry season and are not obviously affected by HR in the wet season.

7.3 IMPACTS OF BIOLOGICAL/HYDROLOGICAL PROCESSES

Scenario simulations are conducted at the Duke site to investigate the effects of HR on water, energy and carbon budgets in the soil-plant-atmosphere continuum under water-limited conditions. The profile of total nighttime uptake over a one year period shows that water is “pumped” from the deep soil layer to the shallow soil layer via the HR process during the nighttime. Simulated soil moisture results indicate that HR has an evident impact on SWC of the shallow soil layer and also affects the SWC vertical profile. The modeled results of one dry year show that HR generally promotes the transpiration, latent heat flux and GPP, and reduces sensible heat flux.

Scenario simulations are also performed at the Blodgett site to investigate the impacts of HR, groundwater dynamics, plant storage and root depth on the water and energy cycles. The modeled results demonstrate that each of the three factors (i.e., HR, groundwater dynamics and plant storage) can evidently increase latent heat flux in the dry season, while they do not have obvious impacts on the latent heat flux in the wet season, no matter whether the maximum root depth is small (2 m) or large (8 m). The combined effects of the three factors can exert larger impacts on the dry-season latent heat flux than each of the three factors alone and can increase the latent heat flux by 82.3% and 40.9%, when the maximum root depth is 2 m and 8 m, respectively.

As the new biological and hydrological processes in the VIC+ model are closely coupled with each other, it enables an investigation of the interactions among these processes. The interactions among roots, groundwater table and HR are investigated through a series of scenario simulations. The modeled results reveal that the impact of one factor (i.e., maximum root depth, groundwater table depth or HR) on dry-season latent heat flux may be influenced by the other

two factors: (1) The increase of root depth is favorable for dry-season latent heat flux, which is more sensitive to root depth when the groundwater table is deeper; (2) The dry-season latent heat flux is promoted by HR more obviously when either the groundwater table or the root depth is deeper ; (3) The rise of groundwater table will increase the dry-season latent heat flux and the effect is more evident when there is no HR or when the root depth is shallow. In addition, the interaction between plant storage and HR is demonstrated by comparing two scenarios in terms of the amount of hydraulically redistributed water in the shallow soil layer. It is found that plant storage can weaken the intensity of the upward HR in the dry summer.

In the wet season, soil water of the shallow layer may be transferred to the deep soil via downward HR. However, downward HR may be restricted by frozen soil in the shallow layer if the wet season is in winter. The effect of frozen soil on the downward HR is investigated with scenario simulations and the results show that frozen soil can evidently reduce the downward HR in winter, which decreases water amount stored in the deep soil and hence can reduce transpiration during the dry season.

7.4 TRANSPIRATION – GROUNDWATER INTERACTIONS

Transpiration–GWTD relationships are investigated based on results of a series of scenario simulations which represent different combinations of precipitation conditions, vegetation types, soil types, GWTDs and the treatment of the HR process. For HR scenarios, the transpiration descent is small while the groundwater table declines within the root zone. In the Transpiration–GWTD curve there is a distinct transitional range where transpiration drops abruptly as the groundwater table declines. When the groundwater table is lower than the transitional range,

transpiration will descend slowly along with the decline of the groundwater table. At this stage, transpiration is mainly sustained and controlled by precipitation and receives less and less supply from groundwater as the groundwater table declines. Transpiration and groundwater tend to be disconnected.

Under the dry precipitation conditions, the impacts of vegetation type, soil type and the HR process on the transpiration–GWTD relationship are evident. The promotion of transpiration caused by the HR process varies with the GWTD (e.g., Figure 5.4a). The promotion of transpiration by HR is very small as the groundwater table is close to the ground surface and increases as the groundwater table declines. The transpiration promotion by HR is most evident as the groundwater table is around the root zone bottom. But when the groundwater table further declines, the impact of HR on transpiration will decrease.

The simulation results show that the upward diffusion of groundwater (also abbreviated as “upward diffusion”) is sensitive to the GWTD (e.g., Figure 5.7). When the groundwater table is close to the root zone bottom, the amount of upward diffusion is evident. In this situation, upward diffusion can also be advanced by HR obviously (Figure 5.9). This is one of the reasons why the transpiration can be promoted by HR. The amount of upward diffusion drops abruptly when the groundwater table declines away from the root zone (e.g., Figure 5.7).

For different forcing data, the Transpiration – GWTD relationship curves have similar shape (Figure 5.14). Transpiration amount is obviously affected by forcing condition. HR plays a more important role under forcing condition with longer dry period.

7.5 DYNAMIC REPRESENTATION OF VEGETATION

The VIC+ model is coupled with the CASACNP biogeochemical model to demonstrate impacts of vegetation on water and energy cycles when dynamic growth of vegetation is represented. Under the observed precipitation condition, LAI values modeled by CASACNP are close to the observed data (Figure 6.1). The coupled model can produce plant transpiration results similar to those of the VIC+ model. Under the decreased precipitation condition, LAI values modeled by CASACNP are obviously lower than the observed LAI data during the latter part of the year (Figure 6.3). The transpiration values produced by the coupled model (where the LAI values are provided by the CASACNP model) are obviously lower than those of the VIC+ model (where the observed LAI values are used) for most months of the year.

7.6 FUTURE WORK

Although this model has been evaluated with an analytical solution and observed data from field sites, it will be helpful to test the model with more observations. The model can be tested against observed data from different sites with various environments (e.g., different climatic conditions, vegetation cover or soil characteristics). Also it will be beneficial to verify the modeled results against observed data in terms of more variables (e.g., soil moisture at different depths, sap flow in roots or stems, leaf water potential, etc.). In this way, we can obtain more understanding on those processes simulated by the model, and assess the model more comprehensively and objectively.

APPENDIX

SOLUTION TO THE COUPLED EQUATIONS FOR WATER MOVEMENT IN ROOTS AND THE SOIL

Soil water dynamics and water transport in roots are described by Equation (1) and Equation (2), respectively. The two equations are coupled to represent the hydraulic redistribution scheme of this study. This appendix presents the finite difference method for solving the two coupled equations simultaneously.

1. Two equations

$$\frac{\partial \theta_s}{\partial t} - \frac{\partial}{\partial z} \left[K_s \left(\frac{\partial \psi_s}{\partial z} \right) \right] + \frac{\partial K_s}{\partial z} + K_{rr} (\psi_s - \psi_r) S_r = 0 \quad (1)$$

$$\frac{\partial}{\partial z} \left[K_{ra} \left(\frac{\partial \psi_r}{\partial z} \right) \right] - \frac{\partial K_{ra}}{\partial z} + K_{rr} (\psi_s - \psi_r) S_r = 0 \quad (2)$$

In the two equations: θ_s is soil moisture content; K_s is soil hydraulic conductivity; ψ_s is soil matric potential; K_{rr} is radial hydraulic conductivity of roots; ψ_r is root pressure potential; S_r is area of root surface per unit volume of soil; K_{ra} is axial hydraulic conductivity of roots.

Downward is positive for the z axis; *downward* is positive for the flow of soil water; *upward* is positive for the flow in roots.

2 Discretization

The implicit difference form of Equation (1) is

$$\frac{\theta_{s,i}^{k+1} - \theta_{s,i}^k}{\Delta t} - \frac{K_{s,i+\frac{1}{2}}^{k+1}(\psi_{s,i+1}^{k+1} - \psi_{s,i}^{k+1}) - K_{s,i-\frac{1}{2}}^{k+1}(\psi_{s,i}^{k+1} - \psi_{s,i-1}^{k+1})}{\Delta z^2} + \frac{K_{s,i+1}^{k+1} - K_{s,i-1}^{k+1}}{2\Delta z} + K_{rr,i}^{k+1}(\psi_{s,i}^{k+1} - \psi_{r,i}^{k+1})S_{r,i}^{k+1} = 0 \quad (3)$$

At the $(m+1)^{\text{th}}$ iteration, write Taylor series expansion for $\theta_{s,i}^{k+1,m+1}$ [Celia et al., 1990]:

$$\theta_{s,i}^{k+1,m+1} = \theta(\psi^{m+1}) = \theta(\psi^m) + \left(\frac{d\theta}{d\psi}\right)_{\psi^m}(\psi^{m+1} - \psi^m) + o[(\psi^{m+1} - \psi^m)^2] \quad (4)$$

Therefore

$$\frac{\theta_{s,i}^{k+1,m+1} - \theta_{s,i}^k}{\Delta t} = C_i^{k+1,m} \frac{\psi_i^{k+1,m+1} - \psi_i^{k+1,m}}{\Delta t} + \frac{\theta_{s,i}^{k+1,m} - \theta_{s,i}^k}{\Delta t} \quad (5)$$

Where C is specific soil moisture capacity ($C(\psi_s) = \frac{\partial \theta_s}{\partial \psi_s}$).

Substituting Equation (5) into Equation (3) and rearranging results in

$$\left(-\frac{K_{s,i-\frac{1}{2}}^{k+1}}{\Delta z^2}\right) \psi_{s,i-1}^{k+1,m+1} + \left(\frac{C_i^{k+1,m}}{\Delta t} + \frac{K_{s,i+\frac{1}{2}}^{k+1}}{\Delta z^2} + \frac{K_{s,i-\frac{1}{2}}^{k+1}}{\Delta z^2} + K_{rr,i}^{k+1} S_{r,i}^{k+1}\right) \psi_{s,i}^{k+1,m+1} + \left(-\frac{K_{s,i+\frac{1}{2}}^{k+1}}{\Delta z^2}\right) \psi_{s,i+1}^{k+1,m+1} + \left(-K_{rr,i}^{k+1} S_{r,i}^{k+1}\right) \psi_{r,i}^{k+1,m+1} + \frac{-C_i^{k+1,m} \psi_{s,i}^{k+1,m}}{\Delta t} + \frac{\theta_{s,i}^{k+1,m} - \theta_{s,i}^k}{\Delta t} + \frac{K_{s,i+1}^{k+1} - K_{s,i-1}^{k+1}}{2\Delta z} = 0 \quad (6)$$

Set

$$\left\{ \begin{array}{l} a_i = -\frac{K_{s,i-\frac{1}{2}}^{k+1}}{\Delta z^2} \\ b_i = \frac{c^{k+1}}{\Delta t} + \frac{K_{s,i+\frac{1}{2}}^{k+1}}{\Delta z^2} + \frac{K_{s,i-\frac{1}{2}}^{k+1}}{\Delta z^2} + K_{rr,i}^{k+1} S_{r,i}^{k+1} \\ c_i = -\frac{K_{s,i+\frac{1}{2}}^{k+1}}{\Delta z^2} \\ d_i = -K_{rr,i}^{k+1} S_{r,i}^{k+1} \\ e_i = \frac{K_{s,i+1}^{k+1} - K_{s,i-1}^{k+1}}{2\Delta z} + \frac{-c_i^{k+1,m} \psi_{s,i}^{k+1,m}}{\Delta t} + \frac{\theta_{s,i}^{k+1,m} - \theta_{s,i}^k}{\Delta t} \end{array} \right. \quad (7)$$

Equation (6) is written as

$$a_i \psi_{s,i-1}^{k+1} + b_i \psi_{s,i}^{k+1} + c_i \psi_{s,i+1}^{k+1} + d_i \psi_{r,i}^{k+1} + e_i = 0 \quad (8)$$

The difference form of Equation (2) is

$$\frac{K_{ra,i+\frac{1}{2}}^{k+1} (\psi_{r,i+1}^{k+1} - \psi_{r,i}^{k+1}) - K_{ra,i-\frac{1}{2}}^{k+1} (\psi_{r,i}^{k+1} - \psi_{r,i-1}^{k+1})}{\Delta z^2} (+) - \frac{K_{ra,i+1}^{k+1} - K_{ra,i-1}^{k+1}}{2\Delta z} + K_{rr,i}^{k+1} (\psi_{s,i}^{k+1} - \psi_{r,i}^{k+1}) S_{r,i}^{k+1} = 0 \quad (9)$$

Rearranging Equation (9) results in

$$\left(\frac{K_{ra,i+\frac{1}{2}}^{k+1}}{\Delta z^2} \right) \psi_{r,i-1}^{k+1} + \left(-\frac{K_{ra,i+\frac{1}{2}}^{k+1}}{\Delta z^2} - \frac{K_{ra,i-\frac{1}{2}}^{k+1}}{\Delta z^2} - K_{rr,i}^{k+1} S_{r,i}^{k+1} \right) \psi_{r,i}^{k+1} + \left(\frac{K_{ra,i+\frac{1}{2}}^{k+1}}{\Delta z^2} \right) \psi_{r,i+1}^{k+1} + (K_{rr,i}^{k+1} S_{r,i}^{k+1}) \psi_{s,i}^{k+1} (+) - \frac{K_{ra,i+1}^{k+1} - K_{ra,i-1}^{k+1}}{2\Delta z} = 0 \quad (10)$$

Set

$$\left\{ \begin{array}{l} l_i = \frac{K_{ra,i-\frac{1}{2}}^{k+1}}{\Delta z^2} \\ m_i = -\frac{K_{ra,i+\frac{1}{2}}^{k+1}}{\Delta z^2} - \frac{K_{ra,i-\frac{1}{2}}^{k+1}}{\Delta z^2} - K_{rr,i}^{k+1} S_{r,i}^{k+1} \\ n_i = \frac{K_{ra,i+\frac{1}{2}}^{k+1}}{\Delta z^2} \\ p_i = K_{rr,i}^{k+1} S_{r,i}^{k+1} \\ q_i = -\frac{K_{ra,i+1}^{k+1} - K_{ra,i-1}^{k+1}}{2\Delta z} \end{array} \right. \quad (11)$$

Equation (10) is written as

$$l_i \psi_{r,i-1}^{k+1} + m_i \psi_{r,i}^{k+1} + n_i \psi_{r,i+1}^{k+1} + p_i \psi_{s,i}^{k+1} + q_i = 0 \quad (12)$$

3 Upper boundary conditions

(1) For root:

$$K_{ra} \left(\frac{\partial \psi_r}{\partial z} \right) - K_{ra} = F_{ru} \quad (z=0, t>0) \quad (13)$$

The difference form is

$$K_{ra,0}^{k+1} \left(\frac{\psi_{r,1}^{k+1} - \psi_{r,0}^{k+1}}{\Delta z} \right) - K_{ra,0}^{k+1} = F_{ru}^{k+1} \quad (14)$$

Rearrange

$$\psi_{r,0}^{k+1} = \psi_{r,1}^{k+1} - \left(\frac{F_{ru}^{k+1}}{K_{ra,0}^{k+1}} + 1 \right) \Delta z \quad (15)$$

(2) For soil:

Mass balance equation for the half layer at the ground surface is [Šimůnek et al., 2005]

$$\frac{\partial \theta}{\partial t} + \frac{\partial q}{\partial z} = 0 \quad (16)$$

The discretization form is

$$\frac{\theta_0^{k+1,m+1} - \theta_0^k}{\Delta t} + \frac{q_1 - F_{su}^{k+1}}{\frac{\Delta z}{2}} = 0 \quad (17)$$

Where, $F_{su} = P - R - E$.

Taylor series expansion of $\theta_0^{k+1,m+1}$ results in

$$\frac{\theta_0^{k+1,m+1} - \theta_0^k}{\Delta t} = C_0^{k+1,m} \frac{\psi_{s,0}^{k+1,m+1} - \psi_{s,0}^{k+1,m}}{\Delta t} + \frac{\theta_0^{k+1,m} - \theta_0^k}{\Delta t} \quad (18)$$

$$q_1 = -\frac{K_{s,0}^{k+1,m} + K_{s,1}^{k+1,m}}{2} \left(\frac{\psi_{s,1}^{k+1,m+1} - \psi_{s,0}^{k+1,m+1}}{\Delta z} - 1 \right) \quad (19)$$

Substituting Equation (18) and Equation (19) into Equation (17) and rearranging gives

$$\left[\frac{C_0^{k+1,m}}{\Delta t} + \frac{K_{s,0}^{k+1,m} + K_{s,1}^{k+1,m}}{(\Delta z)^2} \right] \psi_{s,0}^{k+1,m+1} + \left[-\frac{K_{s,0}^{k+1,m} + K_{s,1}^{k+1,m}}{(\Delta z)^2} \right] \psi_{s,1}^{k+1,m+1} - \frac{C_0^{k+1,m} \psi_{s,0}^{k+1,m}}{\Delta t} + \frac{\theta_0^{k+1,m} - \theta_0^k}{\Delta t} + \frac{2}{\Delta z} \left[\frac{K_{s,0}^{k+1,m} + K_{s,1}^{k+1,m}}{2} - F_{su}^{k+1} \right] = 0 \quad (20)$$

Set

$$\begin{cases} \varepsilon_1 = \frac{C_0^{k+1,m}}{\Delta t} + \frac{K_{s,0}^{k+1,m} + K_{s,1}^{k+1,m}}{(\Delta z)^2} \\ \varepsilon_2 = -\frac{K_{s,0}^{k+1,m} + K_{s,1}^{k+1,m}}{(\Delta z)^2} \\ \varepsilon_3 = -\frac{C_0^{k+1,m} \psi_{s,0}^{k+1,m}}{\Delta t} + \frac{\theta_0^{k+1,m} - \theta_0^k}{\Delta t} + \frac{2}{\Delta z} \left[\frac{K_{s,0}^{k+1,m} + K_{s,1}^{k+1,m}}{2} - F_{su}^{k+1} \right] \end{cases} \quad (21)$$

Equation (20) is written as

$$\varepsilon_1 \psi_{s,0}^{k+1,m+1} + \varepsilon_2 \psi_{s,1}^{k+1,m+1} + \varepsilon_3 = 0 \quad (22)$$

Rearrange

$$\psi_{s,0}^{k+1,m+1} = \frac{1}{\varepsilon_1} \left(-\varepsilon_2 \psi_{s,1}^{k+1,m+1} - \varepsilon_3 \right) \quad (23)$$

4 Deriving coefficients [$i = 2$]

When $i = 1$, Equation (12) is written as

$$l_1 \psi_{r,0}^{k+1} + m_1 \psi_{r,1}^{k+1} + n_1 \psi_{r,2}^{k+1} + p_1 \psi_{s,1}^{k+1} + q_1 = 0 \quad (24)$$

Substituting Equation (15) into Equation (24), we get

$$(l_1 + m_1) \psi_{r,1}^{k+1} + n_1 \psi_{r,2}^{k+1} + p_1 \psi_{s,1}^{k+1} + q_1 - l_1 \Delta z \left(\frac{F_{ru}^{k+1}}{K_{ra,0}^{k+1}} + 1 \right) = 0 \quad (25)$$

Set

$$\left\{ \begin{array}{l} \alpha_{2,1} = l_1 + m_1 \\ \beta_{2,1} = n_1 \\ \delta_{2,1} = p_1 \\ \mu_{2,1} = q_1 - l_1 \Delta z \left(\frac{F_{ru}^{k+1}}{K_{ra,0}^{k+1}} + 1 \right) \end{array} \right. \quad (26)$$

Equation (25) is written as

$$\alpha_{2,1} \psi_{r,1}^{k+1} + \beta_{2,1} \psi_{r,2}^{k+1} + \delta_{2,1} \psi_{s,1}^{k+1} + \mu_{2,1} = 0 \quad (27)$$

Rearrange

$$\psi_{r,1}^{k+1} = \frac{-1}{\alpha_{2,1}} (\beta_{2,1}\psi_{r,2}^{k+1} + \delta_{2,1}\psi_{s,1}^{k+1} + \mu_{2,1}) \quad (28)$$

When $i = 1$, Equation (8) is written as

$$a_1\psi_{s,0}^{k+1} + b_1\psi_{s,1}^{k+1} + c_1\psi_{s,2}^{k+1} + d_1\psi_{r,1}^{k+1} + e_1 = 0 \quad (29)$$

Substituting Equation (23) into Equation (29), we get

$$\left(\frac{-\varepsilon_2}{\varepsilon_1} a_1 + b_1 \right) \psi_{s,1}^{k+1} + c_1 \psi_{s,2}^{k+1} + d_1 \psi_{r,1}^{k+1} + e_1 + \frac{-\varepsilon_3}{\varepsilon_1} a_1 = 0 \quad (30)$$

Set

$$\left\{ \begin{array}{l} \alpha_{1,1} = \frac{-\varepsilon_2}{\varepsilon_1} a_1 + b_1 \\ \beta_{1,1} = c_1 \\ \delta_{1,1} = d_1 \\ \mu_{1,1} = e_1 + \frac{-\varepsilon_3}{\varepsilon_1} a_1 \end{array} \right. \quad (31)$$

Then Equation (30) is written as

$$\alpha_{1,1}\psi_{s,1}^{k+1} + \beta_{1,1}\psi_{s,2}^{k+1} + \delta_{1,1}\psi_{r,1}^{k+1} + \mu_{1,1} = 0 \quad (32)$$

Rearrange

$$\psi_{s,1}^{k+1} = \frac{-1}{\alpha_{1,1}} (\beta_{1,1}\psi_{s,2}^{k+1} + \delta_{1,1}\psi_{r,1}^{k+1} + \mu_{1,1}) \quad (33)$$

Substituting Equation (33) into Equation (27) and rearranging, we get

$$\psi_{r,1}^{k+1} = \frac{\alpha_{1,1}}{\alpha_{1,1}\alpha_{2,1} - \delta_{2,1}\delta_{1,1}} \left(-\beta_{2,1}\psi_{r,2}^{k+1} + \frac{\delta_{2,1}\beta_{1,1}}{\alpha_{1,1}} \psi_{s,2}^{k+1} + \frac{\delta_{2,1}\mu_{1,1}}{\alpha_{1,1}} - \mu_{2,1} \right) \quad (34)$$

Substituting Equation (34) into Equation (32) and rearranging, we get

$$\psi_{s,1}^{k+1} = \frac{\alpha_{2,1}}{\alpha_{1,1}\alpha_{2,1} - \delta_{2,1}\delta_{1,1}} \left(-\beta_{1,1}\psi_{s,2}^{k+1} + \frac{\delta_{1,1}\beta_{2,1}}{\alpha_{2,1}}\psi_{r,2}^{k+1} + \frac{\delta_{1,1}\mu_{2,1}}{\alpha_{2,1}} - \mu_{1,1} \right) \quad (35)$$

When $i=2$, Equation (8) becomes

$$a_2\psi_{s,1}^{k+1} + b_2\psi_{s,2}^{k+1} + c_2\psi_{s,3}^{k+1} + d_2\psi_{r,2}^{k+1} + e_2 = 0 \quad (36)$$

and Equation (12) becomes

$$l_2\psi_{r,1}^{k+1} + m_2\psi_{r,2}^{k+1} + n_2\psi_{r,3}^{k+1} + p_2\psi_{s,2}^{k+1} + q_2 = 0 \quad (37)$$

Substituting Equation (34) into Equation (37) and rearranging, we get

$$\left(\frac{-\alpha_{1,1}l_2\beta_{2,1}}{\alpha_{1,1}\alpha_{2,1} - \delta_{1,1}\delta_{2,1}} + m_2 \right) \psi_{r,2}^{k+1} + n_2\psi_{r,3}^{k+1} + \left(\frac{\alpha_{1,1}l_2}{\alpha_{1,1}\alpha_{2,1} - \delta_{1,1}\delta_{2,1}} \frac{\delta_{2,1}\beta_{1,1}}{\alpha_{1,1}} + p_2 \right) \psi_{s,2}^{k+1} + \frac{\alpha_{1,1}l_2}{\alpha_{1,1}\alpha_{2,1} - \delta_{1,1}\delta_{2,1}} \left(\frac{\delta_{2,1}\mu_{1,1}}{\alpha_{1,1}} - \mu_{2,1} \right) + q_2 = 0 \quad (38)$$

Therefore

$$\begin{cases} \alpha_{2,2} = \frac{-\alpha_{1,1}l_2\beta_{2,1}}{\alpha_{1,1}\alpha_{2,1} - \delta_{1,1}\delta_{2,1}} + m_2 \\ \beta_{2,2} = n_2 \\ \delta_{2,2} = \frac{\alpha_{1,1}l_2}{\alpha_{1,1}\alpha_{2,1} - \delta_{1,1}\delta_{2,1}} \frac{\delta_{2,1}\beta_{1,1}}{\alpha_{1,1}} + p_2 \\ \mu_{2,2} = \frac{\alpha_{1,1}l_2}{\alpha_{1,1}\alpha_{2,1} - \delta_{1,1}\delta_{2,1}} \left(\frac{\delta_{2,1}\mu_{1,1}}{\alpha_{1,1}} - \mu_{2,1} \right) + q_2 \end{cases} \quad (39)$$

Substituting Equation (35) into Equation (36) and rearranging, we get

$$\left(\frac{-\alpha_{2,1}a_2\beta_{1,1}}{\alpha_{1,1}\alpha_{2,1} - \delta_{1,1}\delta_{2,1}} + b_2 \right) \psi_{s,2}^{k+1} + c_2\psi_{s,3}^{k+1} + \left(\frac{\alpha_{2,1}a_2}{\alpha_{1,1}\alpha_{2,1} - \delta_{1,1}\delta_{2,1}} \frac{\delta_{1,1}\beta_{2,1}}{\alpha_{2,1}} + d_2 \right) \psi_{r,2}^{k+1} + \frac{\alpha_{2,1}a_2}{\alpha_{1,1}\alpha_{2,1} - \delta_{1,1}\delta_{2,1}} \left(\frac{\delta_{1,1}\mu_{2,1}}{\alpha_{2,1}} - \mu_{1,1} \right) + e_2 = 0 \quad (40)$$

Therefore

$$\begin{cases} \alpha_{1,2} = \frac{-\alpha_{2,1}a_2\beta_{1,1}}{\alpha_{1,1}\alpha_{2,1} - \delta_{1,1}\delta_{2,1}} + b_2 \\ \beta_{1,2} = c_2 \\ \delta_{1,2} = \frac{\alpha_{2,1}a_2}{\alpha_{1,1}\alpha_{2,1} - \delta_{1,1}\delta_{2,1}} \frac{\delta_{1,1}\beta_{2,1}}{\alpha_{2,1}} + d_2 \\ \mu_{1,2} = \frac{\alpha_{2,1}a_2}{\alpha_{1,1}\alpha_{2,1} - \delta_{1,1}\delta_{2,1}} \left(\frac{\delta_{1,1}\mu_{2,1}}{\alpha_{2,1}} - \mu_{1,1} \right) + e_2 \end{cases} \quad (41)$$

5 Deriving general coefficients

In general, when $i = j$, we have

$$\alpha_{1,j}\psi_{s,j}^{k+1} + \beta_{1,j}\psi_{s,j+1}^{k+1} + \delta_{1,j}\psi_{r,j}^{k+1} + \mu_{1,j} = 0 \quad (42)$$

Rearrange

$$\psi_{s,j}^{k+1} = \frac{-1}{\alpha_{1,j}} \left(\beta_{1,j}\psi_{s,j+1}^{k+1} + \delta_{1,j}\psi_{r,j}^{k+1} + \mu_{1,j} \right) \quad (43)$$

$$\alpha_{2,j}\psi_{r,j}^{k+1} + \beta_{2,j}\psi_{r,j+1}^{k+1} + \delta_{2,j}\psi_{s,j}^{k+1} + \mu_{2,j} = 0 \quad (44)$$

Rearrange

$$\psi_{r,j}^{k+1} = \frac{-1}{\alpha_{2,j}} \left(\beta_{2,j}\psi_{r,j+1}^{k+1} + \delta_{2,j}\psi_{s,j}^{k+1} + \mu_{2,j} \right) \quad (45)$$

Substituting Equation (43) into Equation (44) and rearranging, we get

$$\psi_{r,j}^{k+1} = \frac{\alpha_{1,j}}{\alpha_{1,j}\alpha_{2,j} - \delta_{2,j}\delta_{1,j}} \left(-\beta_{2,j}\psi_{r,j+1}^{k+1} + \frac{\delta_{2,j}\beta_{1,j}}{\alpha_{1,j}}\psi_{s,j+1}^{k+1} + \frac{\delta_{2,j}\mu_{1,j}}{\alpha_{1,j}} - \mu_{2,j} \right) \quad (46)$$

Substituting Equation (45) into Equation (42) and rearranging, we get

$$\psi_{s,j}^{k+1} = \frac{\alpha_{2,j}}{\alpha_{1,j}\alpha_{2,j} - \delta_{1,j}\delta_{2,j}} \left(-\beta_{1,j}\psi_{s,j+1}^{k+1} + \frac{\delta_{1,j}\beta_{2,j}}{\alpha_{2,j}}\psi_{r,j+1}^{k+1} + \frac{\delta_{1,j}\mu_{2,j}}{\alpha_{2,j}} - \mu_{1,j} \right) \quad (47)$$

When $i = j+1$, Equation (8) becomes

$$a_{j+1}\psi_{s,j}^{k+1} + b_{j+1}\psi_{s,j+1}^{k+1} + c_{j+1}\psi_{s,j+2}^{k+1} + d_{j+1}\psi_{r,j+1}^{k+1} + e_{j+1} = 0 \quad (48)$$

and Equation (12) becomes

$$l_{j+1}\psi_{r,j}^{k+1} + m_{j+1}\psi_{r,j+1}^{k+1} + n_{j+1}\psi_{r,j+2}^{k+1} + p_{j+1}\psi_{s,j+1}^{k+1} + q_{j+1} = 0 \quad (49)$$

Substituting Equation (46) into Equation (49) and rearranging, we get

$$\left(\frac{-\alpha_{1,j}l_{j+1}\beta_{2,j}}{\alpha_{1,j}\alpha_{2,j} - \delta_{1,j}\delta_{2,j}} + m_{j+1} \right) \psi_{r,j+1}^{k+1} + n_{j+1}\psi_{r,j+2}^{k+1} + \left(\frac{\alpha_{1,j}l_{j+1}}{\alpha_{1,j}\alpha_{2,j} - \delta_{1,j}\delta_{2,j}} \frac{\delta_{2,j}\beta_{1,j}}{\alpha_{1,j}} + p_{j+1} \right) \psi_{s,j+1}^{k+1} + \frac{\alpha_{1,j}l_{j+1}}{\alpha_{1,j}\alpha_{2,j} - \delta_{1,j}\delta_{2,j}} \left(\frac{\delta_{2,j}\mu_{1,j}}{\alpha_{1,j}} - \mu_{2,j} \right) + q_{j+1} = 0 \quad (50)$$

Therefore

$$\begin{cases} \alpha_{2,j+1} = \frac{-\alpha_{1,j}l_{j+1}\beta_{2,j}}{\alpha_{1,j}\alpha_{2,j} - \delta_{1,j}\delta_{2,j}} + m_{j+1} \\ \beta_{2,j+1} = n_{j+1} \\ \delta_{2,j+1} = \frac{\alpha_{1,j}l_{j+1}}{\alpha_{1,j}\alpha_{2,j} - \delta_{1,j}\delta_{2,j}} \frac{\delta_{2,j}\beta_{1,j}}{\alpha_{1,j}} + p_{j+1} \\ \mu_{2,j+1} = \frac{\alpha_{1,j}l_{j+1}}{\alpha_{1,j}\alpha_{2,j} - \delta_{1,j}\delta_{2,j}} \left(\frac{\delta_{2,j}\mu_{1,j}}{\alpha_{1,j}} - \mu_{2,j} \right) + q_{j+1} \end{cases} \quad (51)$$

Substituting Equation (47) into Equation (48) and rearranging, we get

$$\left(\frac{-\alpha_{2,j}a_{j+1}\beta_{1,j}}{\alpha_{1,j}\alpha_{2,j} - \delta_{1,j}\delta_{2,j}} + b_{j+1} \right) \psi_{s,j+1}^{k+1} + c_{j+1}\psi_{s,j+2}^{k+1} + \left(\frac{\alpha_{2,j}a_{j+1}}{\alpha_{1,j}\alpha_{2,j} - \delta_{1,j}\delta_{2,j}} \frac{\delta_{1,j}\beta_{2,j}}{\alpha_{2,j}} + d_{j+1} \right) \psi_{r,j+1}^{k+1} + \frac{\alpha_{2,j}a_{j+1}}{\alpha_{1,j}\alpha_{2,j} - \delta_{1,j}\delta_{2,j}} \left(\frac{\delta_{1,j}\mu_{2,j}}{\alpha_{2,j}} - \mu_{1,j} \right) + e_{j+1} = 0 \quad (52)$$

Therefore

$$\left\{ \begin{array}{l} \alpha_{1,j+1} = \frac{-\alpha_{2,j}a_{j+1}\beta_{1,j}}{\alpha_{1,j}\alpha_{2,j} - \delta_{1,j}\delta_{2,j}} + b_{j+1} \\ \beta_{1,j+1} = c_{j+1} \\ \delta_{1,j+1} = \frac{\alpha_{2,j}a_{j+1}}{\alpha_{1,j}\alpha_{2,j} - \delta_{1,j}\delta_{2,j}} \frac{\delta_{1,j}\beta_{2,j}}{\alpha_{2,j}} + d_{j+1} \\ \mu_{1,j+1} = \frac{\alpha_{2,j}a_{j+1}}{\alpha_{1,j}\alpha_{2,j} - \delta_{1,j}\delta_{2,j}} \left(\frac{\delta_{1,j}\mu_{2,j}}{\alpha_{2,j}} - \mu_{1,j} \right) + e_{j+1} \end{array} \right. \quad (53)$$

Using Equation (51) and Equation (53), we can derive all the following coefficients:

$$\alpha_{1,i}, \beta_{1,i}, \delta_{1,i}, \mu_{1,i}, \alpha_{2,i}, \beta_{2,i}, \delta_{2,i} \text{ and } \mu_{2,i}, i = 2, 3, \dots, n-1.$$

6 Lower boundary conditions

(1) For root:

$$K_{ra} \left(\frac{\partial \psi_r}{\partial z} \right) - K_{ra} = 0 \quad (z = H_{r,\max}, t > 0) \quad (54)$$

The difference form is

$$K_{ra,n}^{k+1} \left(\frac{\psi_{r,n}^{k+1} - \psi_{r,n-1}^{k+1}}{\Delta z} \right) - K_{ra,n}^{k+1} = 0 \quad (55)$$

Therefore

$$\psi_{r,n}^{k+1} = \psi_{r,n-1}^{k+1} + \Delta z \quad (56)$$

(2) For soil:

Mass balance equation for the half layer at the bottom is

$$\frac{\partial \theta}{\partial t} + \frac{\partial q}{\partial z} = 0 \quad (57)$$

The discretization form is

$$\frac{\theta_n^{k+1,m+1} - \theta_n^k}{\Delta t} + \frac{F_{sl}^{k+1} - q_{n-\frac{1}{2}}}{\frac{\Delta z}{2}} = 0 \quad (58)$$

Where F_{sl} is soil bottom drainage.

Taylor series expansion of $\theta_n^{k+1,m+1}$ results in

$$\frac{\theta_n^{k+1,m+1} - \theta_n^k}{\Delta t} = C_n^{k+1,m} \frac{\psi_{s,n}^{k+1,m+1} - \psi_{s,n}^{k+1,m}}{\Delta t} + \frac{\theta_n^{k+1,m} - \theta_n^k}{\Delta t} \quad (59)$$

$$q_{n-\frac{1}{2}} = -\frac{K_{s,n-1}^{k+1,m} + K_{s,n}^{k+1,m}}{2} \left(\frac{\psi_{s,n}^{k+1,m+1} - \psi_{s,n-1}^{k+1,m+1}}{\Delta z} - 1 \right) \quad (60)$$

Substituting Equations (59) and (60) into Equation (58) and rearranging gives

$$\left[-\frac{K_{s,n-1}^{k+1,m} + K_{s,n}^{k+1,m}}{(\Delta z)^2} \right] \psi_{s,n-1}^{k+1,m+1} + \left[\frac{C_n^{k+1,m}}{\Delta t} + \frac{K_{s,n-1}^{k+1,m} + K_{s,n}^{k+1,m}}{(\Delta z)^2} \right] \psi_{s,n}^{k+1,m+1} - \frac{C_n^{k+1,m} \psi_{s,n}^{k+1,m}}{\Delta t} + \frac{\theta_n^{k+1,m} - \theta_n^k}{\Delta t} + \frac{2}{\Delta z} \left[-\frac{K_{s,n-1}^{k+1,m} + K_{s,n}^{k+1,m}}{2} + F_{sl}^{k+1} \right] = 0 \quad (61)$$

Set

$$\begin{cases} \sigma_1 = -\frac{K_{s,n-1}^{k+1,m} + K_{s,n}^{k+1,m}}{(\Delta z)^2} \\ \sigma_2 = \frac{C_n^{k+1,m}}{\Delta t} + \frac{K_{s,n-1}^{k+1,m} + K_{s,n}^{k+1,m}}{(\Delta z)^2} \\ \sigma_3 = -\frac{C_n^{k+1,m} \psi_{s,n}^{k+1,m}}{\Delta t} + \frac{\theta_n^{k+1,m} - \theta_n^k}{\Delta t} + \frac{2}{\Delta z} \left[-\frac{K_{s,n-1}^{k+1,m} + K_{s,n}^{k+1,m}}{2} + F_{sl}^{k+1} \right] \end{cases} \quad (62)$$

Equation (61) is written as

$$\sigma_1 \psi_{s,n-1}^{k+1,m+1} + \sigma_2 \psi_{s,n}^{k+1,m+1} + \sigma_3 = 0 \quad (63)$$

Rearrange

$$\psi_{s,n}^{k+1,m+1} = \frac{1}{\sigma_2} \left(-\sigma_1 \psi_{s,n-1}^{k+1,m+1} - \sigma_3 \right) \quad (64)$$

7 Computing potential values [$i = n - 1$]

When $i = n - 1$, we have

$$\alpha_{1,n-1} \psi_{s,n-1}^{k+1} + \beta_{1,n-1} \psi_{s,n}^{k+1} + \delta_{1,n-1} \psi_{r,n-1}^{k+1} + \mu_{1,n-1} = 0 \quad (65)$$

$$\alpha_{2,n-1} \psi_{r,n-1}^{k+1} + \beta_{2,n-1} \psi_{r,n}^{k+1} + \delta_{2,n-1} \psi_{s,n-1}^{k+1} + \mu_{2,n-1} = 0 \quad (66)$$

Substituting Equation (56) into Equation (66) results in

$$\left(\alpha_{2,n-1} + \beta_{2,n-1} \right) \psi_{r,n-1}^{k+1} + \delta_{2,n-1} \psi_{s,n-1}^{k+1} + \mu_{2,n-1} + \beta_{2,n-1} \Delta z = 0 \quad (67)$$

Set

$$\begin{cases} v_2 = \alpha_{2,n-1} + \beta_{2,n-1} \\ u_2 = \delta_{2,n-1} \\ w_2 = \mu_{2,n-1} + \beta_{2,n-1} \Delta z \end{cases} \quad (68)$$

Equation (67) is written as

$$v_2 \psi_{r,n-1}^{k+1} + u_2 \psi_{s,n-1}^{k+1} + w_2 = 0 \quad (69)$$

Substituting Equation (64) into Equation (65), we get

$$\left(\alpha_{1,n-1} - \frac{\sigma_1}{\sigma_2} \beta_{1,n-1} \right) \psi_{s,n-1}^{k+1} + \delta_{1,n-1} \psi_{r,n-1}^{k+1} + \mu_{1,n-1} - \frac{\sigma_3}{\sigma_2} \beta_{1,n-1} = 0 \quad (70)$$

Set

$$\begin{cases} u_1 = \alpha_{1,n-1} - \frac{\sigma_1}{\sigma_2} \beta_{1,n-1} \\ v_1 = \delta_{1,n-1} \\ w_1 = \mu_{1,n-1} - \frac{\sigma_3}{\sigma_2} \beta_{1,n-1} \end{cases} \quad (71)$$

Equation (70) is written as

$$u_1 \psi_{s,n-1}^{k+1} + v_1 \psi_{r,n-1}^{k+1} + w_1 = 0 \quad (72)$$

If $K_{rr,j} = 0$ ($j = 1, 2, \dots, n-1$), we have

$$u_1 v_2 - u_2 v_1 = 0 \quad (73)$$

$$\psi_{s,n-1}^{k+1} = -\frac{w_1}{u_1} \quad (74)$$

$$\psi_{r,n-1}^{k+1,m+1} = \psi_{r,n-1}^{k+1,m} \quad (75)$$

If $K_{rr,j} > 0$ ($j = 1, 2, \dots, n-1$), we can solve Equation (69) and Equation (72) to get

$$\psi_{s,n-1}^{k+1} = \frac{\begin{vmatrix} -w_1 & v_1 \\ -w_2 & v_2 \end{vmatrix}}{\begin{vmatrix} u_1 & v_1 \\ u_2 & v_2 \end{vmatrix}} = \frac{v_1 w_2 - v_2 w_1}{u_1 v_2 - u_2 v_1} \quad (76)$$

$$\psi_{r,n-1}^{k+1} = \frac{\begin{vmatrix} u_1 & -w_1 \\ u_2 & -w_2 \end{vmatrix}}{\begin{vmatrix} u_1 & v_1 \\ u_2 & v_2 \end{vmatrix}} = \frac{u_2 w_1 - u_1 w_2}{u_1 v_2 - u_2 v_1} \quad (77)$$

8 Computing other potential values

Use Equations (56) and (64) to get $\psi_{r,n}^{k+1}$ and $\psi_{s,n}^{k+1}$, respectively.

In the above step we get $\psi_{r,n-1}^{k+1}$ and $\psi_{s,n-1}^{k+1}$. Then we can use Equations (46) and (47) to derive all the following unknowns:

$$\psi_{r,j}^{k+1}, \psi_{s,j}^{k+1}, j = n-2, n-3, \dots, 3, 2, 1.$$

Finally, we can use Equations (15) and (23) to get $\psi_{r,0}^{k+1}$ and $\psi_{s,0}^{k+1}$, respectively.

If $K_{rr,j} = 0$ ($j = 1, 2, \dots, n-1$), we have

$$\psi_{r,j}^{k+1,m+1} = \psi_{r,j}^{k+1,m} \quad (j = 0, 1, \dots, n) \quad (78)$$

BIBLIOGRAPHY

- Amenu, G. G., and P. Kumar (2008), A model for hydraulic redistribution incorporating coupled soil-root moisture transport, *Hydrology and Earth System Sciences*, 12(1), 55–74.
- Baker, I. T., L. Prihodko, A. S. Denning, M. Goulden, S. Miller, and H. R. da Rocha (2008), Seasonal drought stress in the Amazon: Reconciling models and observations, *J. Geophys. Res.*, 113, 10 PP., doi:200810.1029/2007JG000644.
- Ball, J. T., I. E. Woodrow, and J. A. Berry (1987), A model predicting stomatal conductance and its contribution to the control of photosynthesis under different environmental conditions, in *Progress in Photosynthesis Research*, Martinus-Nijhoff Publishers, Dordrecht.
- Bonan, G. B. (1995), Land-atmosphere CO₂ exchange simulated by a land surface process model coupled to an atmospheric general circulation model, *Journal of Geophysical Research: Atmospheres*, 100(D2), 2817–2831, doi:10.1029/94JD02961.
- Caldwell, M. M., and J. H. Richards (1989), Hydraulic lift: water efflux from upper roots improves effectiveness of water uptake by deep roots, *Oecologia*, 79(1), 1–5, doi:10.1007/BF00378231.
- Caldwell, M. M., T. E. Dawson, and J. H. Richards (1998), Hydraulic lift: Consequences of water efflux from the roots of plants, *Oecologia*, 113(2), 151–161.
- Campbell, C. S. (2006), *Response of ECH₂O soil moisture sensors to temperature variation*, Decagon Devices, Inc., Pullman.
- Celia, M. A., E. T. Bouloutas, and R. L. Zarba (1990), A general mass-conservative numerical solution for the unsaturated flow equation, *Water Resources Research*, 26(7), 1483–1496, doi:10.1029/WR026i007p01483.
- Cherkauer, K. A., and D. P. Lettenmaier (1999), Hydrologic effects of frozen soils in the upper Mississippi River basin, *J. Geophys. Res.*, 104(D16), 19599–19610, doi:10.1029/1999jd900337.
- Collatz, G. J., J. T. Ball, C. Grivet, and J. A. Berry (1991), Physiological and environmental regulation of stomatal conductance, photosynthesis and transpiration: a model that includes a laminar boundary layer, *Agricultural and Forest Meteorology*, 54(2–4), 107–136, doi:10.1016/0168-1923(91)90002-8.

- Daly, E., A. Porporato, and I. Rodriguez-Iturbe (2004), Coupled dynamics of photosynthesis, transpiration, and soil water balance. Part I: Upscaling from hourly to daily level, *Journal of Hydrometeorology*, 5(3), 546–558.
- Van Dam, J. C., and R. A. Feddes (2000), Numerical simulation of infiltration, evaporation and shallow groundwater levels with the Richards equation, *Journal of Hydrology*, 233(1-4), 72–85.
- Dawson, T. E. (1993), Hydraulic lift and water use by plants: implications for water balance, performance and plant-plant interactions, *Oecologia*, 95(4), 565–574.
- Dawson, T. E. (1996), Determining water use by trees and forests from isotopic, energy balance and transpiration analyses: the roles of tree size and hydraulic lift, *Tree Physiol*, 16(1-2), 263–272, doi:10.1093/treephys/16.1-2.263.
- Domec, J. C., J. S. King, A. Noormets, E. Treasure, M. J. Gavazzi, G. Sun, and S. G. McNulty (2010), Hydraulic redistribution of soil water by roots affects whole-stand evapotranspiration and net ecosystem carbon exchange, *New Phytologist*, 187(1), 171–183.
- Farquhar, G. D., S. Caemmerer, and J. A. Berry (1980), A biochemical model of photosynthetic CO₂ assimilation in leaves of C₃ species, *Planta*, 149(1), 78–90, doi:10.1007/bf00386231.
- Fiscus, E. L. (1975), Interaction between osmotic-induced and pressure-induced water-flow in plant roots, *Plant Physiology*, 55(5), 917–922.
- Flerchinger, G. N., and K. E. Saxton (1987), Simultaneous heat and water model of a freezing snow-residue-soil system, *American Society of Agricultural Engineers*, no. fiche no. 87-2567.
- Foley, J. A., I. C. Prentice, N. Ramankutty, S. Levis, D. Pollard, S. Sitch, and A. Haxeltine (1996), An integrated biosphere model of land surface processes, terrestrial carbon balance, and vegetation dynamics, *Global Biogeochemical Cycles*, 10(4), 603–628, doi:10.1029/96GB02692.
- Franchini, M., and M. Pacciani (1991), Comparative analysis of several conceptual rainfall-runoff models, *Journal of Hydrology*, 122(1-4), 161–219, doi:10.1016/0022-1694(91)90178-k.
- Frensch, J., and E. Steudle (1989), Axial and radial hydraulic resistance to roots of maize (*Zea mays* L.), *Plant Physiology*, 91(2), 719–726.
- Fung, I. Y., S. C. Doney, K. Lindsay, and J. John (2005), Evolution of carbon sinks in a changing climate, *PNAS*, 102(32), 11201–11206, doi:10.1073/pnas.0504949102.

- Gale, M. R., and D. F. Grigal (1987), Vertical root distributions of northern tree species in relation to successional status, *Canadian Journal of Forest Research-Revue Canadienne De Recherche Forestiere*, 17(8), 829–834.
- Van Genuchten, M. T. (1980), A closed-form equation for predicting the hydraulic conductivity of unsaturated soils, *Soil Science Society of America Journal*, 44(5), 892–898.
- Gore, A. (2009), *Our choice: A plan to solve the climate crisis*, Bloomsbury Publishing.
- Herkelrath, W. N., E. E. Miller, and W. R. Gardner (1977), Water uptake by plants: II. The root contact model, *Soil Science Society of America Journal*, 41(6), 1039–1043.
- Van den Honert, T. H. (1948), Water transport in plants as a catenary process, *Discussions of the Faraday Society*, 3, 146–153.
- Houlton, B. Z., Y.-P. Wang, P. M. Vitousek, and C. B. Field (2008), A unifying framework for dinitrogen fixation in the terrestrial biosphere, *Nature*, 454(7202), 327–330, doi:10.1038/nature07028.
- Huang, B. G., and P. S. Nobel (1994), Root hydraulic conductivity and its components: with emphasis on desert succulents, *Agronomy Journal*, 86(5), 767–774.
- Huang, M., and X. Liang (2006), On the assessment of the impact of reducing parameters and identification of parameter uncertainties for a hydrologic model with applications to ungauged basins, *Journal of Hydrology*, 320(1-2), 37–61, doi:10.1016/j.jhydrol.2005.07.010.
- Huang, M., X. Liang, and Y. Liang (2003), A transferability study of model parameters for the variable infiltration capacity land surface scheme, *Journal of Geophysical Research: Atmospheres*, 108(D22), n/a–n/a, doi:10.1029/2003JD003676.
- Hunt, E. R., S. W. Running, and C. A. Federer (1991), Extrapolating plant water flow resistances and capacitances to regional scales, *Agricultural and Forest Meteorology*, 54(2-4), 169–195, doi:10.1016/0168-1923(91)90005-b.
- Jackson, R. B., J. Canadell, J. R. Ehleringer, H. A. Mooney, O. E. Sala, and E. D. Schulze (1996), A global analysis of root distributions for terrestrial biomes, *Oecologia*, 108(3), 389–411.
- Jackson, R. B., H. A. Mooney, and E. D. Schulze (1997), A global budget for fine root biomass, surface area, and nutrient contents, *Proceedings of the National Academy of Sciences of the United States of America*, 94(14), 7362–7366.
- Jackson, R. B., J. S. Sperry, and T. E. Dawson (2000), Root water uptake and transport: using physiological processes in global predictions, *Trends in Plant Science*, 5(11), 482–488, doi:10.1016/S1360-1385(00)01766-0.

- Jarvis, P. G. (1976), The interpretation of the variations in leaf water potential and stomatal conductance found in canopies in the field, *Philosophical Transactions of the Royal Society of London. B, Biological Sciences*, 273(927), 593–610, doi:10.1098/rstb.1976.0035.
- Jeong, S. (2009), Understanding snow process uncertainties and their impacts, Ph.D., University of California, Berkeley, United States -- California.
- Johansen, O. (1977), *Thermal Conductivity of Soils. Ph.D. thesis. CRREL Draft Transl. 637.*
- Jones, H. G. (1992), *Plant and microclimate: A quantitative approach to environmental plant physiology*, Cambridge University Press.
- Katerji, N., M. Hallaire, Y. Menouxboyer, and B. Durand (1986), Modeling diurnal patterns of leaf water potential in field conditions, *Ecological Modelling*, 33(2-4), 185–203.
- Kollet, S. J., and R. M. Maxwell (2008), Capturing the influence of groundwater dynamics on land surface processes using an integrated, distributed watershed model, *Water Resources Research*, 44(2), doi:10.1029/2007wr006004.
- Landsberg, J. J., and N. D. Fowkes (1978), Water movement through plant roots, *Annals of Botany*, 42(179), 493–508.
- Landsberg, J. J., T. W. Blanchard, and B. Warrit (1976), Studies on the movement of water through apple trees, *Journal of Experimental Botany*, 27(4), 579–596, doi:10.1093/jxb/27.4.579.
- Lee, J.-E., R. S. Oliveira, T. E. Dawson, and I. Fung (2005), Root functioning modifies seasonal climate, *Proceedings of the National Academy of Sciences of the United States of America*, 102(49), 17576–17581, doi:10.1073/pnas.0508785102.
- Leuning, R. (1995), A critical appraisal of a combined stomatal-photosynthesis model for C3 plants, *Plant Cell and Environment*, 18(4), 339–355.
- Lhomme, J. P., E. Elguero, A. Chehbouni, and G. Boulet (1998), Stomatal control of transpiration: Examination of Monteith's formulation of canopy resistance, *Water Resour. Res.*, 34(9), 2301–2308, doi:10.1029/98wr01339.
- Lhomme, J. P., A. Rocheteau, J. M. Ourcival, and S. Rambal (2001), Non-steady-state modelling of water transfer in a Mediterranean evergreen canopy, *Agricultural and Forest Meteorology*, 108(1), 67–83.
- Li, L., Y.-P. Wang, Q. Yu, B. Pak, D. Eamus, J. Yan, E. van Gorsel, and I. T. Baker (2012), Improving the responses of the Australian community land surface model (CABLE) to seasonal drought, *Journal of Geophysical Research: Biogeosciences*, 117(G4), n/a–n/a, doi:10.1029/2012JG002038.

- Liang, X., and Z. H. Xie (2001), A new surface runoff parameterization with subgrid-scale soil heterogeneity for land surface models, *Advances in Water Resources*, 24(9-10), 1173–1193.
- Liang, X., D. P. Lettenmaier, E. F. Wood, and S. J. Burges (1994), A simple hydrologically based model of land surface water and energy fluxes for general circulation models, *J. Geophys. Res.*, 99(D7), 14415–14428, doi:10.1029/94jd00483.
- Liang, X., D. P. Lettenmaier, and E. F. Wood (1996a), One-dimensional statistical dynamic representation of subgrid spatial variability of precipitation in the two-layer variable infiltration capacity model, *J. Geophys. Res.*, 101(D16), 21403–21422, doi:10.1029/96jd01448.
- Liang, X., E. F. Wood, and D. P. Lettenmaier (1996b), Surface soil moisture parameterization of the VIC-2L model: Evaluation and modification, *Global and Planetary Change*, 13, 195–206.
- Liang, X., E. F. Wood, and D. P. Lettenmaier (1999), Modeling ground heat flux in land surface parameterization schemes, *J. Geophys. Res.*, 104(D8), 9581–9600, doi:10.1029/98JD02307.
- Liang, X., Z. Xie, and M. Huang (2003), A new parameterization for surface and groundwater interactions and its impact on water budgets with the variable infiltration capacity (VIC) land surface model, *J. Geophys. Res.*, 108(D16), 8613, doi:10.1029/2002jd003090.
- Luo, X., X. Liang, and H. R. McCarthy (2013), VIC+ for water-limited conditions: A study of biological and hydrological processes and their interactions in soil-plant-atmosphere continuum, *Water Resources Research* (Accepted).
- Maxwell, R. M., and S. J. Kollet (2008), Interdependence of groundwater dynamics and land-energy feedbacks under climate change, *Nature Geoscience*, 1(10), 665–669, doi:10.1038/geo315.
- McCarthy, H. R., R. A. M. Oren, A. C. Finzi, D. S. Ellsworth, H.-S. Kim, K. H. Johnsen, and B. Millar (2007), Temporal dynamics and spatial variability in the enhancement of canopy leaf area under elevated atmospheric CO₂, *Global Change Biology*, 13(12), 2479–2497, doi:10.1111/j.1365-2486.2007.01455.x.
- McElrone, A. J., W. T. Pockman, J. Martínez-Vilalta, and R. B. Jackson (2004), Variation in xylem structure and function in stems and roots of trees to 20 m depth, *New Phytologist*, 163(3), 507–517, doi:10.1111/j.1469-8137.2004.01127.x.
- Mendel, M., S. Hergarten, and H. J. Neugebauer (2002), On a better understanding of hydraulic lift: A numerical study, *Water Resources Research*, 38(10), 1183–1192, doi:10.1029/2001WR000911.

- Neumann, R. B., and Z. G. Cardon (2012), The magnitude of hydraulic redistribution by plant roots: a review and synthesis of empirical and modeling studies, *New Phytologist*, 194(2), 337–352, doi:10.1111/j.1469-8137.2012.04088.x.
- Niu, G.-Y., Z.-L. Yang, R. E. Dickinson, L. E. Gulden, and H. Su (2007), Development of a simple groundwater model for use in climate models and evaluation with Gravity Recovery and Climate Experiment data, *J. Geophys. Res.*, 112(D7), D07103, doi:10.1029/2006JD007522.
- Or, D., and J. M. Wraith (1999), Temperature effects on soil bulk dielectric permittivity measured by time domain reflectometry: A physical model, *Water Resources Research*, 35(2), 371–383, doi:10.1029/1998WR900008.
- Pate, J. S., W. D. Jeschke, and M. J. Aylward (1995), Hydraulic architecture and xylem structure of the dimorphic root systems of south-west Australian species of proteaceae, *Journal of Experimental Botany*, 46(289), 907–915.
- Pearcy, R. W., E.-D. Schulze, and R. Zimmermann (1989), Measurement of transpiration and leaf conductance, in *Plant Physiological Ecology: Field methods and instrumentation*, Chapman and Hall, London, New York.
- Pepin, S., N. J. Livingston, and W. R. Hook (1995), Temperature-dependent measurement errors in time domain reflectometry determinations of soil water, *Soil Science Society of America Journal*, 59(1), 38–43.
- Quijano, J. C., P. Kumar, D. T. Drewry, A. Goldstein, and L. Misson (2012), Competitive and mutualistic dependencies in multispecies vegetation dynamics enabled by hydraulic redistribution, *Water Resour. Res.*, 48, 22 PP., doi:201210.1029/2011WR011416.
- Randerson, J. T., M. V. Thompson, T. J. Conway, I. Y. Fung, and C. B. Field (1997), The contribution of terrestrial sources and sinks to trends in the seasonal cycle of atmospheric carbon dioxide, *Global Biogeochemical Cycles*, 11(4), 535–560, doi:10.1029/97GB02268.
- Ren, D., M. Xue, and A. Henderson-Sellers (2004), Incorporating Hydraulic Lift into a Land Surface Model and Its Effects on Surface Soil Moisture Prediction, *Journal of Hydrometeorology*, 5(6), 1181–1191, doi:10.1175/JHM-385.1.
- Richards, L. A. (1931), Capillary conduction of liquids through porous mediums, *Physics*, 1(5), 318–333.
- Runkle, B. R. . (2009), Plant water use and growth in response to soil salinity in irrigated agriculture, Ph.D. dissertation, University of California, Berkeley, California, United States.
- Ryel, R. J., M. M. Caldwell, C. K. Yoder, D. Or, and A. J. Leffler (2002), Hydraulic redistribution in a stand of *Artemisia tridentata*: evaluation of benefits to transpiration

- assessed with a simulation model, *Oecologia*, 130(2), 173–184, doi:DOI 10.1007/s004420100794.
- Sands, R., E. L. Fiscus, and C. P. P. Reid (1982), Hydraulic properties of pine and bean roots with varying degrees of suberization, vascular differentiation and mycorrhizal infection, *Australian Journal of Plant Physiology*, 9(5), 559–569.
- Schäfer, K. V. R., R. Oren, C.-T. Lai, and G. G. Katul (2002), Hydrologic balance in an intact temperate forest ecosystem under ambient and elevated atmospheric CO₂ concentration, *Global Change Biology*, 8(9), 895–911, doi:10.1046/j.1365-2486.2002.00513.x.
- Sellers, P. J., Y. Mintz, Y. C. Sud, and A. Dalcher (1986), A Simple Biosphere Model (SIB) for Use within General Circulation Models, *Journal of the Atmospheric Sciences*, 43(6), 505–531, doi:10.1175/1520-0469(1986)043<0505:ASBMFU>2.0.CO;2.
- Sellers, P. J., D. A. Randall, G. J. Collatz, J. A. Berry, C. B. Field, D. A. Dazlich, C. Zhang, G. D. Collelo, and L. Bounoua (1996), A Revised Land Surface Parameterization (SiB2) for Atmospheric GCMS. Part I: Model Formulation, *Journal of Climate*, 9(4), 676–705, doi:10.1175/1520-0442(1996)009<0676:ARLSPF>2.0.CO;2.
- Šimůnek, J., M. T. van Genuchten, and M. Šejna (2005), *The HYDRUS-1D software package for simulating the one-dimensional movement of water, heat, and multiple solutes in variably-saturated media (version 3.0)*, University of California Riverside, Riverside, California.
- Soylu, M. E., E. Istanbuluoglu, J. D. Lenters, and T. Wang (2011), Quantifying the impact of groundwater depth on evapotranspiration in a semi-arid grassland region, *Hydrol. Earth Syst. Sci.*, 15(3), 787–806, doi:10.5194/hess-15-787-2011.
- Steudle, E., and C. A. Peterson (1998), How does water get through roots?, *Journal of Experimental Botany*, 49(322), 775–788.
- Tuzet, A., A. Perrier, and R. Leuning (2003), A coupled model of stomatal conductance, photosynthesis and transpiration, *Plant Cell and Environment*, 26(7), 1097–1116.
- Wang, G. (2011), Assessing the potential hydrological impacts of hydraulic redistribution in Amazonia using a numerical modeling approach, *Water Resources Research*, 47(2), W02528, doi:10.1029/2010wr009601.
- Wang, L., T. Koike, K. Yang, R. Jin, and H. Li (2010a), Frozen soil parameterization in a distributed biosphere hydrological model, *Hydrol. Earth Syst. Sci.*, 14(3), 557–571, doi:10.5194/hess-14-557-2010.
- Wang, S., R. F. Grant, D. L. Verseghy, and T. Andrew Black (2002), Modelling carbon-coupled energy and water dynamics of a boreal aspen forest in a general circulation model land surface scheme, *International Journal of Climatology*, 22(10), 1249–1265, doi:10.1002/joc.776.

- Wang, Y. P., R. M. Law, and B. Pak (2010b), A global model of carbon, nitrogen and phosphorus cycles for the terrestrial biosphere, *Biogeosciences*, 7(7), 2261–2282, doi:10.5194/bg-7-2261-2010.
- Wang, Y.-P., B. Z. Houlton, and C. B. Field (2007), A model of biogeochemical cycles of carbon, nitrogen, and phosphorus including symbiotic nitrogen fixation and phosphatase production, *Global Biogeochemical Cycles*, 21(1), n/a–n/a, doi:10.1029/2006GB002797.
- Warren, J. M., F. C. Meinzer, J. R. Brooks, J. C. Domec, and R. Coulombe (2007), Hydraulic redistribution of soil water in two old-growth coniferous forests: quantifying patterns and controls, *New Phytologist*, 173(4), 753–765, doi:DOI 10.1111/j.1469-8137.2006.01963.x.
- Wraith, J. M., and D. Or (1999), Temperature effects on soil bulk dielectric permittivity measured by time domain reflectometry: Experimental evidence and hypothesis development, *Water Resources Research*, 35(2), 361–369, doi:10.1029/1998WR900006.
- Wraith, J. M., J. M. Baker, and T. K. Blake (1995), Water uptake resumption following soil drought: a comparison among four barley genotypes, *Journal of Experimental Botany*, 46(288), 873–880.
- Wronski, E. B., J. W. Holmes, and N. C. Turner (1985), Phase and amplitude relations between transpiration, water potential and stem shrinkage, *Plant, Cell & Environment*, 8(8), 613–622, doi:10.1111/j.1365-3040.1985.tb01700.x.
- Zeng, X., and M. Decker (2009), Improving the Numerical Solution of Soil Moisture–Based Richards Equation for Land Models with a Deep or Shallow Water Table, *Journal of Hydrometeorology*, 10(1), 308–319, doi:10.1175/2008JHM1011.1.